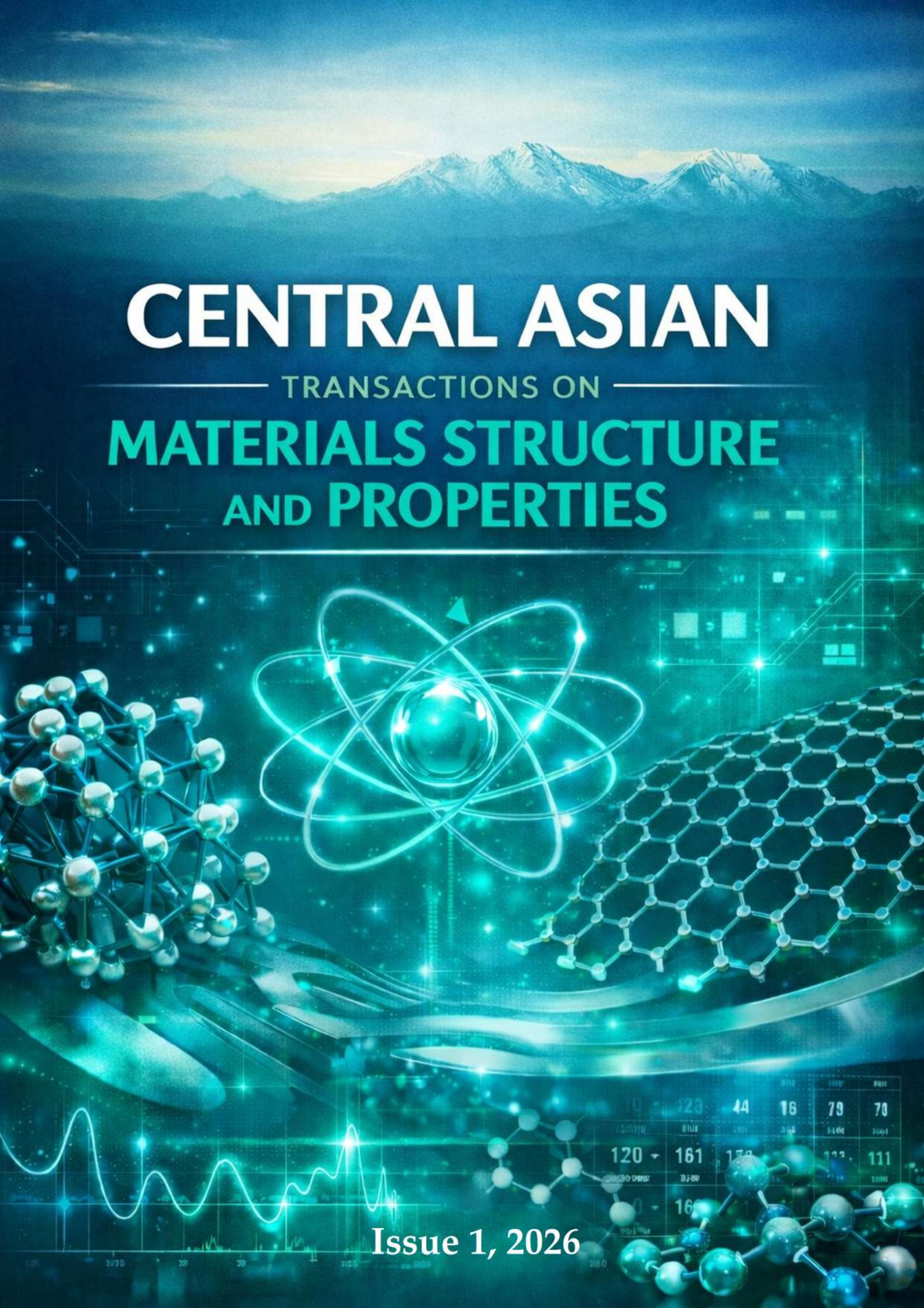
CENTRAL ASIAN
TRANSACTIONS ON
MATERIALS STRUCTURE
AND PROPERTIES
Issue 1, 2026

ISSN (Print): 3134-7983
ISSN (Online): 3134-7991 Vol. 1, Issue 1, March 2026.

CENTRAL ASIAN TRANSACTIONS ON MATERIALS STRUCTURE AND PROPERTIES

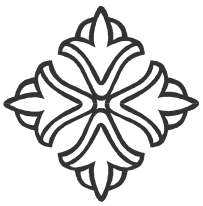

Published 4 times a year

Ust-Kamenogorsk, 2026

Vol. 1, Issue 1, March 2026.
CENTRAL ASIAN TRANSACTIONS ON MATERIALS STRUCTURE AND PROPERTIES

https://doi.org/10.51885/3134-7983_CATMSP_2026_1_1
SRSTI 61.35.33

APPLICATION OF NEW COLLECTORS IN FLOTATION OF COPPER-LEAD-ZINC ORE FROM THE TISHINSKY DEPOSIT

Nazgul Akimbayeva [1], Bekzat Saurbayeva [2*], Raigul Ramazanova [2*],
[1]Kazakh National Women's Teacher Training University, Almaty, Kazakhstan
[2]D. Serikbayev East Kazakhstan Technical University, Ust-Kamenogorsk, Kazakhstan
*Corresponding author: Raigul Ramazanova, e-mail: RRamazanova@edu.ektu.kz

Keywords:
flotation, collecting reagents, surface-active agents, diethanolamine, dithiocarbamates, sulfide ores

ABSTRACT
The work is devoted to improving the technology of flotation enrichment of copper-lead-zinc ore of the Tishinsky deposit based on the development and research of new flotation reagents. It has been shown that increasing the efficiency of separation of sulfide minerals is an important factor in the rational use of mineral resources and improving the technical and economic performance of processing polymetallic raw materials. The aim of this study was to synthesize and evaluate the potential of new surfactants as collectors in the flotation of copper-lead-zinc ore. Alkylated diethanolamines and their dithiocarbamate derivatives were used as the subjects of the study. N-nonyl-N,N-di(2-hydroxyethyl)amine and disodium salt of N-nonyl-N,N-bis(2-xanthateethyl)amine were synthesized. The resulting reagents were found to be useful in copper-lead-zinc ore flotation processes, offering potential for increased selectivity and recovery of valuable components.

INTRODUCTION

At the present stage, the field of mineral processing is developing rapidly, with widespread implementation of new technological solutions aimed at the comprehensive and efficient utilization of mineral raw materials. This trend is directly associated with the decreasing content of valuable components in ores, the increasing complexity of their mineralogical composition, and the tightening of industrial requirements. In this context, rational use of mineral resources, improvement of product quality, reduction of technogenic environmental impact, and minimization of energy consumption represent the key strategic objectives of the modern mining and metallurgical industry (Li et al., 2023).

The effective solution of these challenges requires further advancement of the theoretical and practical foundations of mineral beneficiation processes. In particular, in-depth investigation of the laws governing selective mineral liberation, their physicochemical properties in aqueous media, and the mechanisms of interfacial interactions is of great importance. In the processing of polymetallic ores, achieving high selectivity in mineral separation is one of the main factors determining the efficiency of beneficiation technologies (Zhao et al., 2022).

Flotation is one of the most widely applied and technologically advanced methods for the beneficiation of polymetallic ores. The efficiency of this process largely depends on the type of flotation reagents, their chemical nature, and their interaction with mineral surfaces. When added to the ore pulp, flotation reagents act as essential technological components that ensure or significantly facilitate mineral separation. Without reagents, the flotation process would be limited

to only a few naturally floatable minerals. Among flotation reagents, collectors play a particularly important role. They adsorb onto the surfaces of naturally hydrophilic minerals, imparting hydrophobic properties to them. As a result, mineral particles effectively attach to air bubbles, enhancing both the intensity and selectivity of the flotation process. Therefore, the development of new, highly efficient, and selective collector reagents remains one of the most relevant directions in flotation theory and practice (Otaqulov et al., 2024).

The copper–lead–zinc ores of the Tishin deposit are characterized by a complex mineralogical composition and strong intergrowth of sulfide minerals, which leads to significant technological difficulties during beneficiation. Therefore, the application of next-generation reagents in the flotation processing of these ores can improve beneficiation performance, increase the recovery of valuable components, and enhance the overall economic efficiency of the process (Abramov, 2005).

In this regard, the investigation of novel surfactants based on alkylated diethanolamines and their dithiocarbamate derivatives as flotation collectors is of considerable scientific and practical interest. The use of such reagents can ensure selective flotation of sulfide minerals and contribute to the further improvement of polymetallic ore beneficiation technologies.

The aim of this study is to synthesize new surfactants and evaluate their potential as collectors in the flotation of copper–lead–zinc ores.

MATERIALS AND METHODS

In order to obtain novel surfactants, alkylated diethanolamines and their dithiocarbamate derivatives were synthesized. Their flotation activity was investigated, and as a result, sample **A-3** was found to exhibit high collecting performance in the flotation of sulfide ores.

N-nonyl-N,N-di(2-hydroxyethyl)amine (**A-1**) was synthesized via the reaction of diethanolamine with bromooctane.

Disodium N-nonyl-N,N-bis(2-xanthogenatoethyl)amine (**A-3**) was synthesized by the reaction of N-nonyl-N,N-di(2-hydroxyethyl)amine (**A-1**) with carbon disulfide (CS_2) in an alcoholic medium in the presence of sodium hydroxide (Figure 1).

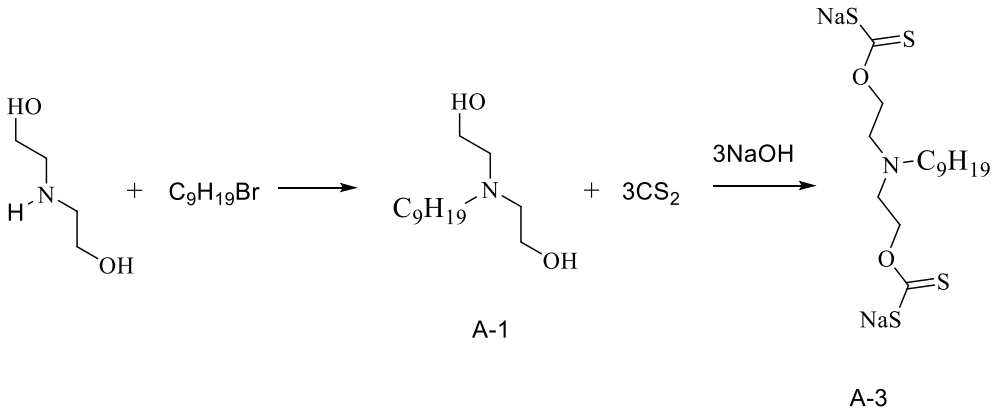

Figure 1. Chemical reaction scheme for the synthesis of the organic compound
Note – Compiled by the authors

The structures of the synthesized compounds were characterized using Fourier-transform infrared (FTIR) spectroscopy and nuclear magnetic resonance (NMR) spectroscopy, while their chemical composition was determined by elemental microanalysis.

In the ^1H NMR spectrum of compound A-1, a singlet characteristic of the CH_3 group protons appears at δ = 0.88 ppm, while multiplets in the range of δ = 1.27 ppm correspond to the protons of the nonyl group $–(CH_2)_9–$. The protons of the NCH_2 group resonate at δ = 4.17 ppm (m). In addition, the hydroxyl proton appears as a broadened singlet at δ = 3.65 ppm.

In the ^13C NMR spectrum of compound A-1, absorption signals corresponding to the carbon atoms of the CH_3 and $–(CH_2)_7–$ groups are observed in the regions of 14.10 and 22.47–22.65 ppm, respectively. The signal at 59.30 ppm is attributed to the carbon atom of the CH_2OH group, whereas the signals at 29.48 and 31.38 ppm correspond to the carbon atoms of the $C_9H_{19}CH_2N$ and $–N(CH_2)–$ groups, respectively.

In the FTIR spectrum of compound A-3, characteristic stretching vibrations of the C=S and C–S bonds are observed at 1262 and 623 cm^{-1}, respectively. Based on the obtained results, a technological scheme for the synthesis of the A-3 collector was developed (Figure 2).

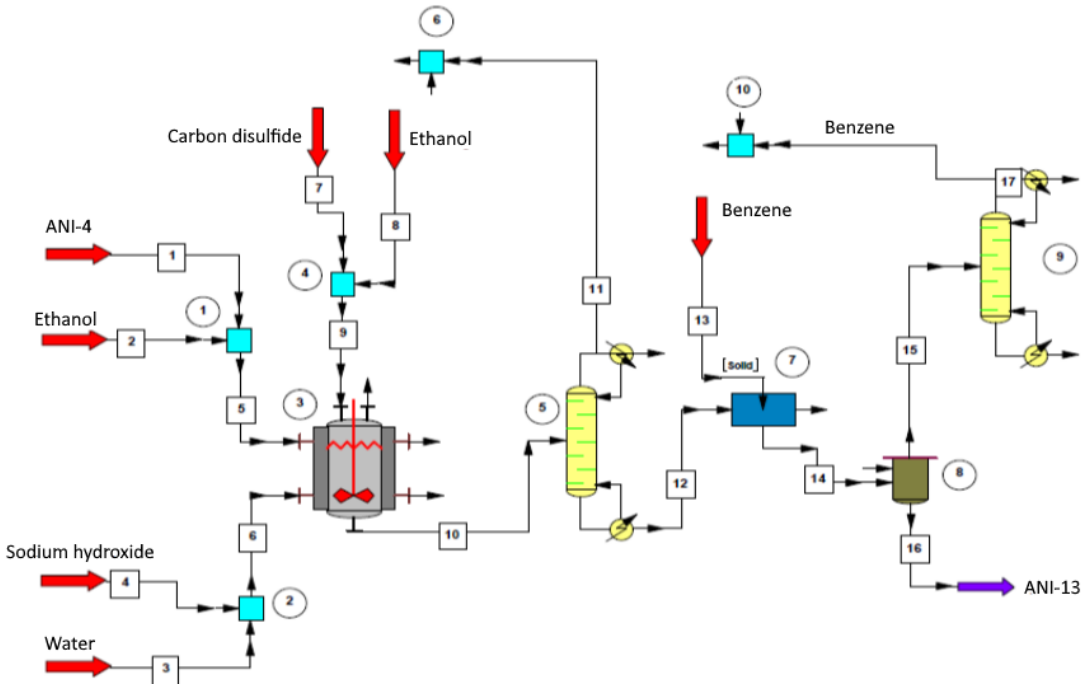

Figure 2. Technological scheme for obtaining the A-3 collector
Note – Compiled by the authors

Description of the technological process (Figure 2):

Compound A-1 was dissolved in ethanol, while sodium hydroxide was dissolved in water, after which the reaction mixture was mixed. A mixture of ethanol and carbon disulfide was introduced at room temperature for one hour, followed by distillation of the solvent (ethanol). Ethanol was then reintroduced into the reaction mixture, the crystalline precipitate was washed with benzene, dried, and the solvent was distilled again, with benzene being reused for washing the precipitate.

The aim of the conducted studies was to increase the flotation activity of the synthesized reagents compared with the base reagent. Reagents A-3 and A-9 containing xanthogenate groups are generally collectors. The lower their activity at the water/air interface, the better they adsorb on the mineral surface. In this case, since reagent A-3 exhibits lower surface activity, it is expected to have higher collecting ability (Figure 3).

In this study, the following reagents were used as collectors: sodium butyl xanthate, which is widely applied at all concentration plants in Kazakhstan, as well as the new collector reagents – sodium N-(nonyl)-N-bis(ethyl xanthogenate) (A-3), N-(heptyl)-N-(2-hydroxyethyl)amino-2-ethyl xanthogenate (A-9), and HET.

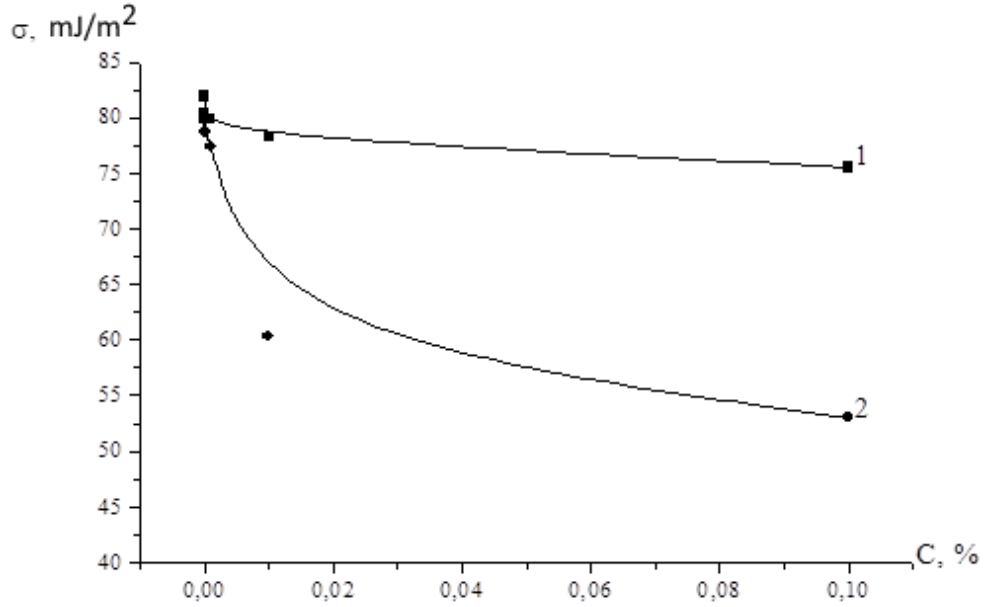

Figure 3. Dependence of surface tension on concentration for solutions of A-3 (1) and A-9 (2)
Note – Compiled by the authors

RESULTS

The results of the studies showed that the use of A-3 and HET as flotation reagents is effective in the processing of zinc–pyrite raw materials. Under the basic reagent regime, the copper content in the collective copper–lead concentrate was 12.8% with a recovery of 86.06%, while the lead content was 10% with a recovery of 78.6%.

The results of flotation experiments demonstrated that when reagent A-3 is used as a collector at a dosage of 23 g/t of ore, the lead content in the collective copper–lead concentrate reaches 11.1%, although the recoveries of copper and lead decrease. When HET is used, the contents of copper and lead in the collective copper–lead concentrate increase: copper rises from 12.88% to 13.6%, and lead from 10% to 18.3%. Consequently, reagents A-3 and HET exhibit selective action toward copper and lead, respectively (Table 1).

Table 1. Results of copper–lead flotation under different reagent regimes

Product name	Yield, %	Composition, %				Recovery, %				Remarks
		Cu	Pb	Zn	Fe	Cu	Pb	Zn	Fe	
Basic reagent mode 500 gr										
Cu–Pb concentrate	3.56	12.8	10	8.4	23.9	86.06	78.6	10.94	25.0	BX – 23 g/t (butyl xanthate) T-80 – 17 g/t
Industrial process 2	2.08	1.76	2.3	7.5	22.9	3.77	5.67	3.11	7.65	
Industrial process 1	6.52	0.3	0.4	4.6	16.7	1.10	1.71	3.27	9.55	
Froth control flotation	9.3	0.1	0.4	4.8	16.7	0.95	4.48	8.91	24.95	
Tailings	78.54	0.1	0.1	4.7	2.6	8.09	9.47	73.75	32.80	
Feed (initial ore)	100	0.67	0.54	5.2	7.6	100	100	100	100	
Cu–Pb concentrate	1.5	11.3	21.1	6.6	13.8	33.0	58	2.0	3.2	A-3 – 23 g/t T-80 – 17 g/t
Industrial process 2	0.82	3.1	4.5	6.2	7.3	4.9	6.8	1.0	0.9	
Industrial process 1	5.48	0.98	1.15	4.9	5.5	10.4	11.6	5.4	4.6	
Froth control flotation	4.56	2.0	0.9	4.9	7.0	17.7	7.5	4.5	4.9	
Tailings	87.6	0.2	0.1	4.9	6.4	34.0	16.1	87.0	86.3	
Feed (initial ore)	100	0.52	0.55	4.94	6.5	100	100	100	100	

end of table 1

Product name	Yield, %	Composition, %				Recovery, %				Remarks
		Cu	Pb	Zn	Fe	Cu	Pb	Zn	Fe	
Basic reagent mode 500 gr										
Cu–Pb concentrate	2.46	13.6	18.3	6.75	23.2	57.1	62.4	3.3	9.0	HET – 30 g/t BX – 23 g/t (butyl xanthate) T-80 – 17 g/t
Industrial process 2	1.2	1.4	2.1	5.7	19.75	2.9	3.5	1.4	3.7	
Industrial process 1	7.08	0.4	1.5	4.6	11.0	4.8	14.7	6.5	12.3	
Froth control flotation	3.92	0.9	1.4	4.6	8.1	6.0	7.6	3.6	5.0	
Tailings	85.34	0,2	0.1	5.0	5.2	29.1	11.8	85.2	70.0	
Feed (initial ore)	100	0.59	0.72	5.01	6.34	100	100	100	100	
Note – Compiled by the authors										

Further studies examined the effect of the new collector on the flotation of the collective copper–lead concentrate. The dosage of the new collector A-3 was varied in the range of 38–76 g/t. When this reagent was used together with butyl xanthate, the copper content and its recovery increased by 3.9%.

The analysis of the obtained results showed that when reagent A-3 was used as a collector in the copper–lead flotation cycle, the contents of copper, lead, and zinc increased from 3.8% to 6.0%; however, the recoveries of copper and lead decreased. At the same time, the recovery of zinc and pyrite in the tailings increased to 84%. As can be seen from the results presented in the table, when reagent A-3 was used as a collector at a dosage of 23 g/t of ore, the lead content in the collective copper–lead concentrate reached 21.1%, although the recoveries of copper and lead decreased. Meanwhile, the recoveries of zinc and pyrite in the tailings increased to 87% and 86.3%, respectively.

Thus, it was established that reagent A-3 exhibits a selective effect toward copper and lead.

Table 2. Flotation results when using new collector reagents.

Product name	Yield, %	Composition, %				Recovery, %				Remarks
		Cu	Pb	Zn	Fe	Cu	Pb	Zn	Fe	
Basic reagent mode 1000 gr										
Cu–Pb concentrate	9.3	4.9	5.8	7.2	33.4	79.8	75.5	13.5	53.7	BX – 76 g/t (butyl xanthate) T-80 – 54 g/t
Industrial process 2	1.8	0.6	1.25	10.4	23.2	1.9	3.2	3.8	7.2	
Industrial process 1	6.9	0.3	0.9	8.7	11.0	3.6	8.7	12.1	13.1	
Froth control flotation	2.0	0.2	0.5	8.6	6.97	0.7	1.4	3.5	2.4	
Tailings	80.0	0.1	0.1	4.15	1.7	14.0	11.2	67.1	23.5	
Feed (initial ore)	100	0.57	0.71	4.95	5.87	100	100	100	100	
Cu–Pb concentrate	7.8	5.05	1.2	8.2	33.4	77.0	40.7	12.7	44.8	BX – 38 g/t (butyl xanthate) A-3 – 38 g/t T-80 – 54 g/t
Industrial process 2	1.17	0.6	1.0	8.2	24.7	1.4	5.1	1.9	5.0	
Industrial process 1	7.9	0.3	0.4	7.2	13.9	4.6	13.8	11.3	18.9	
Froth control flotation	1.95	0.3	0.6	8.1	10.4	1.1	5.1	3.1	3.5	
Tailings	81.18	0.1	0.1	4.4	2.0	15.9	35.3	71.0	27.9	
Feed (initial ore)	100	0.51	0.23	5.03	5.82	100	100	100	100	
Cu–Pb concentrate	3.66	8.7	11.8	9.6	13.1	64.6	71.8	7.1	8.2	A-3 – 76 g/t T-80 – 54 g/t
Industrial process 2	1.5	2.0	2.5	7.95	5.8	6.1	6.2	2.4	1.5	
Industrial process 1	3.82	0.86	0.8	5.2	5.8	6.7	5.1	4.0	3.8	
Froth control flotation	2.1	1.1	0.6	5.5	6.4	4.7	2.1	2.3	2.3	
Tailings	88.92	0.1	0.1	4.7	5.5	18.0	14.8	84.2	84.1	
Feed (initial ore)	100	0.49	0.60	4.96	5.81	100	100	100	100	
Note – Compiled by the authors										

DISCUSSION

The conducted studies confirmed that the synthesized flotation reagents, particularly A-3 and A-9 containing xanthogenate functional groups, demonstrate pronounced flotation activity in the flotation of copper–lead–zinc ore. The mechanism of action of these reagents is closely related to their molecular structure and the specific features of their interaction with mineral surfaces.

It is known that reagents A-3 and A-9 belong to the group of collectors, and for such reagents a lower surface activity at the water/air interface ensures a higher adsorption capacity on the mineral surface. The research results showed that reagent A-3 has low surface activity, which indicates its ability to form a stable adsorption layer on the mineral surface and enhance the hydrophobization of sulfide minerals. In this regard, reagent A-3 exhibits high collecting ability and has a positive effect on the selectivity of the flotation process.

The results of flotation experiments demonstrated the effectiveness of using reagents A-3 and HET in the processing of zinc–pyrite raw materials. Compared with the basic reagent regime, the use of the new reagents altered the content of valuable components in the concentrate and ensured their more selective separation. In particular, the use of reagent A-3 at a dosage of 23 g/t led to an increase in the lead content in the collective copper–lead concentrate, although a decrease in the recovery of copper and lead was observed. This phenomenon can be explained both by the high selectivity of the reagent and by possible re-flotation or partial transfer of minerals to tailings during the flotation process (Abramov, 2010).

When using reagent HET, a significant increase in the content of copper and lead in the collective copper–lead concentrate was observed. This indicates the high frothing ability of HET and its capacity to ensure effective attachment of mineral particles to air bubbles during flotation. As a result, the quality of the concentrate improved and the accumulation of valuable components increased.

Additional studies in which the dosage of reagent A-3 was varied in the range of 38–76 g/t showed that, when used together with butyl xanthate, it allows increasing the copper content and its recovery by up to 3.9%. This synergistic effect is explained by the combination of the selective adsorption of A-3 and the high flotation activity of the basic collector. However, when A-3 was used alone, a decrease in the recovery of copper and lead and an increase in the transfer of zinc and pyrite to tailings were observed, which confirms the selective action of this reagent toward copper and lead (Abramov, 2010).

In general, the obtained results showed that the newly synthesized reagents possess high flotation activity and are characterized by an enhanced ability to hydrophobize mineral surfaces and form stable froth. These properties make it possible to consider reagents A-3 and HET as promising collectors and frothers for the flotation beneficiation of copper–lead–zinc ores.

CONCLUSIONS

The conducted studies demonstrated the effectiveness of newly synthesized flotation reagents for improving the flotation beneficiation technology of copper–lead–zinc ore from the Tishinsky deposit. It was established that under the base reagent regime the copper content in the concentrate was 12.8% (recovery 86.06%) and the lead content was 10% (recovery 78.6%).

When reagent A-3 was used at a dosage of 23 g/t of ore, the lead content increased to 11.1%, while the recoveries of copper and lead slightly decreased; the recovery of zinc and pyrite in the tailings amounted to 84%. When reagent HET was applied, copper increased to 13.6% and lead to 18.3%. When A-3 was used together with butyl xanthate, the contents of copper, lead and zinc increased by 3.8–6.0%, while the recovery of zinc and pyrite in the tailings was 84–87%.

The results show that the synthesized reagents A-3 and HET possess high flotation activity and selective action. This is explained by their ability to enhance the hydrophobization of mineral surfaces and ensure their interaction with air bubbles. Thus, the use of the new reagents makes it possible to improve concentrate quality, increase the recovery of valuable components, and enhance the overall efficiency of the flotation process.

CONFLICT OF INTEREST: The authors declare that they have no conflicts of interest.
FUNDING: This research received no external funding.
INSTITUTIONAL REVIEW BOARD STATEMENT: Not applicable.
INFORMED CONSENT STATEMENT: Not applicable.
DATA AVAILABILITY STATEMENT: All data supporting the findings of this study are included in this article.
ACKNOWLEDGMENTS: The authors express their gratitude to the anonymous reviewers for their valuable comments that contributed to improving the quality of the manuscript.
STATEMENT ON THE USE OF ARTIFICIAL INTELLIGENCE: The authors confirm that no artificial intelligence (AI) tools, including generative language models, were used in the preparation of this article. All textual materials, data, and analytical results were independently prepared by the authors.

REFERENCES

Li, X., Zhang, Y., Wang, J. (2023). Advances in flotation reagents for sulfide ores: A review. Minerals Engineering, 187, 107710. https://doi.org/10.1016/j.mineng.2022.107710

Zhao, L., Chen, H., Li, W. (2022). Novel collectors and modifiers for copper-lead-zinc ore flotation. International Journal of Mineral Processing, 214, 106758. https://doi.org/10.1016/j.minpro.2021.106758

Otaqulov, B., Sadykov, A. (2024). Synthesis and application of alkylated diethanolamine collectors in polymetallic ore flotation. Journal of Mining Science, 60(6), 891–902. https://doi.org/10.1134/S106273912406005X

Abramov, A.A. (2005). Technology of Processing and Enrichment of Non-Ferrous Metal Ores. Vol. 3, Book 1: Ore Preparation and Cu, Cu-Pb, Cu-Fe, Cu-Mo, Cu-Zn Ores. Moscow: MGGU Publishing, 575 p.

Abramov, A.A. (2005). Technology of Processing and Enrichment of Non-Ferrous Metal Ores. Vol. 3, Book 2: Pb, Pb-Cu, Zn, Pb-Zn, Pb-Cu-Zn, Cu-Ni, Co, Bi, Sb, Hg-Containing Ores. Moscow: MGGU Publishing, 461 p.

Kim, T., Park, S., Lee, J. (2021). Dithiocarbamate derivatives as flotation collectors for sulfide minerals. Separation and Purification Technology, 274, 118980. https://doi.org/10.1016/j.seppur.2021.118980

Abdullayev, R., Yermakhanov, S. (2022). Selective flotation of lead and zinc sulfides using new collectors. Minerals, 12(9), 1147. https://doi.org/10.3390/min12091147

Abramov, A.A. (2004). Processing, Enrichment and Complex Utilization of Solid Mineral Resources. Vol. 2: Technology of Mineral Enrichment. Moscow: MGGU Publishing, 509 p.

Abramov, A.A. (2010). Collected Works. Vol. 6: Flotation. Physico-Chemical Modeling of Processes. Moscow: MGGU Publishing, 607 p.

Abramov, A.A. (2010). Collected Works. Vol. 7: Flotation. Collector Reagents. Moscow: MGGU Publishing, 656 p.

Ghosh, A., Sinhamahapatra, S. (2020). Flotation reagents for complex polymetallic ores: Trends and perspectives. In: Bhattacharjee, D., Chakrabarti, S. Future Landscape of Mineral Processing. Springer, Singapore. https://doi.org/10.1007/978-981-15-8523-1_10

Nurzhanov, T., Akhmetov, A., Saparbekov, B. (2023). Application of xanthate and hydroxamate collectors for selective flotation of copper-lead-zinc ores. Applied Sciences, 13(4), 2120. https://doi.org/10.3390/app13042120

Liu, F., Huang, Q., Chen, G. (2021). Effect of novel dithiocarbamate collectors on sulfide mineral flotation efficiency. Minerals, 11(11), 1234. https://doi.org/10.3390/min11111234

Akimbekova, S., Aruova, L., Urkinbaeva, Zh. (2024). Optimization of collector regimes for copper-lead-zinc ores of complex mineralogy. Technobius, 4(4), 0068. https://doi.org/10.54355/tbus/4.4.2024.0068

Zhang, R., Li, Y., Wang, Z. (2025). New trends in collector design for polymetallic sulfide ores flotation. Journal of Materials Research and Technology, 24, 1153–1165. https://doi.org/10.1016/j.jmrt.2025.03.014

Information about authors

Nazgul Akimbayeva – Candidate of Chemical sciences, Associate Professor, Kazakh National Women's Teacher Training University, Almaty, Kazakhstan
e-mail: akimbayeva73@gmail.com
ORCID: https://orcid.org/0000-0001-6371-6688

Bekzat Saurbayeva – Candidate of Chemical sciences, Associate Professor East Kazakhstan Technical University named after D.Serikbaev, Ust-Kamenogorsk, Kazakhstan
e-mail: saurbaeva71@mail.ru
ORCID: https://orcid.org/0009-0002-5022-4814

Raigul Ramazanova – PhD, East Kazakhstan Technical University named after D. Serikbaev, Ust-Kamenogorsk, Kazakhstan
e-mail: RRamazanova@edu.ektu.kz,
ORCID: https://orcid.org/0000-0001-6930-991X

CENTRAL ASIAN TRANSACTIONS ON MATERIALS STRUCTURE AND PROPERTIES

https://doi.org/10.51885/3134-7983_CATMSP_2026_1_2
SRSTI 52.45.19

FEATURES OF COMPOSITION AND PROCESSING OF REFRACTORY GOLD-BEARING ORES OF THE AKTOBE DEPOSIT

Madina Barmenshinova [1]*, **Igor Motovilov** [2], **Marzhangul Inkar** [3], **Rakhymzhan Omar** [4]

[1]K.I. Satpayev Kazakh National Research Technical University, Almaty, Kazakhstan
*Corresponding author: Madina Barmenshinova, *e-mail: m.barmenshinova@satbayev.university*

Keywords:
refractory ores, Aktobe deposit, gold, silver, gravity methods, centrifugal concentration, hydrometallurgy, mineral processing.

ABSTRACT

This article presents the results of studies on the processing of refractory gold-bearing ores from the Aktobe deposit (Zhambyl region, Kazakhstan). The research included chemical and mineralogical characterization, analysis of gold and silver occurrence, and evaluation of physical and mechanical properties. The average gold content was 1.55–1.6 g/t and silver 42–43 g/t. The ore is mainly composed of quartz (up to 79%) and pyrite (up to 10%). Phase analysis revealed that only 46.47% of gold occurs in free form, confirming the refractory nature of the ore. Gravity concentration tests demonstrated the effectiveness of centrifugal separation, achieving up to 35.93% gold recovery with 28.74% of the metal in the concentrate. The findings emphasize the necessity of combined processing technologies. Future research will focus on hydrometallurgical methods, including cyanidation, mechanical activation, and cavitation, to improve recovery and develop optimal flowsheets.

INTRODUCTION

The development of technologies for processing refractory gold-bearing ores is one of the most relevant directions of the modern gold mining industry (Adams, 2016; Marsden & House, 2006; Habashi, 1999). The deterioration of mineral raw material quality, the gradual depletion of easily beneficiable deposits, and the increasing complexity of the mineral composition of newly explored objects necessitate the implementation of advanced and integrated technological solutions (La Brooy et al., 1994; Zhang et al., 2019). According to literature data, a significant portion of the world's gold reserves is currently concentrated in refractory ores, where valuable metals occur in finely dispersed form, associated with sulfide minerals, or locked within a quartz matrix. Such mineralogical features substantially reduce the efficiency of conventional cyanide leaching and require the application of integrated beneficiation and hydrometallurgical processing schemes (Owusu et al., 2021).

The territory of Kazakhstan possesses considerable reserves of refractory gold-bearing raw materials. In this context, one of the promising objects is the Aktobe deposit, explored in 2017 in Zhambyl Region. According to published geological survey data, the ores of this deposit are characterized by relatively low gold content (1.55–1.6 g/t) and silver content (42–43 g/t), as well as a high proportion of quartz (up to 79%) and pyrite (up to 10%). Phase analysis results from several studies indicate that only about 46.47% of gold occurs in free form, while

a substantial portion of the metal is associated with sulfide minerals and disseminated in a finely dispersed state within the host rock. These data confirm the refractory nature of the Aktobe ores and the limited applicability of direct cyanide leaching (Barmenshinova et al., 2023).

In global practice, gravity, flotation, and hydrometallurgical methods are widely used for processing such ores (Corrans, 2017; Mütevellioğlu et al., 2019; Asadi et al., 2019). Analysis of the literature shows that integrated technological schemes involving preliminary recovery of readily liberated gold followed by subsequent processing of obtained concentrates are considered among the most effective approaches (Mutaliyev et al., 2022). Several published studies have comparatively evaluated the efficiency of gravity beneficiation methods for ores similar to those of the Aktobe deposit, including jigging, concentration tables, and centrifugal separation.

Generalization of experimental data indicates that among gravity methods, centrifugal separation provides relatively higher performance in preliminary gold recovery; however, the amount of recovered gold remains insufficient to ensure fully effective industrial-scale processing. In this regard, many authors emphasize the necessity of combining gravity beneficiation with subsequent hydrometallurgical treatment stages.

Hydrometallurgical methods are considered among the most promising directions for processing refractory gold-bearing ores, including direct and intensive leaching processes, the use of alternative reagents, as well as mechanochemical activation and solution cavitation techniques (Amanzholov et al., 2018; Kulenova et al., 2021). Literature data indicate that these approaches have significant potential to improve gold and silver recovery and that their integration with gravity beneficiation enables the development of comprehensive technological schemes for refractory ores.

Thus, the relevance of this study is determined by the need to develop effective processing methods for refractory gold-bearing ores in Kazakhstan. This article is devoted to the analysis and generalization of published scientific research on the processing of ores from the Aktobe deposit. The aim of the work is to characterize the mineralogical features of the Aktobe ores based on a comparative analysis of literature data, evaluate the efficiency of gravity beneficiation methods, and substantiate the feasibility of further hydrometallurgical processing routes.

MATERIALS AND METHODS

This article is based on materials published in various scientific sources concerning the processing of refractory gold-bearing ores from the Aktobe deposit located in the Zhambyl Region. During the study, priority was given to data characterizing the mineralogical, chemical, physical-mechanical, and technological features of the ores from the Aktobe deposit. The deposit was explored in 2017, and geological survey results, as well as subsequent scientific publications, indicate that its ores are characterized by relatively low gold and silver contents and a high proportion of quartz and sulfide minerals. These features create technological limitations in ore processing and necessitate the application of integrated approaches.

In forming the research materials, systematization and comparative analysis of data presented by different authors were applied. When selecting literature sources, attention was paid to the mineralogical composition of the studied ores, the forms of gold occurrence, the reliability of analytical and technological methods used, and the industrial significance of the obtained results. This approach allowed for a comprehensive consideration of technological solutions applicable to ores similar to those of the Aktobe deposit.

The scientific sources included articles published in international and national peer-reviewed journals, monographs, dissertations, and conference proceedings. In selecting literature

data, their scientific level, publication date, reliability of the applied methods, and practical relevance of the results were taken into account. Particular emphasis was placed on information related to the forms of gold distribution, beneficiation efficiency, and regularities in the variation of technological parameters.

During the analysis of published materials, the mineralogical forms of gold, the efficiency of beneficiation and processing methods, as well as the advantages and limitations of various technological approaches were systematized. By comparing results obtained by different authors, common trends and differences were identified, which made it possible to substantiate the main directions for processing refractory gold-bearing ores.

Chemical and Analytical Methods

One of the widely used methods for determining the content of gold and silver is fire assay analysis. This method allows for the evaluation of the total mass fraction of noble metals and is highly reliable for detecting low concentrations of gold and silver. Many scientific studies report that, to improve accuracy, fire assay results were cross-validated using atomic absorption spectroscopy (AAS) and gravimetric methods.

According to literature data, these analytical techniques make it possible to determine gold and silver contents in the range of 0.1–100 g/t and are widely used as standard methods in the gold mining industry (Adams, 2016; Marsden & House, 2006; Zhang et al., 2019). In addition, atomic absorption and X-ray fluorescence (XRF) analysis were used to determine the content of associated elements such as iron, copper, zinc, lead, and manganese. The accuracy of XRF analysis is generally reported within ±3%. The use of infrared analyzers for determining sulfur and carbon content is also widely described in the literature.

Mineralogical Research Methods

Comprehensive mineralogical methods were employed to study the mineral composition of Aktobe ores and the forms of gold occurrence. X-ray diffraction (XRD) analysis identified major mineral phases such as quartz, pyrite, calcite, feldspar, and mica. These data serve as a basis for evaluating ore composition and selecting beneficiation methods.

Polished section microscopy revealed that most gold particles are in micron and submicron sizes and are closely associated with sulfide minerals. Generalization of various studies indicates that gold is frequently associated with minerals such as pyrite, chalcopyrite, and sphalerite. This factor is considered one of the main reasons limiting the efficiency of gravity and flotation beneficiation processes.

Scanning electron microscopy (SEM) combined with energy-dispersive spectroscopy (EDS) allowed clarification of gold morphology, its mineral associations, and interrelations. According to published data, the mineral composition of the ore consists of approximately 78–79% quartz, about 10% pyrite, with the remainder represented by calcite, mica, and feldspar (Barmenshinova et al., 2023; Corrans, 2017). Such mineral composition indicates that a significant portion of gold is not present in free form but is locked within the mineral matrix.

Physical and Mechanical Properties of the Ore

The physical and mechanical properties of the ore play an important role in assessing the efficiency of grinding and beneficiation processes. Literature data consider density, porosity, water absorption, strength, and grindability as key parameters influencing the selection of technological regimes. For ores similar to those of the Aktobe deposit, high Bond work index values indicate significant energy consumption during grinding and highlight the importance of preliminary beneficiation stages (Moldashev & Sarbasov, 2019).

Gravity Beneficiation Methods

The preliminary recovery of gold using gravity methods has been widely discussed in scientific publications. Jigging, shaking tables, and centrifugal concentration are described as separation techniques based on density differences. Comparative analysis of literature data

shows that jigging and shaking tables allow recovery of only a portion of gold, while a significant amount remains in tailings.

Centrifugal concentration, including GRG tests, is frequently cited as one of the most efficient gravity methods. According to published data, this method can achieve preliminary gold recovery of approximately 30–40%, but this level is often insufficient for fully effective industrial-scale processing (Owusu et al., 2021). Therefore, the necessity of combining gravity beneficiation with subsequent processing stages is commonly emphasized.

Hydrometallurgical Processing Directions

Hydrometallurgical methods are considered among the most promising approaches for processing refractory gold-bearing ores. Literature describes direct and intensive leaching processes, the use of alternative reagents, as well as mechanochemical activation and solution cavitation techniques as effective means of additional gold and silver recovery. These methods are reported to accelerate the breakdown of sulfide and silicate matrices and enhance reaction activity (Kulenova & Abdrakhmanova, 2021; Shestaev & Zhaksygulova, 2020).

In processing published experimental data, mathematical statistics methods were widely applied. Mean values, standard deviations, and correlation and regression dependencies were calculated, and the reliability of results was assessed using statistical criteria. These approaches made it possible to comparatively analyze the influence of various technological parameters on gold recovery indicators.

RESULTS AND DISCUSSION

A comprehensive and comparative analysis of published scientific studies on the processing of gold-bearing ores from the Aktobe deposit shows that their mineralogical, chemical, physical-mechanical, and technological features are the key factors determining the possibilities for effective gold recovery. Literature data repeatedly emphasize that these ores are characterized by a predominance of quartz rocks, a significant proportion of sulfide minerals – particularly pyrite—and the finely dispersed and locked distribution of gold. Such features result in a considerable portion of gold being confined within the mineral matrix rather than occurring in free form, which significantly limits the efficiency of conventional beneficiation and hydrometallurgical processing methods. The combination of these factors fully justifies classifying the ores of the Aktobe deposit as refractory gold-bearing raw materials.

According to published chemical data, the average gold content in the Aktobe ores is approximately 1.55–1.6 g/t, while the silver content is around 42–43 g/t. These values do not preclude the industrial development of the deposit; however, the relatively low concentration of precious metals imposes high technological requirements for their efficient processing. Analysis of the literature indicates that direct hydrometallurgical treatment of low-grade gold ores tends to be economically inefficient, whereas the introduction of preliminary beneficiation stages can improve overall technological performance. At the same time, the relatively high silver content increases the potential value of the ore from the perspective of complex processing; however, the different mineralogical distribution of gold and silver complicates their complete recovery under a single technological regime. Therefore, chemical composition data can only serve as a basis for technologically sound decisions when considered together with mineralogical and phase characteristics.

Generalization of mineralogical studies shows that the ores of the Aktobe deposit predominantly belong to quartz-rich rocks, with quartz content ranging from 75 to 79%. Pyrite accounts for approximately 8–10%, while minerals such as calcite, feldspar, and muscovite occur as minor components. This mineralogical composition indicates that a significant portion of gold is not present in free form but is closely associated with sulfide and silicate minerals. Phase analysis data suggest that only about 45–47% of gold occurs as free or partially liberated grains,

while the remainder is associated with pyrite and other sulfide minerals or dispersed within the quartz matrix in micron and submicron sizes. Literature widely reports that this situation considerably reduces the efficiency of direct cyanide leaching, making the application of preliminary beneficiation stages a mandatory technological element for refractory ores.

A generalized description of the characteristic mineralogical features of these ores is presented in Table 1, which shows the proportions of the main minerals and their influence on beneficiation and processing operations.

Table 1. Mineralogical composition of the ores from the Aktobe deposit

Mineral	Content, %	Technological effect
Quartz	75-79	Enhances microdispersed distribution of gold and reduces beneficiation efficiency
Pyrite	8-10	Main carrier of gold in locked form
Calcite	4-6	Indirect influence on reagent regimes
Feldspar	3-5	Complicates grinding and slime formation processes
Muscovite	1-3	Affects selectivity during flotation
Note – Compiled by the author		

Published physico-mechanical data indicate that the ore is characterized by high strength and difficult grindability. For ores similar to those of the Aktobe deposit, a Bond work index of approximately 19 kWh/t^0.5 and a strength index of f ≈ 12 according to the Protodyakonov scale indicate significant energy consumption during grinding. These factors complicate the complete liberation of gold and necessitate the introduction of additional grinding stages; however, an increase in the degree of grinding raises the energy intensity of the technological process and may negatively affect the economic efficiency of processing. In this regard, literature data emphasize the need to optimize grinding regimes taking into account mineralogical and physico-mechanical characteristics.

A comparative analysis of published studies on the efficiency of gravity beneficiation methods shows that these techniques demonstrate different levels of performance at the preliminary beneficiation stage. Although jigging and shaking tables enable the recovery of free and coarse-grained gold, several studies note that a significant portion of gold remains in the tailings. Centrifugal concentration, including GRG tests, is described as one of the most effective gravity methods and can provide an average preliminary gold recovery of approximately 30–40%. Nevertheless, these values are insufficient to ensure complete gold recovery, since a considerable portion of gold remains locked in sulfide and microdispersed phases.

Generalized data on the comparative efficiency of gravity beneficiation methods are presented in Table 2.

Table 2. Test results of gravity beneficiation methods for ores from the Aktobe deposit

Method	Gold recovery, %	Gold content in concentrate, g/t	Remarks
Jigging	12–15	8	Significant metal losses
Shaking table	20–22	18	Improved, but still limited
Centrifugal concentration	28–35.93	36	Most effective method
Note – Compiled by the author			

Despite the relatively high efficiency of gravity beneficiation, published data indicate that its use as an independent technology is insufficient for refractory gold-bearing ores. In this regard, many authors recommend applying multistage technological schemes that combine gravity beneficiation with flotation and hydrometallurgical processing stages. In such schemes, free and coarse gold is recovered at the preliminary gravity stage, while subsequent stages are aimed at additional recovery of sulfide-associated and microdispersed gold.

Numerous scientific studies show that the application of hydrometallurgical processing methods makes it possible to effectively treat difficult-to-leach and locked forms of gold. Although direct cyanide leaching is effective for free gold, its efficiency decreases when processing gold associated with sulfide minerals. In this context, approaches such as intensive leaching, the use of alternative reagents, mechanochemical activation, and solution cavitation are reported to accelerate the liberation of gold from the mineral matrix and increase overall recovery to 70–80%.

In general, the systematization of published scientific results clearly demonstrates the necessity of applying multistage and integrated technological approaches for the effective processing of gold-bearing ores from the Aktobe deposit. Preliminary gravity beneficiation allows the recovery of the readily liberated portion of gold, while subsequent flotation and hydrometallurgical stages enable efficient extraction of locked and microdispersed gold forms. Such technological strategies form the scientific and technological basis for the industrial development of ores from the Aktobe deposit.

CONCLUSIONS

A comprehensive analysis of published scientific data on the processing of gold-bearing ores from the Aktobe deposit demonstrates that, based on their mineralogical composition and the distribution patterns of gold, they belong to the category of refractory ores. Literature sources identify the predominance of quartz, a significant presence of pyrite, and the locked and finely dispersed distribution of gold as the key factors that make these ores technologically complex. These features limit the efficient recovery of gold using conventional technological approaches, including direct cyanide leaching, and substantiate the necessity of applying preliminary beneficiation stages.

A comparative evaluation of gravity beneficiation results reported in published studies reveals considerable differences in the efficiency of various methods. Generalization of literature data indicates that centrifugal concentration is one of the most effective techniques at the preliminary beneficiation stage. This method allows for relatively high recovery of free and coarse-grained gold and is shown by many authors to outperform jigging and shaking table methods. At the same time, it is emphasized that the main advantage of gravity technologies lies in their ability to recover the readily liberated portion of gold at the initial stage.

However, analysis of published data also shows that a substantial fraction of gold remains locked within sulfide minerals or in the microdispersed phases of the host rock. This circumstance demonstrates the insufficiency of gravity methods as a standalone technology and highlights the need for further integrated processing of the ore. In this regard, many researchers consider the combination of gravity beneficiation with subsequent technological stages as an essential condition for effective and complete gold recovery.

Literature data propose hydrometallurgical methods as one of the most promising technological directions. In particular, direct and intensive leaching, mechanochemical activation, and cavitation treatment of solutions are described as advanced approaches that can enhance the leachability of microscopic and dispersed gold forms. These methods improve reagent penetration into mineral surfaces and accelerate process kinetics, thereby increasing gold

recovery. Numerous scientific studies substantiate that the combined application of gravity beneficiation and hydrometallurgical treatment enables the development of an effective integrated processing scheme for refractory gold-bearing ores.

Thus, the synthesis of the reviewed data clearly demonstrates the importance of applying multistage and integrated technological approaches for the efficient processing of gold-bearing ores from the Aktobe deposit. From a theoretical perspective, this work contributes to clarifying the mineralogical and technological patterns characteristic of refractory gold ores and supplements the general scientific foundation for their processing. From a practical standpoint, the conclusions obtained provide a scientific basis for developing effective technological solutions aimed at the industrial exploitation of the deposit.

The technological directions proposed based on the analysis of published results can be applied to the development of other refractory gold-bearing deposits in Kazakhstan with similar geological and mineralogical characteristics. These approaches can enhance the efficiency of integrated mineral resource utilization and serve as a scientific foundation for the technological advancement of the domestic gold mining industry.

CONFLICT OF INTEREST: The authors declare no conflicts of interest.

FUNDING: This research was funded by the Science Committee of the Ministry of Science and Higher Education of the Republic of Kazakhstan (Grant No. AP19680182 — Development of an effective technology for the integrated beneficiation and processing of gold-bearing raw materials from the Aktobe deposit).

REFERENCES

Adams, M.D. (2016). Gold ore processing: Project development and operations (2nd ed.). Elsevier. https://www.sciencedirect.com/book/9780444636584/gold-ore-processing

Marsden, J., & House, C. (2006). The chemistry of gold extraction (2nd ed.). SME. https://smemi.-personifycloud.com/personifyebusiness/Store/Product-Details/productId/116858?utm_-source=chatgpt.com

Zhang, D., Xu, B., & Li, J. (2019). Advances in pretreatment of refractory gold ores by bioleaching. Minerals Engineering, 138, 110–121. https://doi.org/10.1016/j.mineng.2019.04.005

Corrans, I.J. (2017). Application of centrifugal separators in the gold industry. Journal of the Southern African Institute of Mining and Metallurgy, 117(3), 249–254. https://doi.org/10.17159/2411-9717/2017/v117n3a9

Barmenshinova, M., Motovilov, I., Telkov, S., & Omar, R. (2023). Study of the material composition of refractory gold-bearing ore from the Aktobe deposit. Complex Use of Mineral Resources, 331(4), 5–11. https://doi.org/10.31643/2024/6445.34

Mütevellioğlu, N.A., & Yekeler, M. (2019). Beneficiation of oxidized lead-zinc ores by flotation using different chemicals and test conditions. Journal of Mining Science, 55(2), 327–332. https://doi.org/10.1134/S1062739119025623

Asadi, T., & Azizi, A. (2017). Leaching of zinc from a lead-zinc flotation tailing sample using ferric sulphate and sulfuric acid media. Hydrometallurgy, 185, 48–56. https://www.sciencedirect.-com/science/article/abs/pii/S2213343717304438?utm_source=chatgpt.com

Habashi, F. (1999). Extractive metallurgy of gold. Québec: Métallurgie Extractive Québec. https://www.worldcat.org/oclc/42790893

La Brooy, S.R., Linge, H.G., & Walker, G.S. (1994). Review of gold extraction from ores. Minerals Engineering, 7(10), 1213–1241. https://doi.org/10.1016/0892-6875(94)90114-7

Owusu, C., Yalcin, T., Stopic, S., & Friedrich, B. (2021). Gold recovery from refractory gold concentrates by pressure oxidation, thiosulfate leaching and resin adsorption. Journal of Sustainable Metallurgy, 7(2), 695–709. https://doi.org/10.1007/s40831-020-00313-6

Шестаев А.Ж., Жаксыгулова Г.Е. (2020). Особенности переработки упорных золотосодержащих руд Казахстана. Горный журнал Казахстана, 3, 25–31. https://-doi.org/10.31643/gzk-2020-3 // Shestaev A.Zh., Zhaksygulova G.E. (2020). Osobennosti pererabotki upornykh zolotosoderzhashchikh rud Kazakhstana [Features of processing refractory gold ores of Kazakhstan]. Gornyi Zhurnal Kazakhstana, 3, 25–31. (In Russ.)

Куленова Н.А., Абдрахманова Г.С. (2021). Новые подходы к комплексной переработке золотосодержащего сырья. Вестник КазНТУ, 5, 87–94. https://vestnik.kazntu.kz/index.php/-en/article/view/2021-5-87 // Kulenova N.A., Abdrakhmanova G.S. (2021). Novye podkhody k kompleksnoi pererabotke zolotosoderzhashchego syr'ya [New approaches to comprehensive processing of gold-bearing raw materials]. Vestnik KazNTU, 5, 87–94. (In Russ.)

Аманжолов С.А., Бектурганов Д.А. (2018). Технологические аспекты флотации упорных золотосодержащих руд. Комплексное использование минерального сырья, 3, 33–40. https://-doi.org/10.31643/2018/33 // Amanzholov S.A., Bekturganov D.A. (2018). Tekhnologicheskie aspekty flotatsii upornykh zolotosoderzhashchikh rud [Technological aspects of flotation of refractory gold ores]. Kompleksnoe ispol'zovanie mineral'nogo syr'ya, 3, 33–40. (In Russ.)

Молдашев Ж.К., Сарбасов К.М. (2019). Применение центробежных сепараторов при обогащении золотосодержащих руд. Известия НАН РК. Серия геологии и технических наук, 4, 57–63. https://doi.org/10.32014/2019.2518-170X.57// Moldashev Zh.K., Sarbasov K.M. (2019). Primenenie tsentrobezhnykh separatorov pri obogashchenii zolotosoderzhashchikh rud [Application of centrifugal separators in gold ore beneficiation]. Izvestiya NAN RK. Seriya geologii i tekhnicheskikh nauk, 4, 57–63. (In Russ.)

Mutaliyev, A., Zhunusov, A., & Duisenova, A. (2022). Refractory gold ores of Kazakhstan: Problems and prospects of processing. Eurasian Mining, 1, 38–44. https://doi.org/10.17580/em.2022.01.07

Information about authors

Madina Barmenshinova – Candidate of Technical Sciences, Associate Professor, Head of the Department of Metallurgy and Mineral Processing, Kazakh National Research Technical University named after K.I. Satpayev,
e-mail: m.barmenshinova@satbayev.university,
ORCID: https://orcid.org/0000-0003-0534-2387

Igor Motovilov – PhD, Associate Professor of the Department of Metallurgy and Mineral Processing, Kazakh National Research Technical University named after K.I. Satpayev,
e-mail: i.motovilov@satbayev.university,
ORCID: https://orcid.org/0000-0002-0716-402X

Marzhangul Ingkar – doctoral Student of the Department of Metallurgy and Mineral Processing, Kazakh National Research Technical University named after K.I. Satpayev,
e-mail: m.ingkar@mail.ru,
ORCID: https://orcid.org/0009-0002-7304-9326

Rakhymzhan Omar – master of technical sciences, Engineer of the Department of Metallurgy and Mineral Processing, Kazakh National Research Technical University named after K.I. Satpayev,
e-mail: r.omar@satbayev.university,
ORCID: https://orcid.org/0000-0002-3269-7549

https://doi.org/10.51885/3134-7983_CATMSP_2026_1_3
SRSTI 05.12.15

INTEGRATED LADLE TREATMENT OF 40HN3MF STEEL USING FESIAL AND FEMN FOR METALLURGICAL ROLLERS

Ardak Dostayeva [1], **Aristotel Issagulov** [1], **Mirhat Abdrakhmanov** [1], **Aigerim Zhalel** [1]*, **Ainagul Toleuova** [1]
[1]Abylkas Saginov Karaganda Technical University, Karaganda, Kazakhstan
*Corresponding author: Zhalel Aigerim Toleugazykyzy, e-mail: a.zhalel@ktu.edu.kz

Keywords:
thermo-Calc software, phase diagram, complex alloy steels, out-of-furnace treat-ment.

ABSTRACT
This paper is a review and deals with the study of manufacturing rollers for met-allurgical furnaces with improved performance characteristics. The main attention is paid to complex extra-furnace treatment aimed at improving the mechanical and thermal properties of materials. The study includes the analysis of existing steels and technological approaches. Steel 40HN3MF was selected as the main ob-ject of study.
The chemical composition was optimized using the ThermoCalc software pack-age, where the silicon and aluminum content was varied. The effect of FeSiAl and FeMn deoxidizers was studied to increase strength and heat resistance of materi-als. The work uses literature data that reflect modern trends in the development of steels for metallurgical equipment.
The results obtained allowed formulating recommendations for improving the structure and performance characteristics of metallurgical furnace rollers.

INTRODUCTION

Metallurgical furnaces used in various metallurgical processes such as smelting, rolling and heat treatment operate under extreme temperatures and are ex-posed to mechanical and chemical stress. Stability and durability of these fur-naces directly depend on the quality of the materials they are made of, as well as on the technologies used to treat them. In recent decades, special attention has been paid to the development of methods of improving the performance of furnace components. One of the most promising areas is complex out-of-furnace treatment that can significantly improve the strength, heat-resistant and corrosion properties of materials, thereby increasing the service life of furnaces and improving the efficiency of metallurgical processes. According to the existing research, adding manganese to steel can improve its performance.

Adding manganese to steel has a significant effect on its mechanical and performance properties. Manganese is an important alloying element that im-proves various characteristics of steel, including strength, wear resistance and machinability. Depending on the manganese content, various effects can be achieved, which allows using the steel in various industries and for different types of applications.

The use of manganese steels:

– High-manganese steels (with the manganese content of 10 to 14 %) are used in conditions of intense wear, for example, for the production of crushers, jaw and cone crushers, excavator parts and mining equipment.

– Manganese steels with a lower manganese content (up to 1-2 %) are used in various areas of mechanical engineering, including the manufacturing of such structural components as shafts, gears and axles operating under normal or increased loads.

Thus, adding manganese to steel significantly improves its mechanical properties and expands the areas of application of the material.

High-manganese steels that contain 8.5–15 % manganese, due to their high wear resistance under impact loads, for many years have remained an indispensable structural material for manufacturing replaceable parts of machines and equipment in mechanical engineering, mining, metallurgy, railway and the other industries. Linings of vortex and ball mills, tram and railway frogs and turnouts, track links, sprockets, excavator bucket teeth and other parts are made of these steels (Likholobov, 2012). Such steels can also be used to manufacture various parts of metallurgical furnaces with increased performance properties. Some of them include: furnace fireboxes, masonry furnace and crucible components, grates, components for cooling systems, screw elements and ladles, burning elements. The use of high-manganese steels in these components improves their performance characteristics, reduces the frequency of maintenance and improves the overall efficiency of metallurgical processes.

High-manganese steel can also be used to make furnace rollers, especially for furnaces that are subject to high temperatures and mechanical stress.

Metallurgical furnace rollers play an important role in the metalworking process. They are an integral part of many types of furnaces, such as smelting, annealing, roasting, and rolling furnaces. These devices help to ensure stability of the furnace and also contribute to the improvement of technological processes.

Metallurgical furnace rollers perform several main functions:

– Supporting and moving materials. They ensure the movement of metal blanks, ingots, products, and other materials inside the furnace, which is necessary for uniform heating or melting. In some cases, rollers can be part of a system for automatic feeding or extraction of materials;

– Minimizing friction. Rollers reduce friction between the workpiece and the furnace walls, which is important for increasing the service life of both the workpiece and the equipment, as well as improving furnace efficiency;

– Providing high temperature resistance. Rollers are used to move materials through areas with extreme temperatures. This is a very important function, as metallurgical furnaces can operate at temperatures reaching 1000-2000°C, de-pending on the type of metal and the process. Rollers must be made of high-strength materials that can withstand such conditions;

– Reducing mechanical stress. They also help to distribute the load and to reduce wear of the other furnace components, such as screws, conveyor belts or other mechanisms.

Rollers for metallurgical furnaces can be solid-cast, composite (with a steel core and heat-resistant shell), water-cooled and floating to compensate for thermal expansion. Depending on the material, they are made of heat-resistant steel, ceramics, cast iron or have a protective coating to increase wear resistance. According to the area of application, rollers are used for heating and annealing furnaces, cooling sections and continuous casting furnaces where high heat resistance and resistance to mechanical loads are required. They are also divided into driven that actively move the blanks, and non-driven (support) that perform a supporting function.

EXPERIMENTAL PART

The study of manufacturing rollers for metallurgical furnaces with improved performance through com-plex out-of-furnace treatment is key to enhancing their durability and efficiency under high temperatures and mechanical loads. Such treatment methods significantly boost wear resistance, heat resistance, and resistance to mechanical damage. To achieve increased

performance characteristics of rollers, various methods of material treatment are used, which can significantly improve their wear resistance, heat resistance, and resistance to mechanical damage. Let's consider the main aspects of this approach.

1. Selecting the material for manufacturing rollers

High-manganese steels with good wear resistance and resistance to high temperatures are often used to manufacture rollers for metallurgical furnaces. However, various methods of out-of-furnace treatment can be used to improve the performance characteristics of the material.

2. Complex out-of-furnace treatment

Complex out-of-furnace treatment includes several processes that can significantly improve the properties of the material and the rollers in particular. Here is a histogram comparing the properties of the material before and after different types of out-of-furnace treatment. It shows how each method affects the material hardness, wear resistance, corrosion resistance, heat resistance and viscosity.

The diagram (Figure 1) shows how different treatment methods affect such material properties as hardness, wear resistance, corrosion resistance, heat resistance and toughness. Heat treatment (quenching and tempering) in-creases hardness and wear resistance (up to level 7), improves toughness, which is critical for rollers operating under mechanical loads. Nitrocar-burizing/nitriding significantly increases wear resistance (up to 8) and corrosion resistance (up to 6) by developing a durable surface layer. Inert gas treatment increases heat resistance (up to 7) and reduces oxidation maintaining the chemical stability of the material. Plasma spraying significantly improves hard-ness, wear resistance and heat resistance (up to level 8) forming a protective layer. Plasma-activated spraying (PAS) provides maximum performance for most properties: wear resistance and heat resistance reach level 9, and hard-ness and corrosion resistance level 8. This makes PAS especially effective for rollers in metallurgical furnaces.

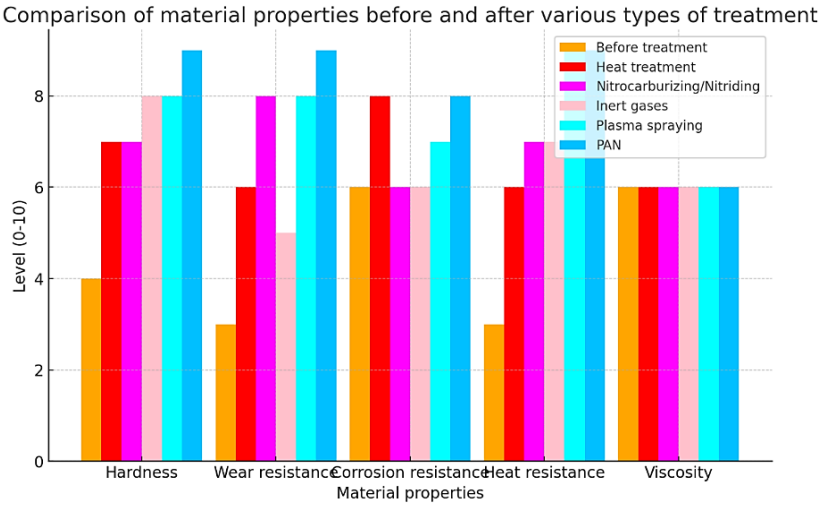

Figure 1. Different methods affecting the material properties

Note – compiled by the authors

High-manganese steels are commonly used for furnace rollers due to their good wear and heat resistance. However, out-of-furnace treatments can further enhance their properties.

This includes processes like heat treatment, nitriding, inert gas treatment, plasma spraying, and plasma activated spraying (PAS).

At the initial stage of this study, a literature review was conducted to analyze current approaches to improving furnace roller properties. Recent research emphasizes the use of inoculants to enhance the crystallization process in casting (Zatulovsky, 1989; Morton & Bryant,

1979; Grigorenko, Kostin, Golovko, et al., 2015; Petrova, 2006; Harvey & Noble, 2007; Scaland, 2001). Studies (Zatulovsky, 1989; Morton & Bryant, 1979) highlight the long-standing use of inoculants of various origins, while modern works focus on updated compositions, particle sizes, and innovative introduction methods. In (Petrova, 2006; Harvey & Noble, 2007), inoculants containing Ce, FeSi and Ca demonstrated positive effects on primary crystallization, acting as both modifiers and microcoolers.

Active development of this area is caused by the fact that traditional methods of improving the properties of materials, such as alloying, heat treatment and modification of ingots, have almost reached the limit of their effectiveness. It should be emphasized that high-alloy steels, including wear-resistant, heat-resistant and corrosion-resistant alloys, are most often selected as objects of research. This is due to the high cost of nanomodifiers, which significantly increases the cost of the final product. In addition, the process of adding nanomodifiers to molten steel is a complex technological task that requires introducing an additional production stage (Vladimirov & Golubev, 1999; Orlov, Malyshevsky, Khlusova, & Golosienko, 2014; Kovalev, Ryaboshuk, Issagulov, Sultamurat, & Jironkin, 2016).

Studies (Russian Federation, 2009a; Russian Federation, 2009b; USSR, 1971; Gulyaev, 2001; Issagulov, Kvon, & Kulikov, 2019; Goldstein, Grachev, & Veksler, 1989; Perelygin, 2008; New high-strength weldable wear-resistant steel, 2005; Duzcukohfu, 2015) are focused on the analysis of the effect of nanomodifiers on increasing the material wear resistance. Structured composite materials and chemical compounds such as SiC, TiO_2 and others were used as nanomodifiers. All the studies showed an increase in wear resistance from 5 to 20% as a result of nanomodification with these compositions.

The analysis of the effect of nanomodifiers on the characteristics of steels is one of the promising areas in modern metal science.

For manufacturing rollers for metallurgical furnaces using high-manganese steels, steel grades are usually selected that have high wear resistance, heat resistance and good mechanical strength. The main element affecting these characteristics is manganese, which, in combination with the other alloying elements, improves the properties of steel.

Various grades can be used for the manufacture of rollers for metallurgical furnaces. These steels must contain a large amount of manganese. As an example, the following steel grades can be mentioned: 110G13L, 20H13, 27HGSA, 16HN60, 30HGSA, 40HNMA, 40HNMF, 40HN3MF, etc.

In work (Likholobov, 2012), steel grade 110G13L was selected as the material. This steel was melted in an arc furnace with the basic lining, ensuring an effective process of remelting and alloying of components. In another work (Issagulov, Ibatov, Kvon, & Arinova, 2019), the object of study was steel grade 30H3MF, which belongs to the group of chromium-molybdenum steels with the possibility of improving properties.

The chemical composition of steel 30H3MF is similar to grade 30HN3MF but the absence of nickel causes reduced viscosity indices. The study focused on increasing the material wear resistance through additional microalloying with vanadium and titanium, which are effective carbide-forming elements. The consequence of this is decreasing the Mn concentration in (Al) in the cast state and decreasing the amount of Al_6Mn dispersoids formed during annealing (Toleuova, Dostayeva, Zharkevich, & Adilkanova, 2020; Kulikov, Aubakirov, Kvon, et al., 2019; Batessova, Omirbay, Sattarova, et al., 2023; Aubakirov, Issagulov, Akberdin, et al., 2022; Dostayeva, Yerahtina, Zholmagambetov, Medeubayev, & Zholmagambetov, 2021; Kovalyova, Yeremin, Arinova, Medvedeva, & Dostayeva, 2017; Belov, Dostaeva, Shurkin, et al., 2016). Table 1 shows comparative indicators for steels 40HNMF and 110G13L.

Steel 110G13L is suitable for rollers operating under conditions of intense abrasive wear and impact loads at moderate temperatures. It is a good choice for furnace areas with high

mechanical impact.

Steel 40HN3MF is better used for rollers that are exposed to high temperatures and require corrosion resistance and heat resistance. It is suitable for areas with stable thermal loads and moderate mechanical impacts.

Table 1. Comparative indicators for steels 40HNMF and 110G13L

Characteristic	Steel 40HNMF	Steel 110G13L
Composition (basic elements)	C (0.4%), Cr (1.0-1.5%), Ni (1.5-2.5%), Mo (0.2-0.3%), Mn	C (0.95-1.05%), Cr (11-13%), Mn
Strenth	High	Medium
Wear resistance	Medium (uncreases after treatment)	Very high
Heat resistance	High, up to 600°C	High, up to 400°C
Corrosion resistance	High (due to Ni and Mo)	Medium (less stable in aggressive environments)
Impact toughness	High	Medium
Treatability	Good	bad
Welding	Good	Complicated
Use	High temperatures, aggressive media	High mechanical loads, intense wear
Note – compiled by the authors		

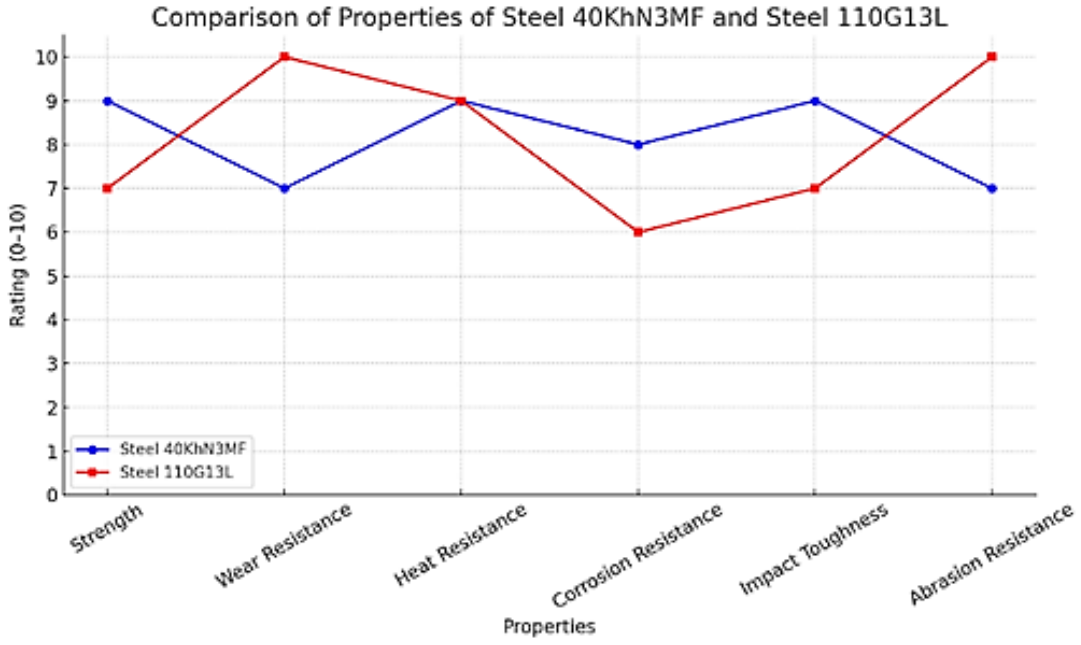

Figure 2. Comparison of steels 40HN3MF and 110G13L properties
Note – compiled by the authors

Based on the conducted monitoring and information analysis, steels of the 40HN3MF grade were determined as the object of research. Grades of this type are widely used at the plants of the Republic of Kazakhstan for producing various parts of metallurgical equipment: couplings of conveyor belts, baskets, elements of shut-off valves, as well as for furnace rollers.

The 40HN3MF grade of steel is complex-alloyed, since it contains alloying elements of different nature. The steel has a unique set of strength and ductility properties, which makes it a

promising material for the production of critical parts.

Table 2. Chemical composition of steel 40HN3MF (SS 4543-2016)

Main elements content, %					Mechanical properties		
C	Mn	Cr	Ni	Other elements	σ_B, MPa	δ, %	KC, J/cm^2
0.33-0.40	0.3-0.8	1.2-1.5	3.0-3.5	0.35-0.45 Mo 0.1-0.18	880	≥ 10	≥ 59
Note – compiled by the authors							

This steel belongs to the class of improved chromium-nickel-molybdenum steels; it is one of the best grades of structural engineering steels. Due to nickel alloying, this steel has a large reserve of toughness; the presence of molybdenum in the composition significantly reduces the tendency to temper brittleness that is typical for steels of this class. The main advantage of chromium-nickel-molybdenum steels is their high hardenability, up to sections of 80-100 mm; they provide a martensite and lower bainite structure after complete quenching in oil. This combination of properties makes this steel extremely common for producing large-sized parts that require a combination of high strength and toughness. However, the possibilities for improving the properties of steels of this class are almost exhausted. This steel is alloyed with a small amount of vanadium, which provides a fine-grained structure and some increase in strength properties compared to the 40HN2M grade. However, it should be noted that additional vanadium alloying requires additional introduction of scarce nickel to maintain toughness, which is undesirable. Thus, the use of modification-type treatment is a good alternative for improving properties compared to changing the steel composition.

One of the ways to improve the properties of this steel by developing a defect-free homogeneous structure, the combined effect of introducing nanomodifiers and inoculants was determined as an internal factor.

DISCUSSION

To conduct experimental studies and to determine the optimal steel composition, the analysis was performed using the Thermo-Calc software package. The results obtained allowed studying in detail phase transformations, thermodynamic characteristics and the effect of alloying elements on the properties of the alloy.

Phase transformations in the Fe-Si-Al ligature were studied using the Thermo-Calc software package by constructing polythermal sections for this ternary system. The con-tents of silicon in the range of 45 % and aluminum 15% were considered as variable parameters.

Figure 3 shows an example of polythermal sections for Fe-45Si-15Al alloys. The analysis of the diagrams shows that crystallization of the Fe-Si-Al alloy begins with the release of a double eutectic from the liquid phase, including crystals of silicon and the intermetallic compound FeSi2 (in the range of 49-50 at. % Si).

At the temperature of about 800°C, the intermetallic compound Al13Fe4 undergoes peritectic formation from the residual liquid phase and silicon. Subsequently, when the temperature decreases to 600°C, this intermetallic compound decomposes with the release of aluminum and the formation of the FeSi2_L phase. However, in real conditions, this transformation may not occur due to the low mobility of atoms at such temperatures.

Micro-X-ray spectral analysis of the phase composition of ferrosilicon aluminum shows that the alloy structure consists mainly of silicon grains, iron-aluminum intermetallic compounds Al13Fe4 and the iron-silicon phase FeSi2.

According to the diagrams, the Fe-45Si-15Al alloy is eutectic or near-eutectic with the melting-solidification temperature in the range of 1005-1018°C. When ferrosilicon aluminum is introduced into liquid steel, the phase transformations occur in the reverse order. However, due

to a high speed of the processes of extra-furnace treatment and crystallization of steel, these transformations may not have time to be fully realized. In particular, the intermetallic compound Al13Fe4 can be temporarily preserved in liquid steel.

If particles of this phase remain in the melt before crystallization begins, they can serve as nucleation centers for austenite grains that help to refine the structure of cast steel. This is especially true for steel cast at 1400-1450°C, where the ladle processing temperature is relatively low.

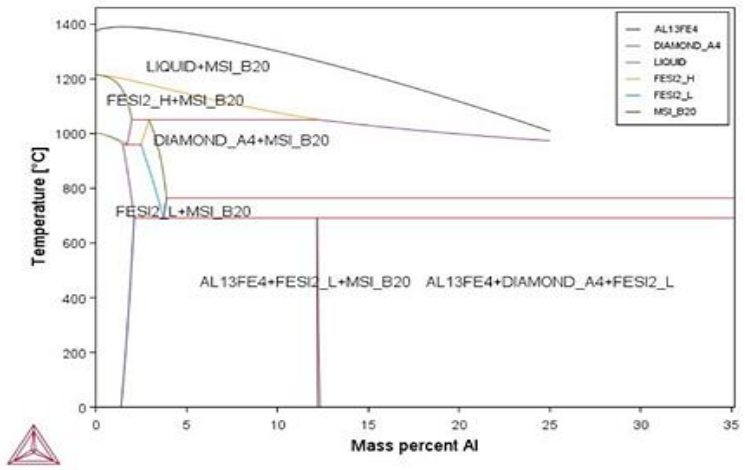

a

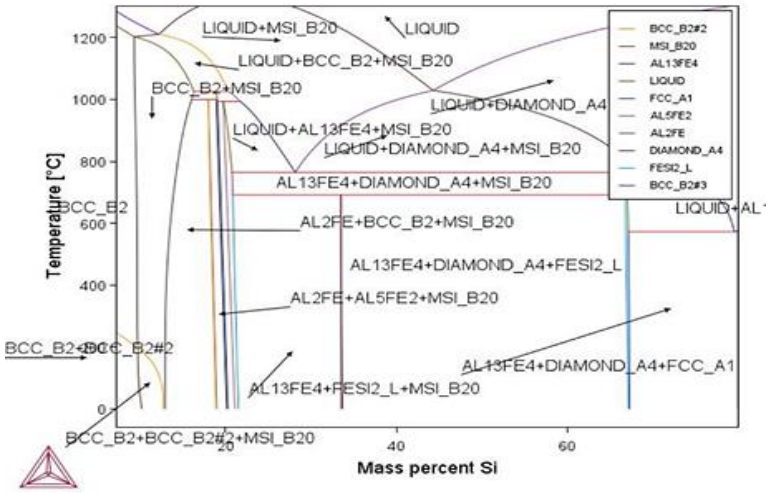

b

Figure 3. Polythermal sections for Fe-45Si-15Al alloys:
(a) With different aluminum content; (b) With different silicon contents.
Note – compiled by the authors

Left Diagram – Al-Fe-Si Based Phase Diagram

The left diagram shows the phase transformations in the Al–Fe–Si system depending on the aluminum content (mass percent Al) and temperature.

The upper region labeled LIQUID indicates the temperatures at which the alloy is completely molten.

Areas marked LIQUID + MSI_B20, LIQUID + DIAMOND_A4, etc., represent two-phase fields, where liquid metal coexists with solid phases such as:

1. MSI_B20

2. DIAMOND_A4
3. FESI2_H

The horizontal lines show invariant reactions or phase transformation temperatures, including fields where:

1. FESI2_L + MSI_B20
2. AL13FE4 + FESI2_L + MSI_B20
3. AL13FE4 + DIAMOND_A4 + MSI_B20
4. coexist.

As the aluminum concentration increases, the stability fields of intermetallic phases shift, indicating how the alloy structure changes upon solidification or during heat treatment.

Right Diagram - Si-Fe-Al Based Phase Diagram

The right diagram shows phase transformations depending on silicon content (mass percent Si) and temperature. The upper region labeled LIQUID corresponds to fully molten alloy at high Si concentrations. As temperature decreases, liquid metal coexists with solid phases:

1. MSI_B20
2. DIAMOND_A4
3. AL13FE4
4. FCC_A1
5. BCC_B2

Several two- and three-phase regions are visible, for example:

1. LIQUID + BCC_B2 + MSI_B20
2. AL13FE4 + DIAMOND_A4 + MSI_B20
3. AL2FE + AL5FE2 + FESI2_L

At lower temperatures, stable solid phases such as BCC_B2 and FCC_A1 begin to form, defining the final structure of the alloy after solidification. In general, both diagrams demonstrate how temperature affects the formation of various intermetallic compounds and how changes in aluminum or silicon content influence the melting behavior, the solidification process, and the development of stable structural phases. Together, these diagrams make it possible to evaluate the optimal alloy composition and select appropriate heat-treatment parameters to achieve the required mechanical and thermal properties for metallurgical applications, including the production of furnace rollers.

CONCLUSIONS

In the course of the study, a literature review was conducted on the technology of manufacturing metallurgical rollers and methods of improving the properties of the materials used. Based on a comparative analysis of various approaches, the most effective strategy for improving the performance characteristics of the rollers was identified.

The optimal option was recognized as ladle extra-furnace treatment of 40HN3MF steel with the addition of ferrosilicon aluminum (FeSiAl) and manganese (FeMn). This method can significantly improve the quality of steel due to deoxidation, structure modification, stabilization of the chemical composition and improvement of mechanical properties.

The choice of FeSiAl as the main deoxidizer is due to its ability to effectively bind oxygen and to prevent unwanted oxidation of the alloy. The complex composition of FeSiAl (aluminum content of 5-15% and silicon 20-50%) provides a high degree of deoxidation and improvement of the steel structure. The addition of manganese (FeMn) helps to increase the impact toughness, hardenability and heat resistance of the alloy, as well re-duces the risk of cracking during thermal cycling.

In further planned experimental studies, it is intended to investigate in more detail the parameters of ladle treatment, including the temperature range, sequence, and amount of

alloying additions. Melting of 40HN3MF steel is planned to be carried out in an induction furnace at a temperature of 1400-1500 C using a base metal charge of 230 g. During the furnace melting stage, the addition of nickel — 10.6 g and aluminum — 0.33 g is planned. After tapping the melt from the furnace, alloying and modification during secondary (ladle) treatment are planned to be performed by stepwise addition of FeCrAl — 1.92 g and FeMn – 0.64 g.

After completion of ladle treatment, the molten metal is planned to be poured into pre-prepared and preheated molds made of a sand–polymer mixture, followed by cooling at room temperature. It is anticipated that separating alloying between the furnace and ladle stages will allow for more precise control of the chemical composition, improved metal homogeneity, and enhanced stability of steel structure modification.

The use of the selected treatment method helps to increase the service life of metallurgical rollers operating under conditions of high temperatures, intense mechanical loads and abrasive wear. Further studies are planned to include a detailed study of the effect of out-of-furnace treatment modes on steel characteristics, as well as experimental testing of the obtained material under conditions close to real operation. After heat treatment, ladle treatment is carried out using a mold made from a sand-polymer mixture. This material was chosen for its strength, density, porosity, and good technological properties such as flowability, gas permeability, and moldability, which ensure casting accuracy and mold durability.

CONFLICT OF INTEREST: The authors declare that they have no conflict of interest.

FUNDING: The work was carried out within the framework of the implementation of the IRN Program BR24993020 “Developing and implementing the technology of producing complex-alloyed steels with a homogeneous defect-free structure due to the synergy of external and internal effects on the melt” (agreement with the Committee of Science of the Ministry of Education and Science of the Republic of Kazakhstan No. 363-PTsF-24-26 dated october 01, 2024), funded by the Ministry of Science and Higher Education of the Republic of Kazakhstan. Additionally, the research was supported by the project AP26103581 “Development and research of a cost-effective technology for manufacturing precision castings in sand-resin molds obtained using variable static pressure”.

REFERENCES

Likholobov, E. Yu. (2012). Improving the quality of high-manganese steel castings by improving the process of melting and out-of-furnace treatment. Moscow, pp. 3–4.

Zatulovsky, S. S. (1989). Suspension casting. Kyiv: Naukova Dumka, 260 p.

Morton, D. O., & Bryant, M. D. (1979). Inoculation techniques for cast iron. British Foundryman, 183–186.

Grigorenko, G. M., Kostin, V. A., Golovko, V. V., et al. (2015). The effect of nanopowder inoculators on the structure and properties of cast metal of high-strength low-alloy steels. General Issues of Metallurgy, (2), 32–41.

Petrova, V. F. (2006). Study of the influence of inoculators on the structural parameters of cast metal and service properties of forged products of heavy engineering (Doctoral dissertation). Volgograd.

Harvey, J. N., & Noble, G. A. (2007). Inoculation of cast irons. In Proceedings of the 55th Indian Foundry Congress.

Scaland, T. (2001). Inoculation and solidification studies. Modern Casting, (6), 158–160.

Vladimirov, N. F., & Golubev, A. A. (1999). Development of production technology of sheet hull steels. Issues of Materials Science, 3(20).

Orlov, V. V., Malyshevsky, V. A., Khlusova, E. A., & Golosienko, S. A. (2014). Development of structural steels for marine equipment and main pipelines intended for operation in the

Arctic. Steel, (9), 79–88.

Kovalev, P. V., Ryaboshuk, S. V., Issagulov, A. Z., Sultamurat, G. I., & Jironkin, M. V. (2016). Improving production technology of tube steel grades in converter process. Metalurgija, 55(4), 715–718.

Russian Federation. (2009). Wear-resistant cast iron composition (Patent No. 2345160).

Russian Federation. (2009). Wear-resistant cast iron composition (Patent No. 2347839).

USSR. (1971). Wear-resistant cast iron composition (Author's Certificate No. 309971).

Gulyaev, A. P. (2001). Metal science. Moscow: Metallurgy.

Issagulov, A. Z., Kvon, S. S., & Kulikov, V. Yu. (2019). Increasing the wear resistance of 30H3MF steel by additional alloying. In Proceedings of the XXIII International Scientific and Production Conference "Innovative Solutions in Agricultural Science – A Look into the Future" (pp. 80–82). Maisky, Russia.

Goldstein, M. N., Grachev, S. V., & Veksler, Yu. G. (1989). Special steels. Moscow: Metallurgy.

Perelygin, V. (2008). Hardox: Let's sort it out calmly. Fixed Assets, (12).

New high-strength weldable wear-resistant steel with a tensile strength of at least 1050 N/mm². (2005). Metallurgist, (1), 51–54.

Duzcukohfu, H. (2015). Effect of boron addition on mechanical properties of 60SiCr7 steel. International Journal of Materials, Mechanics and Manufacturing, 3(2).

Issagulov, A. Z., Ibatov, M. K., Kvon, S. S., & Arinova, S. K. (2019). Studying the properties and microstructure of 30CrMnV9 steel on wear resistance. Metalurgija, 58(3–4), 326–328.

Toleuova, A. R., Dostayeva, A. M., Zharkevich, O. M., & Adilkanova, M. A. (2020). Calculating and experimental studying of phase transformations in Al–Zr–Fe–Si system alloys. Metalurgija, 59(4), 543–546.

Kulikov, V. Y., Aubakirov, D. R., Kvon, S. S., et al. (2019). Use of wear-resistant materials in the Kazakhstani metallurgical industry. Metallurgist, 62, 1068–1072.

https://doi.org/10.1007/s11015-019-00755-5

Batessova, F., Omirbay, S., Sattarova, A., Zholmagambetov, N., Zholmagambetov, S., Dostayeva, A., Suleimenov, N., & Medeubayev, N. (2023). Reducing industrial noise by the use of damping alloys when manufacturing mining equipment parts. Heliyon, 9(6), e17152.

https://doi.org/10.1016/j.heliyon.2023.e17152

Aubakirov, D. R., Issagulov, A. Z., Akberdin, A. A., Kvon, S. S., Kulikov, V. Y., Arinova, S. K., Dostayeva, A. M., Shcherbakova, Ye. P., Sarkenov, B. B., & Narembekova, A. K. (2022). Influence of boron- and barium-containing modifiers on the structure of low-chromium cast iron. Heliyon, 8(11), e11496.

https://doi.org/10.1016/j.heliyon.2022.e11496

Dostayeva, A. M., Yerahtina, I. I., Zholmagambetov, N. R., Medeubayev, N. A., & Zholmagambetov, S. R. (2021). Investigation of aluminum–titanium alloys production and labor safety in metal smelting process. Metalurgija, 60(3–4), 403–406.

Kovalyova, T., Yeremin, E., Arinova, S., Medvedeva, I., & Dostayeva, A. (2017). Enhancing surface roughness of castings when sand–resin mold casting. Metalurgija, 56(1–2), 135–138.

Belov, N. A., Dostaeva, A. M., Shurkin, P. K., et al. (2016). Influence of annealing on electrical resistance and hardness of hot-rolled aluminum alloy sheets containing up to 0.5% Zr. Russian Journal of Non-Ferrous Metals, 57, 429–435.

https://doi.org/10.3103/S1067821216050035

Information about authors

Ardak Dostayeva – professor, Abylkas Saginov Karaganda Technical University, Karaganda, Kazakhstan
E-mail: a.dostayeva@ktu.edu.kz
ORCID: https://orcid.org/0000-0002-1982-2368

Aristotel Issagulov – Doctor of Technical Sciences, professor, Abylkas Saginov Karaganda Technical University, Karaganda, Kazakhstan.
E-mail: a.issagulov@ktu.edu.kz
ORCID: https://orcid.org/0000-0003-2174-9072

Mirhat Abdrahmanov – M.Eng., Abylkas Saginov Karaganda Technical University, Karaganda, Kazakhstan.
E-mail: m.abdrakhmanov@ktu.edu.kz
ORCID: https://orcid.org/0000-0003-3915-3293

Aigerim Zhalel – doctoral student., Abylkas Saginov Karaganda Technical University, Karaganda, Kazakhstan.
E-mail: a.zhalel@ktu.edu.kz
ORCID: https://orcid.org/0009-0000-8178-9602

Ainagul Toleuova – PhD ass. professor, Abylkas Saginov Karaganda Technical University, Karaganda, Kazakhstan
E-mail: a.toleuova@ktu.edu.kz
ORCID: https://orcid.org/0000-0002-3216-1824

Vol. 1, Issue 1, March 2026.

CENTRAL ASIAN TRANSACTIONS ON MATERIALS STRUCTURE AND PROPERTIES

https://doi.org/10.51885/3134-7983_CATMSP_2026_1_4
SRSTI 31.15.31

ANALYSIS OF THE EFFECTIVENESS OF THE USE OF LIQUID DEICING REAGENTS TO REDUCE THE FREEZING FORCE OF ICE FORMATIONS ABOVE THE ROAD SURFACE

Zhuldyz Zhamigazina [1]*, **Saniya Kiyalbay** [1]
[1]L.B. Goncharov Kazakh Automobile and Road Institute, Almaty, Kazakhstan
*Corresponding author: Zhuldyz Zhamigazina, ZhZhamigazina@gmail.com

Keywords:
snow and ice formation, deicing reagents, bischofite, concentration of liquid deicing solutions, coefficient of adhesion, density of snow and ice formation, climatic conditions of Kazakhstan, winter content.

ABSTRACT

One of the key problems of winter maintenance of highways in Central Asia and Kazakhstan remains the inefficiency of traditional methods of dealing with snow and ice in conditions of variable temperature and high humidity. In particular, various types of snow and ice formations are observed on a number of sections of the road network, which cannot be removed mechanically without damaging the coating. In this regard, there was a need to evaluate the effectiveness of the use of deicing reagents in liquid form. The article presents the results of experimental studies conducted by the authors on sections of the Almaty - Ust–Kamenogorsk highway and on the entrance roads to Almaty and Ust-Kamenogorsk. The physico-mechanical characteristics of snow and ice rolling and the effectiveness of anti-icing solutions based on bischofite (MgCl2·6H2O) with concentrations of 5, 10, 15 and 18% were studied. Field measurements were carried out with an interval of 10 minutes, recording changes in the coefficient of adhesion. Correlations have been established between the concentration of the reagent, the time of action and the adhesion parameters, as well as the distribution rates of solutions depending on the density and thickness of the ice.

INTRODUCTION

The winter period is the most unfavorable in terms of ensuring continuous and safe transport operation. The unevenness of roads due to untimely snow removal and the reduction of the coefficient of adhesion lead to an increase in braking distance and, consequently, to a higher risk of loss of vehicle control. The probability of road traffic accidents on pavements fully or partially covered with snow or ice is 4.5 and 1.5 times higher, respectively, compared to clean dry pavements. Considering that winter slipperiness resulting from icing of road surfaces occupies a significant part of the road operation period, ensuring proper quality of road maintenance is one of the priority tasks of road operating services.

Within the territory of the Republic of Kazakhstan, there are a considerable number of road sections where the use of specialized equipment for removing snow and ice deposits is limited due to technical reasons. Moreover, under conditions of long-term pavement operation, the effectiveness of alternative methods for combating ice has not been sufficiently supported by empirical data and requires additional scientific justification.

Currently, many methods for combating snow accumulation and slipperiness on highways

are known. The use of chemical deicing reagents is considered the most economically reasonable and effective way to eliminate snow and ice formations. The application of friction materials such as sand and waste provides only short-term improvement in pavement adhesion (within 1–1.5 hours), after which their effectiveness decreases significantly. Similarly, the use of solid chemical reagents yields insufficient results due to their limited active duration.

For the climatic conditions of the Republic of Kazakhstan, characterized by a long winter period and variable weather conditions (alternation of daytime thawing and nighttime freezing), the use of liquid deicing reagents (VN RK 6.1-001-2024, 2024) represents an optimal solution. However, this technology has not yet become widespread. On the one hand, this is due to the lack of comprehensive scientific studies confirming the effectiveness of liquid reagents under conditions of frequent alternation of thawing and freezing, which promotes the formation of dense and hard-to-remove ice. On the other hand, there are no methodological recommendations for applying this technology under specific climatic and road-operating conditions, and the material and technical base remains insufficiently developed, including the lack of specialized equipment for distributing liquid reagents as well as facilities for their preparation and storage.

In this regard, within the framework of this study, it is planned to conduct a field analysis of the application of liquid reagents on various sections of highways in order to assess their effectiveness under snow and ice conditions typical for Kazakhstan.

MATERIALS AND METHODS

In 2022, based on the considerations outlined above, field experimental studies were conducted by researchers from the Kazakh Automobile and Road Institute (KazARI) and D. Serikbayev East Kazakhstan Technical University (EKSTU) to determine the effect of chemical deicing reagents on the destruction of snow–ice formations. The study was carried out on sections of the Almaty–Ust-Kamenogorsk highway, as well as on entrance roads to Almaty (from the Kaskelen direction via the upper highway) and to Ust-Kamenogorsk.

One of the main reasons for conducting field tests was the presence of road sections where traditional mechanical methods for removing snow–ice compaction were ineffective. In particular, in a number of locations the pavement was characterized by the presence of a thin but very strong ice layer, the mechanical removal of which led to damage to the asphalt concrete surface when using available equipment. As a result, such sections remained covered with ice, creating a high accident risk.

Under these conditions, it was hypothesized that complete removal of snow–ice compaction could be achieved through the application of liquid chemical deicing reagents. It was assumed that liquid reagents would not only facilitate the melting of ice and effectively disrupt its structure, but would also remain on the pavement surface and perform a preventive function by inhibiting the re-formation of ice. This is particularly relevant for the variable winter climate typical of Kazakhstan, where daytime solar radiation causes partial melting of ice, followed by nighttime refreezing into an even denser and more slippery layer.

The objective of the experimental study was to evaluate the effectiveness of liquid deicing reagents in combating winter slipperiness on the most hazardous road sections, as well as to determine optimal application conditions, including solution concentration, distribution method, and duration of action.

RESULTS AND DISCUSSION

In East Kazakhstan, experimental studies were conducted on two sections of the Almaty–Ust-Kamenogorsk highway. Site No. 1 (Figure 1a), located at the entrance to Ust-Kamenogorsk at km 1820, was investigated on March 2, 2022, from 12:00 to 18:30 under wind speeds of 10–12 m/s and air temperatures of minus 10 to minus 12 °C. The thickness of the snow–ice compaction

on the pavement ranged from 1.5 to 6 cm, with a density of 0.3–0.6 t/m³.

At Site No. 2 (km 1120, Figure 1b), studies were carried out on March 18, 2022, from 12:00 to 19:30 under clear, calm weather conditions with an air temperature of minus 6 to minus 8 °C and relative humidity of 71.8%. The thickness of the snow–ice layer on the pavement ranged from 2 to 11 cm, with a density of 0.1–0.22 t/m³. The average daily traffic volume at both sites was 2 887 vehicles per day.

The transport and operational characteristics of the studied sites differed significantly from each other. At the first site, partial melting of the snow–ice formation was observed on the pavement surface, which considerably deteriorated road conditions and hindered vehicle movement. After the application of the deicing solution, the snow–ice compaction completely melted within 1.0–1.2 hours, as shown in Figure 1b.

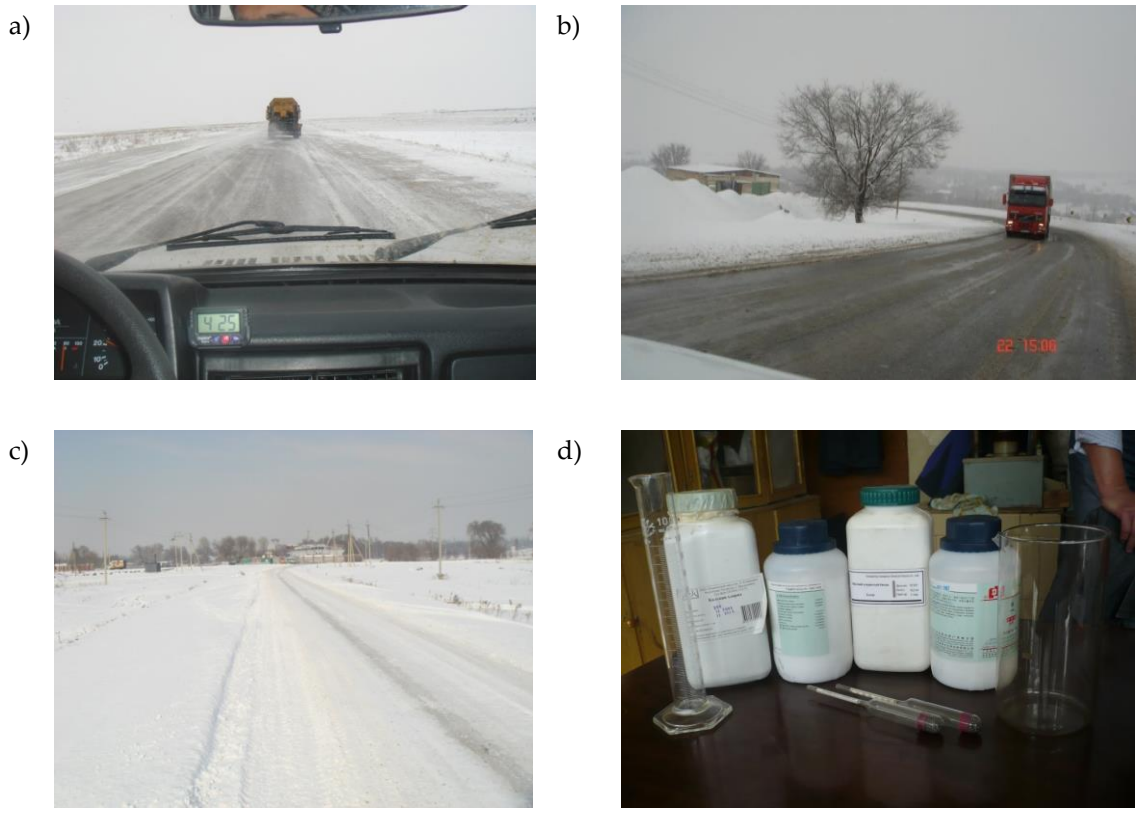

Figure 1. General view of the studied sites: (a) Site No. 1 on the Almaty–Ust-Kamenogorsk highway; (b) Site No. 2 at the same location; (c) entrance road to Almaty (upper highway "Almaty–Kaskelen"); (d) tested deicing reagents and hydrometers used for density determination.
Note – prepared by the authors.

In addition, on some sections of this road, the formation of melted snow crusts and wheel tracks on the surface of the snow–ice layer due to solar radiation was observed (Figure 1), which is typical for roads with high traffic intensity.

Similar studies were conducted on the entrance roads to Almaty. As an experimental site, the entrance to Almaty between Almaty and Kaskelen (upper highway) was selected. Field tests were carried out on February 11, 2022, from 12:00 to 18:00. At Site No. 3, the studies were conducted at air temperatures of minus 5 to minus 8 °C and relative humidity of 86%. The daytime traffic volume at this site did not exceed 560 vehicles per day. The thickness of the dry

snow layer ranged from 2.6 to 8 cm, while its density did not exceed 0.38 t/m³.

Methodology for preparing liquid chemical solutions for field tests. To conduct experimental tests and determine the concentration and distribution rate of liquid reagents, a universal spreader manufactured by Renault was used (Figure 2a). The slipperiness of the pavement was measured using a portable IKSp device (Figure 2b).

a) b)

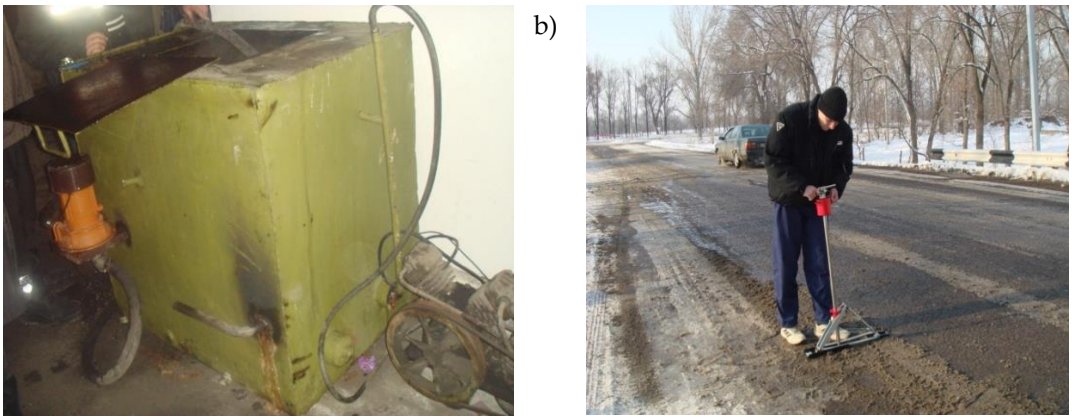

Figure 2. Preparation of liquid deicing reagents for field tests: (a) installation for preparing deicing solution; (b) process of measuring the coefficient of adhesion using the IKSp device.
Note – prepared by the authors

The mixing of the solution used as a deicing material was carried out in a stationary mixing unit (Figure 2a). Its design consisted of an electric pump, a tank for preparing the liquid solution (Ve = 0.75 m³), a hose for supplying compressed air, and a compressor. During solution preparation, the water in the tank was preheated to the boiling point (+100 °C). This increased the dissolution efficiency of the chemical reagents and significantly reduced their dissolution time (PR RK 218-64-2007, 2008).

Under laboratory conditions, three types of chloride salts were tested: sodium chloride (NaCl), calcium chloride ($CaCl_2$), and bischofite ($MgCl_2 \cdot 6H_2O$), and their concentrations were determined (Table 2). During field tests, only bischofite ($MgCl_2 \cdot 6H_2O$) and the deicing solution prepared from this reagent were used. The solution was prepared in four concentrations: 5%, 10%, 15%, and 18%. Bischofite was selected as the primary deicing material (Figure 1d).

Table 1. Selection of chemical solution concentrations

Concentration of sodium chloride solution			Concentration of calcium chloride solution			Concentration of bischofite solution		
Solution density, t/m³	NaCl content in 100 g of solution, g	Freezing temperature, °C	Solution density, t/m³	NaCl content in 100 g of solution, g	Freezing temperature, °C	Solution density, t/m³	NaCl content in 100 g of solution, g	Freezing temperature, °C
1	2	3	4	5	6	7	8	9
1.04	5.6	-3.5	1.04	4.8	-2.4	1.04	5.2	-3.56
1.05	7.0	-4.4	1.05	5.9	-3.0	1.05	6.4	-5.25
1.06	8.3	-5.4	1.06	7.1	-3.7	1.06	7.8	-6.40
1.07	9.6	-6.4	1.07	8.3	-4.4	1.07	9.0	-7.38

End of table 1

1	2	3	4	5	6	7	8	9
1.08	11.0	-7.5	1.08	9.4	-5.2	1.08	10.1	-8.28
1.09	12.2	-8.6	1.09	10.5	-6.1	1.09	11.1	-9.10
1.10	13.6	-9.8	1.10	11.5	-7.1	1.10	11.5	-10.00
1.11	14.9	-11.0	1.11	12.6	-8.1	1.11	12.1	-12.90
1.12	16.2	-12.2	1.12	13.7	-9.1	1.12	12.8	-14.20
1.13	17.5	-13.6	1.13	14.7	-10.2	1.13	13.5	-16.10
1.14	18.0	-15.1	1.14	15.8	-11.4	1.14	14.5	-18.70
1.15	20.0	-16.0	1.15	16.8	-12.7	1.15	15.6	-20.30
1.16	21.2	-18.2	1.16	17.8	-14.2	1.16	16.7	-22.10
1.17	22.4	-20.0	1.17	18.9	-15.7	1.17	17.8	-24.50
1.175	23.1	-21.2	1.18	19.9	-17.4	1.18	18.5	-26.80
			1.19	20.9	-19.2	1.19	19.6	-29.20
			1.20	21.9	-21.2	1.20	20.5	-31.20
			1.21	22.8	-23.3	1.21	21.4	-33.40
			1.22	23.8	-25.7	1.22	22.1	-35.50
			1.23	24.7	-28.3			
			1.24	25.7	-31.2			
			1.25	26.6	-34.6			
			1.26	27.5	-38.6			
			1.27	28.4	-43.6			
			1.28	29.4	-50.1			

Note – the dissolution time of chemical reagents depends on the temperature of water heating

Note – compiled by the authors

Table 2. Results of slipperiness measurements at 5-minute intervals

Time, min	Solution concentration, %			
	5	10	15	18
1	2	3	4	5
0	0.09	0.09	0.09	0.09
5	0.10	0.11	0.13	0.14
10	0.12	0.14	0.17	0.19
15	0.14	0.15	0.19	0.21
20	0.15	0.17	0.21	0.23
25	0.17	0.19	0.24	0.25
30	0.19	0.22	0.27	0.28
35	0.21	0.24	0.30	0.34
40	0.22	0.27	0.34	0.37
45	0.24	0.29	0.38	0.40
50	0.27	0.33	0.41	0.44
55	0.29	0.35	0.44	0.48
60	0.31	0.38	0.46	0.52
65	0.34	0.43	0.49	0.56
70	0.36	0.47	0.54	0.61
75	0.39	0.51	0.58	0.63
80	0.41	0.54	0.63	0.68

Note – compiled by the authors

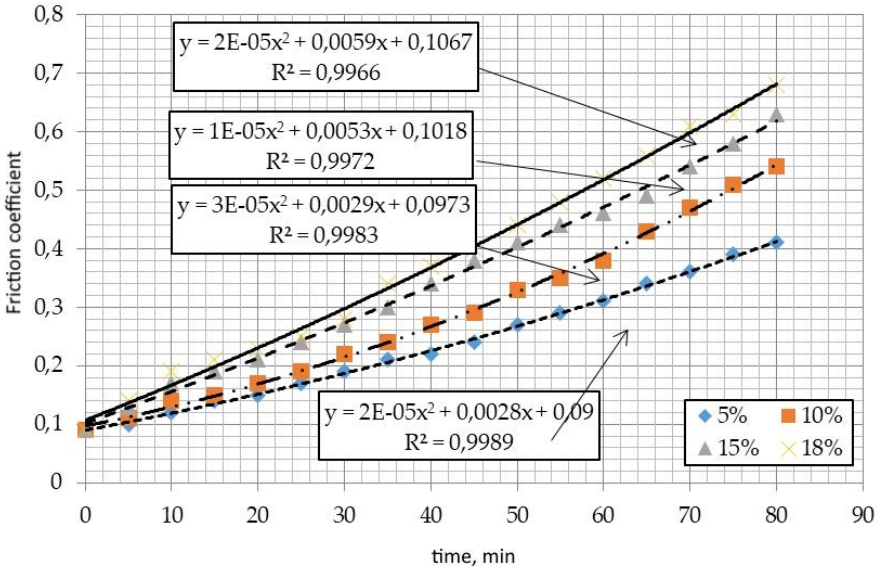

Figure 3. Correlation between the duration of solution action and the coefficient of adhesion of road pavements depending on reagent concentration

Note – prepared by the authors

Figure 3 presents the results of field tests aimed at determining the effective duration of action of a deicing solution based on bischofite. As can be seen from the curves, the effectiveness of the solution increases over time with higher concentrations. At low concentrations, the snow–ice compaction cannot be completely melted; consequently, the coefficient of adhesion does not exceed 0.41. The main reason is that at air temperatures below minus 8 °C, solutions of low concentration (5–7%) are not sufficiently effective.

Regulation of deicing reagent distribution rates and assessment of pavement slipperiness under field conditions. At the experimental sites, chemical reagents were applied using an emergency method, i.e., directly onto the snow–ice layer. The distribution rates were adopted in accordance with calculated data: for solid reagents, the maximum rate was 350 g/m² and the minimum was 90 g/m²; for liquid reagents, the maximum rate was 450 mL/m² and the minimum was 60 mL/m².

As noted above, the distribution of liquid chemical reagents was carried out using a universal spreader manufactured by Renault, provided by the East Kazakhstan branch of JSC "KazAvtoZhol".

Technology for distributing liquid deicing reagents. In this universal spreader, the distribution of reagents was regulated by: a) an external shutter (Figure 4a); b) an onboard computer controlling the material spreading width (Figure 4b); c) adjusting the operating speed of the vehicle.

Processing of field test results.

Considering the variability of numerous factors affecting the value of the coefficient of adhesion (thickness, density, hardness of snow–ice formations, etc.), it is reasonable to apply a sampling method for its evaluation, even under approximately similar pavement conditions. The sampling method consists of determining generalized characteristics of a population not by measuring all its elements, but by examining only a representative part selected randomly. The applicability of this method is based on the law of large numbers. According to this law, as demonstrated by M.A. Chebyshev's theorem (Khovanskii, 2013), with a sufficiently large number of observations, the sample mean of a measured parameter approaches its mathematical expectation.

a) b)

Figure 4. Regulation of chemical reagent distribution rates using (a) the external shutter of the spreader and (b) the onboard computer.
Note – prepared by the authors.

The sample size n (number of measurements) depends on the required confidence level. In engineering practice, a confidence level of $P = 0.95$ is commonly adopted (less frequently 0.997). For a very large population, the required sample size is determined by the expression given in VN RK 6.1-001-2024 (2024).

$$\sigma = \frac{t^2 \cdot \sigma^2}{\Delta^2}, \quad (1)$$

where t is a parameter characterizing the confidence level, i.e., the probability that the deviation does not exceed Δ^2, which equals $t = 2$ for a confidence level of $P = 0.95$ and $t = 3$ for $P = 0.997$.

Pavement slipperiness is evaluated as follows (VN RK 6.1-001-2024, 2024):

$$K_{ck} = \frac{\varphi_{fact}}{\varphi_{allow}}, \quad (2)$$

where: φ_{fact} is the actual value of the coefficient of adhesion; φ_{allow} is the permissible value of the coefficient of adhesion, equal to $\varphi_{allow} = 0.28$ under winter slipperiness conditions and $\varphi_{allow} = 0.40$ during the dry season.

For a comprehensive evaluation of the performance of bischofite solution ($MgCl_2 \cdot 6H_2O$) (Table 3, column 4), its characteristics were compared with those of traditionally used deicing reagents — sodium chloride NaCl (Table 3, column 2) and calcium chloride $CaCl_2$ (Table 3, column 3). The comparison was carried out under identical laboratory and field conditions, with equal application rates and temperature regimes. The analysis included key indicators such as: solution freezing temperature, duration of action, pavement adhesion coefficient after treatment, braking distance, and residual effect in preventing secondary ice formation.

Table 3. Results of comparative analysis of deicing reagents

Indicator	NaCl (15%)	$CaCl_2$ (15%)	$MgCl_2 \cdot 6H_2O$ (15%)
Freezing temperature, °C	–13.6	–10.2	–16.1
Increase in adhesion (after 60 min)	0.38	0.36	0.46
Duration of action, min	up to 90	up to 120	up to 160
Reduction of braking distance, %	12 %	16 %	23 %
Braking distance on ice (at 50 km/h)	28 m	26 m	21,5 m
Residual effect (prevention of secondary icing)	weak	moderate	distinct
Note – compiled by the authors			

The bischofite-based deicing reagent ($MgCl_2 \cdot 6H_2O$) has a number of operational advantages that enable its effective use under the climatic conditions of Kazakhstan. Due to its low crystallization temperature (down to −16.1 °C at a 15% concentration), the solution remains active even under sustained frost conditions. One of its key advantages is a pronounced residual effect: after application, the reagent remains on the pavement surface for a long time, preventing the re-freezing of ice.

At low concentrations of deicing solution (5–7% and below), their action is insufficient to fully disrupt the structure of the snow–ice layer; as a result, the pavement adhesion coefficient does not exceed 0.41. The main reason is that at air temperatures below −8 °C, low-concentration solutions (5–7%) are not effective enough.

CONCLUSIONS

The destruction of the snow–ice structure is strongly influenced by both the concentration of the solution and the duration of the interaction between the snow–ice formation and the chemical reagent. For example, a solution prepared at a 5% concentration increases adhesion from 0.10 to 0.23 within 80 minutes, whereas a 15% solution increases it from 0.10 to 0.41 over the same period. Moreover, this performance indicator depends not only on the solution concentration but also on the density of the snow–ice formation.

After the structure of the snow–ice layer is disrupted, it is necessary to clear the road of melted snow. Typically, the melted snow is in a liquefied state, as shown in Figure 1b.

Field tests demonstrated that, in terms of braking distance reduction, bischofite outperforms traditional NaCl- and $CaCl_2$-based reagents by 20–25%. At the same time, it enables an increase in the adhesion coefficient to 0.46 and above, which corresponds to safe operating conditions for roads in winter.

The use of bischofite solutions is recommended under the following conditions:

- Road conditions**:** compacted snow–ice layer, glazed ice, variable temperatures (thaw–freeze cycles), and high air humidity;
- Road sections**:** bridges, steep ascents and descents, intersections, accident-prone zones, and high-traffic urban areas;
- Application mode**:** emergency and preventive treatment of the pavement prior to expected precipitation or a sharp drop in temperature.

CONFLICT OF INTEREST: The authors declare that there is no conflict of interest.

DECLARATION ON THE USE OF ARTIFICIAL INTELLIGENCE TECHNOLOGIES: The authors did not use artificial intelligence (AI) tools at any stage of preparing this scientific article.

REFERENCES

Kiyalbaev, A., Kiyalbay, S., Tolkynbaev, T., & Tleulenova, G. (2022). Theoretical model for anchoring a particle of preheated sand into an ice formation. *International Journal of GEOMATE, 23*(96), 112–120. https://geomatejournal.com/geomate/article/view/3333/2922 (In Eng.)

New friction measuring device – for driving winter. (2000). *Nordic Road and Transport Research, 2*, 11–12. https://trid.trb.org/View/687131 (In Eng.)

Omirzak, Y., Espayeva, G., Kiyalbayev, A., Kiyalbay, S., & Sagybekova, A. (2024). Snow pressure zoning for road safety: Snow mechanical characteristics and climatic factors. *EVERGREEN Joint Journal of Novel Carbon Resource Sciences & Green Asia Strategy, 11*(3), 1602–1612. https://www.tj.kyushu-u.ac.jp/evergreen/contents/EG2024-11_3_content/pdf/p1602-1612.pdf (In Eng.)

Rosenberg, A.M., Gaidis, J.M., Kossivas, T.G., & Previte, R.W. (1977). A corrosion inhibitor formulated with calcium nitrite for use in reinforced concrete. *ASTM STR – 629*, 89–99. https://trid.trb.org/View/72000 (In Eng.)

Борисюк, Н.В. (2019). Зимнее содержание городских дорог: учебное пособие. М.: Инфра-Инженерия. / Borisyuk, N.V. Zimnee soderzhanie gorodskikh dorog: uchebnoe posobie [Winter maintenance of urban roads: textbook] (In Russ.) https://znanium.ru/catalog/document?id=346684

ВН РК 6.1-001-2024. (2024). Ведомственный норматив. Зимнее содержание автомобильных дорог общего пользования. Астана: Минтранском РК. / VN RK 6.1-001-2024. Vedomstvennyi normativ. Zimnee soderzhanie avtomobil'nykh dorog obshchego pol'zovaniya [Departmental standard. Winter maintenance of public roads] (In Russ.) https://online.zakon.kz/Document/?doc_id=39626184

РГП «Казгидромет». (2021). Ежегодный бюллетень мониторинга состояния и изменения климата Казахстана: 2020 год. Нур-Султан: РГП «Казгидромет». / RGP «Kazgidromet». Ezhegodnyi byulleten' monitoringa sostoyaniya i izmeneniya klimata Kazakhstana: 2020 god [Annual bulletin of monitoring the state and climate change of Kazakhstan: 2020] (In Russ.) https://www.kazhydromet.kz/ru/klimat/ezhegodnyy-byulleten-monitoringa-sostoyaniya-i-izmeneniya-klimata-kazahstana

Киялбаев, А.К., Киялбай, С.Н., Еспаева, Г.А., & Маданбеков, Н.Ж. (2023). Теоретические и экспериментальные методы транспортного строительства. Учебник. Часть 1. Дорожные условия и основы дорожной теплотехники. Алматы–Бишкек: ADAL KITAP. / Kiyalbaev, A.K., Kiyalbai, S.N., Espaeva, G.A., Madanbekov, N.Zh. Teoreticheskie i eksperimental'nye metody transportnogo stroitel'stva. Uchebnik. Chast' 1. Dorozhnye usloviya i osnovy dorozhnoi teplotekhniki [Theoretical and experimental methods of transport construction. Textbook. Part 1. Road conditions and basics of road thermal engineering] (In Russ.) https://ebsadal.kz/book/249/en

Кингери, У.Д. (1996). *Лед* и снег. М.: Мир. / Kingeri, U.D. Led i sneg [Ice and snow] (In Russ.) https://www.rassep.ru/academy/perevodnye-knigi/?sortBy=name&orderBy=asc,nulls&PAGEN_1=157

Гидрометреоиздат. (2019). Метрологический справочник по климатическим условиям Казахстана. Ежегодник. Алматы: Гидрометреоиздат. / Gidrometreozidat. Metrologicheskii spravochnik po klimaticheskim usloviyam Kazakhstana. Ezhegodnik [Metrological handbook on climatic conditions of Kazakhstan. Yearbook] (In Russ.) https://www.kazhydromet.kz/ru/klimat/ezhegodnyy-byulleten-monitoringa-sostoyaniya-i-izmeneniya-klimata-kazahstana

Дорожный учебно-инженерный центр. (1995). Методы зимнего содержания дорог в Финляндии. Санкт-Петербург–Павловск. / Dorozhnyi uchebno-inzhenernyi tsentr. Metody zimnego soderzhaniya dorog v Finlyandii [Methods of winter road maintenance in Finland] (In Russ.)

Минтранском РК. (2008). ПР РК 218-64-2007 Инструкция по борьбе с зимней скользкостью на автомобильных дорогах общего пользования. Астана: Минтранском РК. / PR RK 218-64-2007 Instruktsiya po bor'be s zimnei skol'zkost'yu na avtomobil'nykh dorogakh obshchego pol'zovaniya [Instruction on combating winter slipperiness on public roads] (In Russ.) https://adilet.zan.kz/rus/docs/E17000178AD

Грей, Д.М., & Мейл, Д.Х. (1986). Снег: справочник. *Л.*: Гидрометеоиздат. / Greya, D.M., & Meila, D.Kh. Sneg: spravochnik [Snow: Handbook] (In Russ.) https://www.amazon.-ca/Handbook-Snow-Principles-Processes-Management/dp/1932846069#

Хованский, А.Г. (2013). Полиномы Чебышёва и их обращения. Математическое просвещение, 17, 93–106. / Khovanskii, A.G. Polinomy Chebysheva i ikh obrashcheniya

[Chebyshev polynomials and their inverses] (In Russ.) https://www.mathnet.ru-/links/bf7e6ec405b028c297bcb8218e869946/mp272.pdf

Gufo.me. (n.d.). Glaciology dictionary online resource. [Online]. (In Eng.) https://gufo.me/dict/glaciology

Information about authors

Zhuldyz Zhamigazina – is a PhD student at L.B. Goncharov Kazakh Automobile and Road Institute, Almaty, Kazakhstan.
Her research interests are related to road engineering, transport infrastructure, and materials for transport construction.
e-mail: ZhZhamigazina@gmail.com,
ORCID: https://orcid.org/0009-0005-7616-1630

Saniya Kiyalbay – received her Candidate of Technical Sciences degree in 05.23.11 — Design and Construction of Roads, Metros, Airfields, Bridges and Transport Tunnels. She is currently an Associate Professor at L.B. Goncharov Kazakh Automobile and Road Institute named after, Almaty, Kazakhstan. Her research interests include operation of highways, transport planning, and development of intelligent systems for predicting landslide processes and their impact on technical and operational characteristics of roads in mountainous areas.
e-mail: sanina8@mail.ru,
ORCID: https://orcid.org/0000-0003-3880-2773,

CENTRAL ASIAN TRANSACTIONS ON MATERIALS STRUCTURE AND PROPERTIES

https://doi.org/10.51885/3134-7983_CATMSP_2026_1_5
SRSTI 53.31.21

MICROSTRUCTURAL CHARACTERIZATION OF LOW-GRADE RAW MATERIALS FOR CHROMIUM-MANGANESE LIGATURE SMELTING

Sultan Kabylkanov[1,2]*, **Saule Abdulina**[1], **Yerbolat Makhambetov**[2], **Yucel Onuralp**[3]
[1]D. Serikbaev East Kazakhstan Technical University, Ust-Kamenogorsk, Kazakhstan
[2]Chemical-Metallurgical Institute, Karaganda, Kazakhstan
[3]Istanbul Technical University, Istanbul, Turkey
*Corresponding author: Sultan Kabylkanov, e-mail: kabylkanov.s@edu.ektu.kz

Keywords:
steel, ferrochrome, ferromanganese, chromium-manganese ligature, alloying process, phase analysis, microstructural analysis.

ABSTRACT

This article examines the mineralogical and structural features of chromite ore from the Kempirsai deposit and iron-manganese ore from the Kerege-Tas deposit. The relevance of the study is determined by the need to assess the suitability of these complex, multicomponent ores for metallurgical processing. The aim of the research is to conduct a comprehensive analysis of the morphology, mineral phases, and elemental composition of the ore samples using modern methods. Scanning electron microscopy (SEM) was applied to characterize the surface structure of the samples, while energy-dispersive spectroscopy (EDS) was used to determine the distribution and relative concentrations of elements. The results revealed the predominance of chromite in the chromite ore and Mn and Fe minerals in the iron-manganese ore, as well as their close association with silicate and oxide phases. The findings are fully consistent with the results of chemical analysis and X-ray diffraction (XRD) studies previously performed by the authors. The scientific novelty lies in the comprehensive characterization of the morphological and phase features of the ores, while the practical significance is in substantiating their suitability as an effective raw material for the production of Cr-Mn ligature.

INTRODUCTION

It is well known that the technological progress of modern civilization is closely linked to the development of new materials with predetermined operational properties (Backeberg, Bedder, & Sardain, 2021; Zhang et al., 2024). In this process, the ferrous metallurgy sector continues to play a leading role, as it forms the fundamental basis for the sustainable development of industrial production, energy, and transport infrastructure. In particular, the production of high-quality alloyed steels remains one of the key indicators of a country's industrial strength and scientific-technological potential (Akbari, Zamani, & Mostafaei, 2024).

In established industrial practice, the conventional method of steel alloying is applied, whereby standard ferroalloys such as FeCr and FeMn are introduced separately into the melt (Zhou, Tang & Wang, 2020). This approach makes it possible to comprehensively ensure the strength, plasticity, and corrosion resistance of steel (Wang, Liu, Li & Zheng, 2022; Cheng et al., 2019). However, this traditional technology also has inherent limitations. First of all, it imposes

strict requirements on raw material quality. The stable chemical composition and high quality of ferroalloys used for alloying are based solely on the use of pre-enriched, high-grade ore concentrates. This, in turn, increases dependence on high-quality raw material resources and raises production costs. Moreover, the use of low-grade or poor-quality ores under conventional technological conditions is considered complex and economically inefficient.

In recent years, the observed depletion of high-grade ore reserves, combined with the abundant availability of low-grade and lean ores widespread across Kazakhstan, has posed new scientific and technological challenges for the metallurgical industry. At present, processing such ores using conventional methods requires expensive beneficiation stages, which significantly increase production costs and reduce overall economic efficiency. As a result, a significant contradiction has emerged between the existing technological paradigm and the actual capabilities of the available mineral resource base. This situation necessitates the search for innovative, resource-efficient, and environmentally sustainable solutions based on new technological approaches (Daver et al., 2016).

One of the most effective ways to overcome this fundamental contradiction is the development of modern technologies capable of directly processing low-grade raw materials. Such technologies would make it possible to bypass costly beneficiation stages and fully utilize the natural composition of the original ore.

In this regard, a particularly promising direction is the development of a technology for directly smelting a Cr–Mn ligature from low-grade local ores, specifically chromite ore from the Kempirsai deposit and iron-manganese ore from the Keregetas deposit. On the one hand, this approach offers an effective alternative under conditions of high-grade raw material scarcity, and on the other hand, it enables more complete and rational utilization of Kazakhstan's mineral resource potential.

Nevertheless, a mandatory and crucial prerequisite for developing such a new technology is a comprehensive and in-depth investigation of the physicochemical properties, mineralogical composition, and morphological and structural characteristics of the initial raw materials. Only the results of such scientifically grounded analysis can ensure the correct development of the future technological process and its effective implementation at an industrial scale.

In previous studies (Kabylkanov, Makhambetov, Abdullina, Zhakan, & Yucel, 2025), low-grade chromite ores and iron-manganese ores were comprehensively characterized using X-ray diffraction (XRD) and differential thermal analysis (DTA). XRD results demonstrated that chromite ($FeCr_2O_4$, $MgCr_2O_4$) is the predominant mineral phase in the Kempirsai ore, along with associated phases such as hematite (Fe_2O_3), hercynite ($FeAl_2O_4$), quartz (SiO_2), and Cr_2O_3. In samples from the Keregetas deposit, compounds such as MnO, Mn_3O_4, and Fe_2O_3 were identified, as well as a stable spinel-type $MnFe_2O_4$ phase. In addition, SiO_2 and Al_2O_3 phases were also detected in the ore composition.

Derivatographic studies revealed that the ores undergo multi-stage physicochemical transformations upon heating. In the low-temperature range (100–400 °C), an endothermic effect was observed due to the release of moisture and volatile compounds. In the medium temperature range (500–750 °C), distinct exothermic peaks were recorded, associated with the oxidation of Cr and Fe and the formation of stable Cr_2O_3 and Fe_2O_3 phases. In the iron-manganese ore, the formation of intermediate phases such as MnO and Mn_2O_3 was identified in this temperature interval. At high temperatures (750–1400 °C), recrystallization of mixed oxide phases and the formation of spinel-type compounds were observed, while above 1400 °C the system reached relative stability (Kabylkanov, Abdullina, Makhambetov, & Yucel, 2025).

The results of the conducted analyses confirmed that the Kempirsai chromite ore and Keregetas iron-manganese ore possess a complex and multicomponent mineralogical nature. Their mineral composition is heterogeneous, characterized by the coexistence of various phases

and their intricate interrelationships. Furthermore, their thermal behavior is defined by multi-stage reactions involving different phase transformations, which increase process complexity. Based on these findings, the main objective of this study is to comprehensively characterize the morphological and microstructural features of these ores using modern scanning electron microscopy (SEM) and energy-dispersive spectroscopy (EDS) techniques.

The relevance of the present study is justified by several important aspects. From a scientific perspective, it focuses on the comprehensive characterization of low-grade chromite and manganese-containing raw materials. This includes not only determining their overall chemical composition but also analyzing mineral phase morphology, grain size parameters, structural features, and phase transformation behavior under thermal treatment. Such an integrated investigation provides a reliable scientific foundation for developing a direct Cr–Mn ligature smelting technology (Makhambetov et al., 2025).

From an industrial standpoint, the obtained results provide accurate and reliable baseline data for developing new technological regulations, conducting thermodynamic modeling, and performing engineering calculations. This helps reduce uncertainties in planning industrial trials and minimizes technical and economic risks associated with implementing new technologies. Moreover, these scientific data facilitate practical solutions related to efficient raw material utilization, energy optimization, slag formation control, and enhancement of process stability (Kabylkanov et al., 2025).

Thus, the present work represents a comprehensive study of both scientific and applied significance. The research results not only demonstrate the feasibility of utilizing low-grade and complex ores but also lay the groundwork for developing new technological solutions aimed at improving metallurgical processing. This has strategic importance for expanding the domestic mineral resource base, reducing production costs, and decreasing dependence on imported raw materials in Kazakhstan's metallurgical industry.

MATERIALS AND METHODS

In this study, natural raw material samples obtained from two major ore deposits in Kazakhstan were used as research objects. The first sample was chromite ore from the Kempirsai deposit located in the Khromtau district of Aktobe Region, while the second sample was iron–manganese ore from the Keregetas deposit situated in the Zhanaarka district of Karaganda Region. These ores are characterized by their low grade, multicomponent composition, and complex mineralogical nature; therefore, the development of scientifically grounded methods for their metallurgical processing represents a relevant and important task.

For the purpose of the study, several kilograms of samples were collected from each deposit. Each sample was initially crushed and ground, after which it was analyzed in the "Chemical Analysis" laboratory of the Zh. Abishev Institute of Chemical and Metallurgical Processes using wet chemical analysis methods. As a result, the overall chemical composition of the ores was determined, providing a basis for subsequent experimental and theoretical investigations. The main chemical characteristics of the studied ores are presented in Table 1, while the external appearance of the lump samples is shown in Figure 1.

Table 1. Chemical composition of the studied ores, wt.%.

Material	Composition, wt.%								
	Cr_2O_3	$Mn_{ж}$	Fe_2O_3	SiO_2	Al_2O_3	MgO	CaO	P_2O_5	S
Chromite ore	40.49	–	12.03	11.10	8.99	28.29	0.65	0.006	0.013
Iron-manganese ore	–	26.62	21.78	16.74	2.57	0.15	2.34	0.43	0.17
Note – Compiled by the authors based on chemical analysis data									

For morphological and microstructural investigations, selected ore lumps were placed into special molds and impregnated with epoxy resin. After complete curing of the resin, the samples were firmly fixed and subjected to multistage mechanical preparation. This process included stepwise grinding using abrasive materials of different grain sizes, followed by final polishing with diamond pastes to achieve a mirror-like surface finish. This sample preparation method ensured the preservation of the natural microstructure without distortion during processing, thereby enabling the acquisition of high-quality and well-defined SEM images.

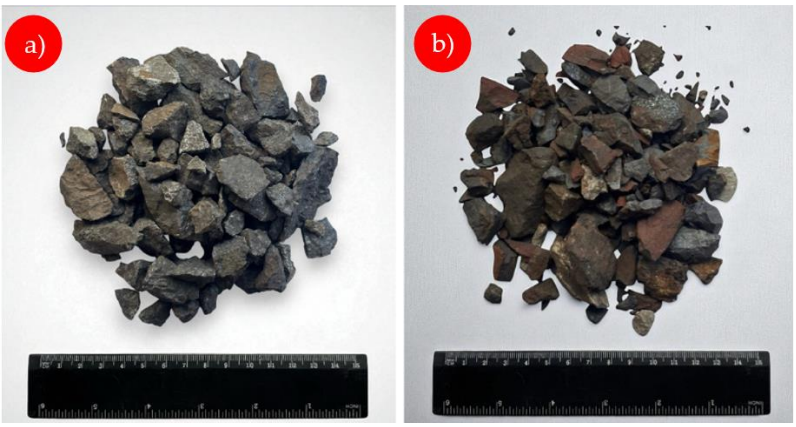

Figure 1. Studied raw materials: (a) chromite ore; (b) iron–manganese ore
Note – Prepared by the authors

The study was conducted using a modern ZEPTOOLS–ZEM20 scanning electron microscope manufactured in China. This analytical system provides high technical performance, including magnification up to 360,000× and resolution down to 5 nm at an accelerating voltage of 20 kV (Nogayev et al., 2025). A key advantage of this microscope is its capability to examine non-conductive samples without conductive coating and under low-vacuum conditions. This is particularly important for metallurgical studies, as it allows the preservation of the sample's original natural structure.

The microscope is equipped with an Oxford Energy Dispersive Spectroscopy (EDS) system, which significantly enhances its analytical capabilities. This system enables rapid qualitative and quantitative determination of the elemental composition in selected micro-areas, as well as the construction of elemental distribution maps (mapping) on the sample surface (Jones, Roberts, Wuhrer, & Madsen, 2022). EDS analysis provides critical information for determining the stoichiometry of mineral phases, investigating phase boundaries, and evaluating the morphology of micro-inclusions (Kato, Sano, & Yamaguchi, 2025).

Thus, the synergistic application of SEM (for microstructure) and EDS (for microcomposition) ensures the acquisition of comprehensive and reliable data on the structural and morphological characteristics of the raw material samples (Hyde, McFadden, & Carter, 2024). The obtained dataset forms a microstructural basis for predicting the high-temperature interaction mechanisms between slag-forming and metal-forming components.

RESULTS AND DISCUSSION

The results obtained in this study enabled a comprehensive characterization of the mineralogical composition, morphological features, and chemical properties of the investigated ores. These data serve as a fundamental basis for assessing the technological potential of low-grade chromite and manganese-containing raw materials, as well as for evaluating their metallurgical behavior. Figure 2 presents the SEM image of the Kempirsai chromite ore together with the elemental distribution maps of its main constituents.

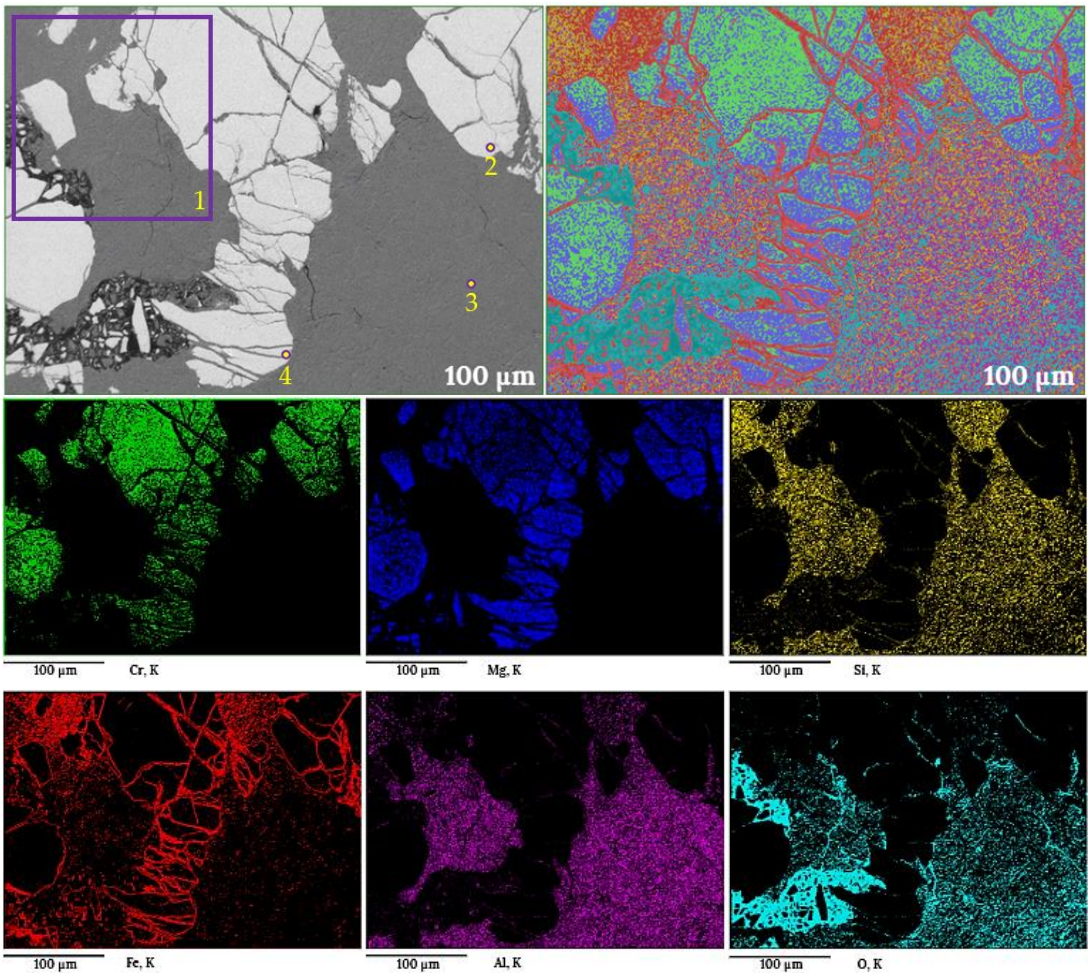

Figure 2. SEM image and elemental distribution maps of the Kempirsai chromite ore
Note – Prepared by the authors based on SEM analysis

Microstructural analysis clearly demonstrated that the mineral composition of the ore is heterogeneous. The bright regions were identified primarily as chromite grains. These grains exhibit a variety of shapes: some are close to regular geometric forms, while others are elongated or angular. The gray matrix corresponds to silicate minerals, which completely surround the chromite grains. Such a structure confirms the multicomponent mineralogical nature of the ore.

In addition, very fine dark particles were observed in certain areas. Their morphology is characteristic of iron-bearing or aluminosilicate inclusions, and they were identified as secondary phases. SEM analysis performed at magnifications up to 100 nm made it possible to clearly distinguish these fine structural features. As a result, the overall morphological characterization of the ore sample revealed a complex microstructural architecture.

To clarify the chemical elemental composition of the Kempirsai chromite ore, EDS analysis was performed. This method made it possible to determine the relative proportions of the main elements and to assess their distribution across different areas of the sample. The EDS results are presented in Figure 3 and Table 2; together with the morphological observations, they provide a deeper understanding of the phase relationships and elemental distribution patterns within the ore.

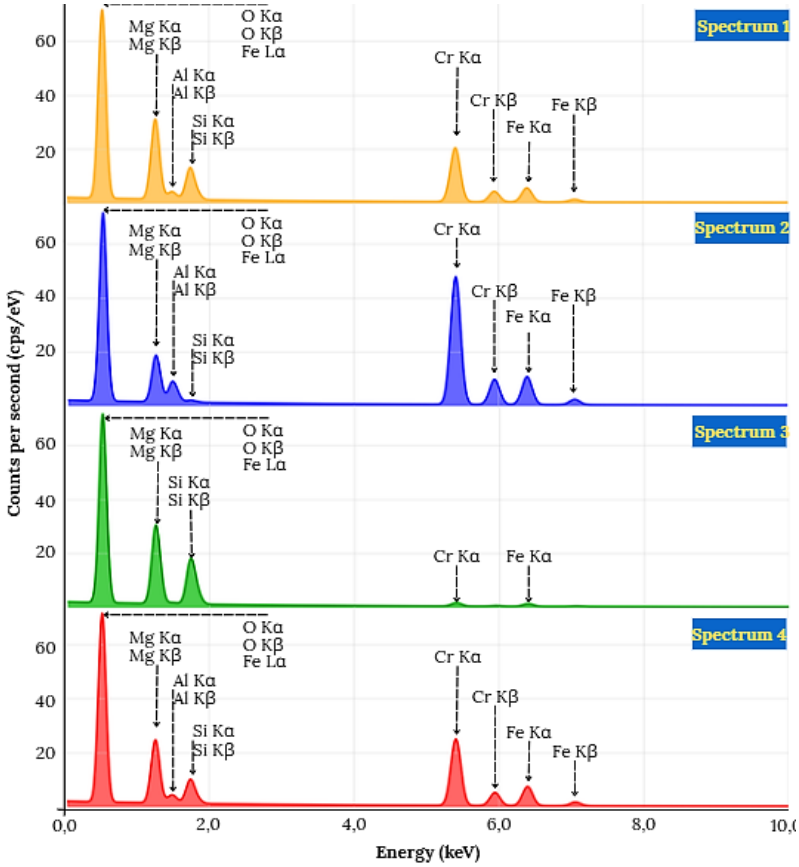

Figure 3. EDS spectra of the main elements identified in four selected areas of the chromite ore sample

Note – Prepared by the authors based on EDS analysis

Table 2. Mass fractions of the main elements in the chromite ore sample, wt.%

Spectrum No.	Composition, wt.%					
	O	Mg	Si	Cr	Al	Fe
1	43.99	17.55	7.91	16.50	1.82	4.42
2	38.16	8.85	0.46	33.85	4.20	7.62
3	53.59	20.95	13.73	1.28	0.37	1.06
4	48.80	15.30	6.62	22.45	2.15	6.68

Note – Compiled by the authors based on EDS analysis

Based on the spectra obtained from four selected areas of the ore sample (Figure 3 and Table 2), the mass fractions of the main elements were determined. Spectral analysis enabled the assessment of the mineralogical composition of the sample and the distribution patterns of elements across different regions.

The results showed that in the low-energy range (0.5–2.0 keV), distinct peaks of O, Mg, Al, and Si were recorded. These data confirm the predominance of silicate and oxide phases in the ore composition. In the high-energy range (5–7 keV), characteristic peaks of Cr and Fe were observed, indicating that these elements constitute the main mineral phases of the ore. The intensity variations of the spectral curves demonstrated that the elements are not uniformly distributed across the sample; in certain areas, specific elements were found to be dominant. Such heterogeneity may significantly influence the thermal and technological properties of the ore.

Analysis of individual spectra revealed the following:

• In Spectrum 1, a high concentration of Cr was detected alongside O and Mg, suggesting the predominance of a spinel-type $MgCr_2O_4$ phase.

• In Spectrum 2, the content of Cr reached 33.85 wt.%, Mg was 8.85 wt.%, and Fe was 7.62 wt.%, which is characteristic of chromite mineral composition.

• In Spectrum 3, elevated levels of Si (13.73 wt.%) and Mg (20.95 wt.%) were observed, while Cr was only 1.28 wt.%, indicating that this area corresponds to a silicate matrix.

• In Spectrum 4, Cr amounted to 22.45 wt.%, Mg to 15.30 wt.%, and Fe to 6.68 wt.%, characterizing a mixed region containing both chromite and iron-bearing inclusions.

In all spectra, Al was detected only in minor amounts (0.37–4.20 wt.%). Overall, the obtained data clearly reflect the complex mineralogical composition of the sample, revealing the distribution patterns of spinel phases, chromite-rich areas, and the surrounding silicate matrix.

At the next stage, in order to investigate the structural features of the iron–manganese ore from the Keregetas deposit in greater depth, its morphological characteristics were examined using SEM. The high magnification capability and excellent resolution of this method made it possible to conduct a detailed analysis of the sample's surface morphology, identify its textural and structural features, and evaluate the spatial arrangement, distribution patterns, and interrelationships of different mineral phases, particularly at phase boundaries. As a result, the obtained data confirmed the complex multiphase structure of the ore and demonstrated the heterogeneity of its mineralogical composition from a morphological perspective. The SEM image of the studied iron–manganese ore is presented in Figure 4.

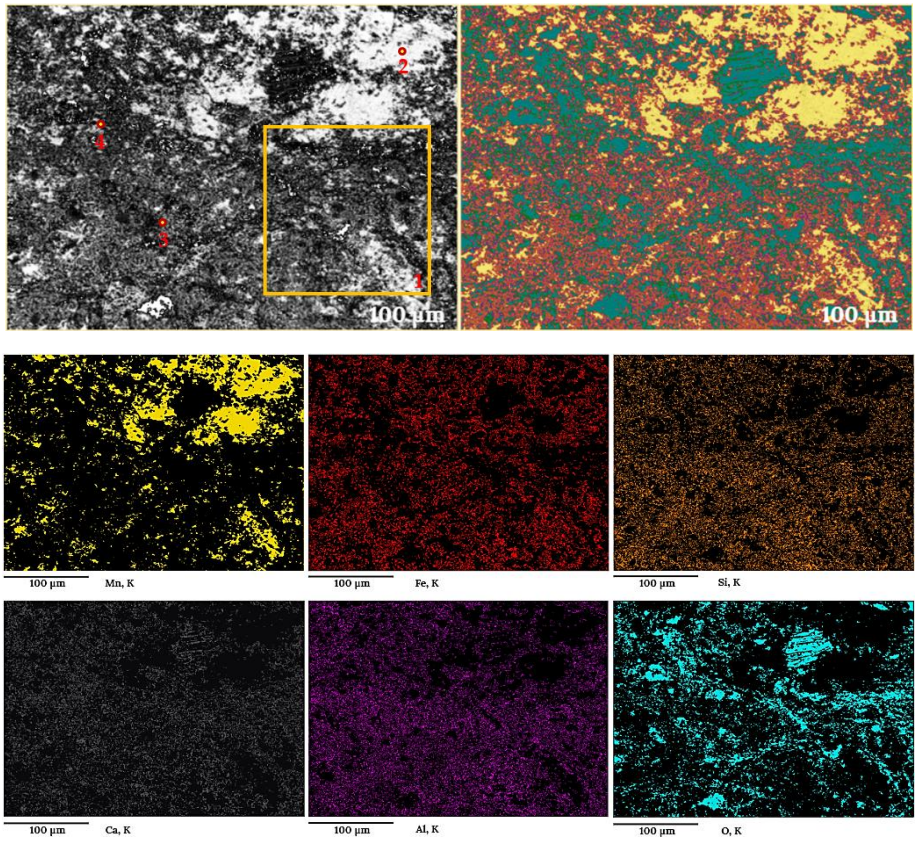

Figure 4. SEM image and elemental distribution maps of the Keregetas iron-manganese ore

Note – Prepared by the authors based on SEM analysis

In addition to SEM imaging, Energy Dispersive Spectroscopy (EDS) was employed to clarify the elemental composition of the sample and to obtain a deeper understanding of its chemical characteristics. This method not only enabled the identification of the distribution of major and minor elements within the studied ore but also allowed quantitative assessment of their relative proportions.

EDS analysis revealed that in different areas of the iron–manganese ore sample, key elements such as Fe, Mn, Si, and O are concentrated in varying amounts. At the same time, the presence of minor quantities of elements such as Al, Ca, and Cr indicates the existence of additional mineral phases. These data confirm the multiphase nature of the sample and highlight the complexity of its mineralogical composition.

The results of the conducted analysis are illustrated in Figure 5, while Table 3 summarizes the EDS spectral data of the main elements recorded in selected regions of the iron-manganese ore sample.

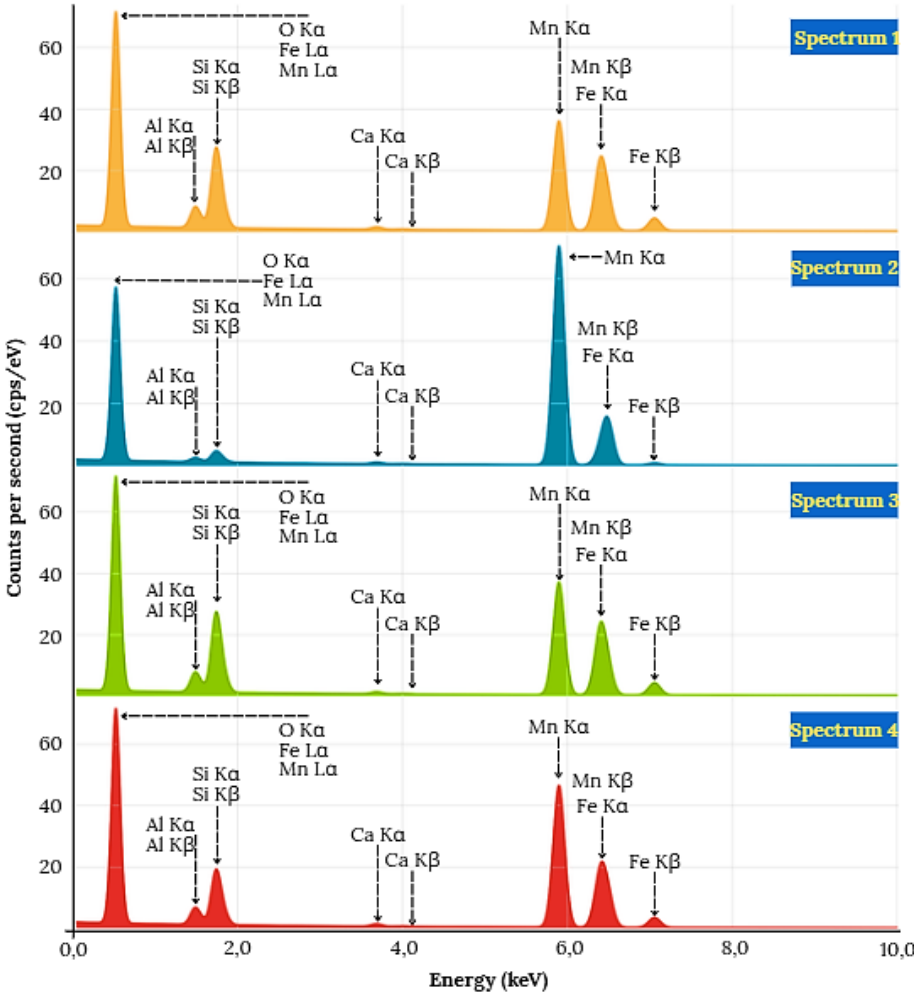

Figure 5. EDS spectra of the main elements identified in four selected areas of the iron–manganese ore sample

Note – Prepared by the authors based on EDS analysis

As part of the study, EDS spectra obtained from four selected areas of the iron–manganese ore sample were analyzed. Each spectrum exhibited clear characteristic peaks corresponding to the main elements comprising the mineral composition of the ore.

In the low-energy range (0.5–2.0 keV), intense peaks of O, Al, and Si, as well as Mn Lα lines, were recorded, indicating their significant concentration in the silicate and oxide phases of the ore. In the mid-energy range (3–4 keV), weak Ca Kα and Kβ lines were detected, suggesting the presence of minor accessory mineral phases. In the high-energy range (5–7 keV), distinct Mn and Fe Kα and Kβ peaks were observed, confirming that these elements are the primary metal-forming components in the ore. The relative intensities of the spectral curves made it possible to assess the proportional distribution and spatial variability of elements in different regions of the sample.

Table 3. Mass fractions of the main elements in the iron–manganese ore sample, wt.%

Spectrum No.	Composition, wt.%					
	O	Ca	Si	Mn	Al	Fe
1	34.15	0.50	13.52	23.10	3.35	13.64
2	31.35	0.36	2.12	52.56	0.72	2.60
3	34.39	0.41	13.63	24.00	3.20	13.44
4	32.80	0.47	8.95	28.75	2.60	10.43

Note – Compiled by the authors based on EDS analysis

Based on the study of the iron–manganese ore, spectra obtained from four selected areas were analyzed. In Spectrum 1, significant amounts of O (34.15 wt.%) and Si (13.52 wt.%) were recorded, while Mn (23.10 wt.%) and Fe (13.64 wt.%) were also present in considerable proportions. Such a composition indicates the coexistence of iron–manganese minerals together with silicate phases.

In Spectrum 2, the Mn content increased sharply to 52.56 wt.%, while O reached 31.35 wt.%, Fe 2.60 wt.%, and Si 2.12 wt.%. These data demonstrate that this region is rich in manganese-bearing minerals.

In Spectrum 3, Mn amounted to 24.00 wt.%, Fe to 13.44 wt.%, Si to 13.63 wt.%, and O to 34.39 wt.%. This composition confirms the distribution of Fe–Mn minerals within a silicate–oxide matrix.

In Spectrum 4, Mn (28.75 wt.%) and Fe (10.43 wt.%) were present in relatively high proportions, while O reached 32.80 wt.%. This region corresponds to a complex mineral assemblage containing both iron–manganese inclusions and silicate phases.

Overall, in all four spectra Al was detected only in minor amounts (0.72–3.35 wt.%), while Ca content was very low (0.36–0.50 wt.%). The data presented in Table 3, together with the spectral analysis results, clearly characterize the complex mineralogical composition of the sample and reveal the distribution of Mn- and Fe-rich areas as well as silicate phases. Furthermore, morphological SEM investigations highlighted the textural features of the sample and confirmed the presence of localized concentrations of Mn and Fe minerals on its surface.

CONCLUSION

In this study, the mineralogical and structural features of the Kempirsai chromite ore and the Keregetas iron–manganese ore were comprehensively investigated using a complex of modern analytical methods. The results revealed the multicomponent and complex nature of these ores and enabled a metallurgical assessment of their morphological and phase behavior.

SEM analysis characterized the surface morphology of the samples and demonstrated that chromite ($FeCr_2O_4$) is the dominant mineral phase in the chromite ore from Kempirsai. In addition, the heterogeneous distribution of ferrospinels and silicate inclusions was identified. In

the iron–manganese ore, Mn- and Fe-bearing minerals were found to exhibit complex textural relationships and to coexist with silicate and oxide phases. These features confirm the heterogeneity and multiphase structure of the studied ores.

According to EDS results, the high Cr content in the Kempirsai chromite ore confirms that chromite is the main mineral-forming component. In the Keregetas iron–manganese ore, elevated concentrations of Mn and Fe indicate that these elements define the principal phase composition of the material. Minor elements such as Al, Ca, and Si were detected only in small amounts, confirming the presence of accessory mineral phases.

Overall, the obtained results demonstrate that the investigated ores possess a multiphase and structurally complex mineralogical nature. Such characteristics directly influence their thermal stability, susceptibility to phase transformations, and technological behavior during metallurgical processing.

The findings of this study are in full agreement with the results of chemical analysis and previously conducted XRD investigations. This confirms the complementarity of the applied methods and the reliability of the scientific conclusions drawn.

From a practical standpoint, the mineralogical composition of the Kempirsai chromite ore and the Keregetas iron–manganese ore indicates their suitability for metallurgical use. In particular, the obtained results demonstrate that these ores can serve as promising raw materials for the production of Cr–Mn ligatures.

CONFLICT OF INTEREST: The authors declare that they have no conflicts of interest.

FUNDING: This research was funded by the Ministry of Science and Higher Education of the Republic of Kazakhstan (Grant Nos. AP23488918 and BR24992854).

ACKNOWLEDGEMENTS: The authors express their gratitude to their colleagues for methodological support and valuable comments, as well as to the anonymous reviewers whose suggestions contributed to improving the quality of this manuscript.

STATEMENT ON THE USE OF ARTIFICIAL INTELLIGENCE TECHNOLOGIES: The authors declare that no artificial intelligence (AI) tools were used in the preparation of this article.

REFERENCES

Akbari, P., Zamani, M., & Mostafaei, A. (2024). Machine learning prediction of mechanical properties in metal additive manufacturing. Additive Manufacturing, 91, 104320. https://doi.org/10.1016/j.addma.2024.104320

Backeberg, N. A., Bedder, J. C. M., & Sardain, E. (2021). Bulk and stainless ferroalloys markets: Fundamentals, trends and forecasts. In Proceedings of the 16th International Ferro-Alloys Congress (INFACON XVI). https://doi.org/10.2139/ssrn.3927686

Cheng, L., Li, W., Li, Y., Yang, Y., Li, Y., Cheng, Y., & Song, D. (2019). Thermal analysis and decomposition kinetics of the dehydration of copper sulfate pentahydrate. Journal of Thermal Analysis and Calorimetry, 135(6), 2697–2703. https://doi.org/10.1007/s10973-018-7595-y

Daver, F., Kajtaz, M., Brandt, M., & Shanks, R. A. (2016). Creep and recovery behaviour of polyolefin-rubber nanocomposites developed for additive manufacturing. Polymers, 8(12), 437. https://doi.org/10.3390/polym8120437

Hyde, A., McFadden, N., & Carter, P. (2024). Installation and operation of SEM–EDS analysis in a multidisciplinary laboratory. Microscopy and Microanalysis, 30(S1), ozae044.449. https://doi.org/10.1093/mam/ozae044.449

Jones, R., Roberts, A., Wuhrer, R., & Madsen, I. (2022). Enhanced compositional mapping on the SEM through combined EDS–WDS mapping in AZtecWave. Microscopy and Microanalysis, 28(S1), 546–548. https://doi.org/10.1017/S1431927622002823

Kabylkanov, S., Makhambetov, Y., Abdulina, S., Burumbayev, A., Zhakan, A., & Onuralp, Y. (2025). Production of chrome-manganese ligature using ferrosilicochrome dust as a reducing agent. Acta Metallurgica Slovaca, 31(3), 141–148. https://doi.org/10.36547/ams.31.3.2221

Kabylkanov, S., Makhambetov, Ye., Abdullina, S., Zhakan, A., & Yucel, O. (2025). Research of physico-chemical properties of charge materials for the production of chromium-manganese ligature. Science and Technology of Kazakhstan, 1(53), 233–247. https://doi.org/10.48081/IDDG9941

Kabylkanov, S. K., Abdullina, S. A., Makhambetov, Ye. N., & Yucel, O. (2025). Differential thermal analysis of charge materials for the production of chromium-manganese ligature. D. Serikbayev EKSTU Bulletin (Vestnik EKTU), 1(3), 60–69. https://doi.org/10.51885/1561-4212_2025_3_60

Kato, T., Sano, S., & Yamaguchi, T. (2025). A comprehensive and quantitative SEM–EDS analytical method. Scientific Reports, 15, 89362. https://doi.org/10.1038/s41598-025-89362-w

Makhambetov, Y., Abdulina, S., Kabylkanov, S., Burumbayev, A., Zhakan, A., Sadyk, Z., & Akhmetov, A. (2025). Production of Chromium–Manganese Ligature from Low-Grade Chromium and Iron–Manganese Ores Using Silicon–Aluminum Alloys as Reductants. Processes, 13(10), 3158. https://doi.org/10.3390/pr13103158

Nogayev, K., Abishkenov, M., Ashkeyev, Z., Akhmetova, G., Kydyrbayeva, S., & Tavshanov, I. (2025). Effect of imposed shear during oval-caliber rolling on the properties of Mn–Si low-alloy steel. Eng, 6(10), 265. https://doi.org/10.3390/eng6100265

Wang, Y., Liu, W., Li, N., & Zheng, C. (2022). The Importance of Structure and Corrosion Resistance of Steels/Alloys. Coatings, 12(7), 997. https://doi.org/10.3390/coatings12070997

Zhang, G., Zhang, H., Liu, X., Xin, Y., Yin, S., Gao, L., & Shi, Z. (2024). Effect of Mn on corrosion resistance of low-Cr weathering steel. Metals, 14(12), 1433. https://doi.org/10.3390/met14121433

Zhou, L., Tang, J., & Wang, Y. (2020). Effect of ferroalloys on the properties of steel. Materials Science Forum, 1016, 187–194.

Information about authors

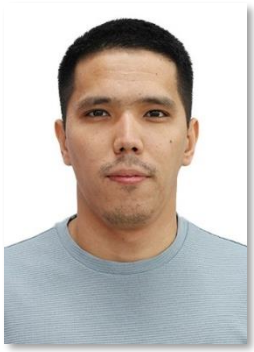

Sultan Kabylkanov – PhD student, D. Serikbayev East Kazakhstan Technical University, Ust-Kamenogorsk, Kazakhstan
e-mail: kabylkanov.s@edu.ektu.kz,
ORCID: https://orcid.org/0000-0002-1272-2065

Saule Abdulina – PhD, Professor, D. Serikbayev East Kazakhstan Technical University, Ust-Kamenogorsk, Kazakhstan, Ust-Kamenogorsk, Kazakhstan,
e-mail: abdulina.saule@mail.ru,
ORCID: https://orcid.org/0000-0001-6328-8652

Yerbolat Makhambetov – PhD, Associate Professor, Chemical-Metallurgical Institute, Karaganda, Kazakhstan,
e-mail: m.ye.n@mail.ru,
ORCID: https://orcid.org/0000-0001-8613-9932

Onuralp Yucel – PhD, Professor, Istanbul Technical University, Istanbul, Turkey,
e-mail: yucel@itu.edu.tr,
ORCID: https://orcid.org/0000-0002-3879-0410

CENTRAL ASIAN TRANSACTIONS ON MATERIALS STRUCTURE AND PROPERTIES

https://doi.org/10.51885/3134-7983_CATMSP_2026_1_6
SRSTI 53.31.23

SELECTIVE REDUCTION OF IRON FROM IRON–MANGANESE ORE USING HYDROGEN

Yerbol Kuatbay [1], **Asylbek Nurumgaliev** [2], **Gulzat Bulekova** [1]*, **Ainagul Otarbayeva** [3], **Semyon Salikhov** [4]

[1]Karaganda Industrial University, Temirtau, Kazakhstan
[2]Abilkas Saginov Karaganda Technical University, Karaganda, Kazakhstan
[3]K. Zhubanov Aktobe Regional University, Aktobe, Kazakhstan
[4]South Ural State University (National Research University), Chelyabinsk, Russian Federation
*Corresponding author: Gulzat Bulekova, e-mail: g.bulekova@tttu.edu.kz

Keywords:
iron–manganese ore, hydrogen, manganese, iron, arsenic, phosphorus, reduction.

ABSTRACT

The results of the study indicate that the iron–manganese ore is characterized by a complex mineralogical composition comprising Fe-, Mn-, and Si-bearing oxides as well as complex aluminosilicate phases. X-ray diffraction (XRD) of the as-received material confirmed goethite (FeO(OH)), hematite (Fe_2O_3), quartzite (SiO_2), and manganese dioxide (MnO_2) as the dominant phases.

During oxidative roasting, goethite underwent dehydroxylation with the formation of hematite, and the emergence of Mn_2O_3 and Mn_3O_4 phases was also identified. The formation of Mn_7SiO_{12} indicates high-temperature interaction between manganese species and silica, suggesting the development of solid-state synthesis processes in the Mn–Si–O system.

Thus, hydrogen proved to be an efficient and environmentally benign reductant, enabling selective iron reduction at relatively low temperatures. The reduced metal and the oxide residue can be separated by smelting or magnetic separation, which opens prospects for developing processing flowsheets for Kazakhstan's iron–manganese ores with minimal environmental impact.

INTRODUCTION

Hydrogen is currently considered one of the key instruments enabling low-carbon transformation of the global energy system. According to projections by the International Renewable Energy Agency (IRENA), by 2050 the share of hydrogen in global energy consumption could increase to 12% (IRENA, 2023). The European Union countries and other advanced industrial economies are actively investing in technological solutions in this field, which strengthens the prospects for the widespread use of hydrogen as an energy carrier. In October 2024, Kazakhstan also adopted a national Concept for the Development of Hydrogen Energy to accelerate the transition to a low-carbon economy, initiating targeted measures at the national level. In this concept, hydrogen is defined as a strategic element for decarbonizing industry and the transport sector (Baisanov et al., 2021).

One of the major initiatives in Kazakhstan is the world's largest green hydrogen production hub in Mangystau Region, implemented by Svevind Group. The project includes a seawater desalination plant with a capacity of 255,000 m^3 per day, wind and solar power plants with a total installed capacity of 40 GW, and 20 GW of electrolyzer systems. In addition, KazMunayGas Engineering is considering underground water as an alternative source for hydrogen production under water scarcity conditions (KMG Engineering, 2024). These initiatives demonstrate the growing strategic role of hydrogen in Kazakhstan's energy system.

In the metallurgical sector, the use of hydrogen as a reducing agent has been actively studied in recent years. In the processing of iron and manganese ores, hydrogen exhibits the ability to selectively reduce iron (Ngoy et al., 2020; Ernst et al., 2024). It has been shown that in complex minerals containing hematite, magnetite, and titanium-bearing phases, hydrogen demonstrates higher kinetic efficiency compared to traditional carbon-based reductants (Naseri Seftejani & Schenk, 2018; John & Hayes, 1982). While carbon-based reduction releases CO_2 as a by-product, hydrogen reduction produces water, which not only enhances the environmental advantages of the technology but also significantly reduces greenhouse gas emissions from metallurgical processes (Matthew et al., 1990). Furthermore, hydrogen's ability to selectively separate iron from manganese enables better control of phase composition and reduces energy consumption.

The mineralogical structure of iron–manganese ores in Kazakhstan is complex and characterized by high concentrations of iron and silicon, which makes traditional blast furnace or electric furnace processing inefficient (Yerbolat et al., 2024; Pavlov et al., 2012). Such methods lead to increased energy consumption, higher manganese losses, and additional environmental pollution (Suleimen & Salikhov, 2022; Kosdauletov et al., 2021). Although physical and physicochemical beneficiation methods can partially separate mineral phases based on density or magnetic properties, the heterogeneous structure of the ore limits their effectiveness (Baisanov et al., 2021; Tastanova et al., 2023).

Carbon-based reduction also has well-known drawbacks, including high CO_2 emissions and incomplete recovery of manganese, which negatively affect metallurgical performance (Kosdauletov & Roshchin, 2020; Kosdauletov et al., 2022). Previously proposed two-stage pyrometallurgical schemes—initial reduction of iron and phosphorus followed by melting of the product—have environmental and technological limitations, since the use of CO as a reductant causes persistent environmental harm (Roshchin et al., 2023). In this context, the transition to hydrogen is considered a more environmentally friendly and efficient approach to processing iron–manganese ores.

MATERIALS AND METHODS

For the experiments, iron–manganese ore from the "Keregetas" deposit in Kazakhstan was used. Prior to testing, the ore was ground in an IDA-175 mill to a particle size of −1 mm to ensure homogeneity of its chemical composition. The ground material was then moistened, placed in a mold, and dried at 150 °C for 1 hour to completely remove moisture.

The reduction process was carried out in an RB Automazione MM 6000 laboratory vertical furnace designed for testing iron-bearing materials (Figure 1). Samples weighing up to 30 g were placed in a reaction tube made of heat-resistant AISI 310 steel with a diameter of 75 mm. The temperature was controlled by a system consisting of five independent heating zones equipped with silicon carbide heaters, ensuring uniformity of the thermal field.

Reduction was performed in the temperature range of 700–1100 °C with a holding time of 60 minutes. High-purity hydrogen (99.99%), compliant with GOST 3022-80, was used as the reducing agent. It was supplied at a flow rate of 0.5 L/min and monitored using a digital mass flow controller. High-grade argon (99.993%), compliant with GOST 10157-2016, was used as the inert gas.

The furnace was equipped with an automated control system that allowed programming of the temperature profile, real-time monitoring of process parameters, and continuous recording of sample mass changes during the experiment.

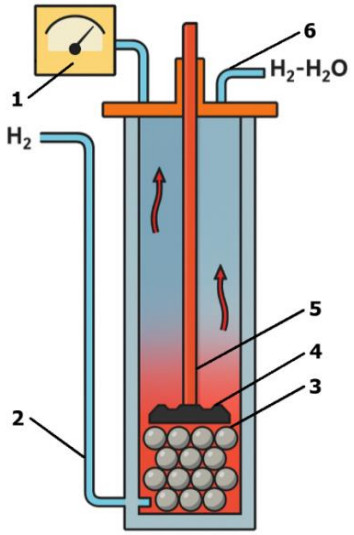

Figure 1. Schematic diagram of the reactor setup for the experiment: 1 – multimeter; 2 – hydrogen gas supply system; 3 – corundum balls for uniform gas distribution; 4 – samples; 5 – thermocouple; 6 – exhaust system for outlet (residual) gases
Note – prepared by the authors

The microstructure and elemental composition were investigated using a JEOL JSM-7001F scanning electron microscope equipped with an OXFORD X-Max 80 energy-dispersive detector. The analysis was performed at an accelerating voltage of 30 kV with magnification up to 1.2 nm. Composition was determined in both point and area analysis modes, and data processing was carried out using the microscope's proprietary software.

X-ray diffraction analysis (XRD) was conducted on a Rigaku Ultima IV diffractometer with a CuKα X-ray tube (λ = 1.5406 Å). Measurements were performed at 40 kV and 30 mA. Diffractograms were recorded over the range 2θ = 5–90° at a scanning rate of 5°/min. Powder samples (< 0.063 mm fraction) were placed in flat sample holders for analysis. Phase identification was carried out using the Match software (Crystal Impact, Germany) with the PDF2 (2009) database, which enabled the detection of newly formed oxide and silicate phases resulting from the reduction process.

Ores from the "Keregetas" deposit are characterized by a complex mineralogical composition and heterogeneous structure. They contain iron, manganese, silicon, barium, potassium, and aluminum. The presence of phosphorus and arsenic impurities complicates their metallurgical processing.

To obtain an averaged chemical composition, the raw ore was melted in a Nabertherm resistance furnace at 1650 °C in a corundum crucible. The melt was then rapidly cooled in a metal mold. The resulting quenched material was analyzed using a JEOL JSM-7001F scanning electron microscope equipped with an OXFORD X-Max 80 energy-dispersive detector. The study was conducted at accelerating voltages of 0.5–30 kV over a sample area magnified up to 600 μm, enabling high-precision determination of the elemental composition.

The average chemical composition of the ore after melting and quenching is presented in Table 1.

Table 1. Elemental composition of the ore

Analysis of the sample area	O	Al	Si	K	Ca	Mn	Fe	As	Ba
at.% (atomic percent)	66,6	4,5	9,9	0,9	0,5	11,8	5,4	0,4	0,1
wt.% (weight percent)	42,5	4,8	11,1	1,5	0,7	25,8	12,0	1,1	0,5
Note – prepared by the authors									

Figure 2 presents the results of X-ray diffraction (XRD) analysis of the initial iron–manganese ore. The analysis was performed using a Rigaku Ultima IV diffractometer with Match software. Based on the results, the main mineral phases of the ore were identified as goethite FeO(OH), hematite Fe_2O_3, manganese dioxide MnO_2, a combined iron–manganese oxide phase $FeMnO_3$, and silicon dioxide SiO_2.

Due to the relatively low peak intensities of other compounds, accurate identification of phases containing potassium (K), aluminum (Al), arsenic (As), and barium (Ba) was difficult.

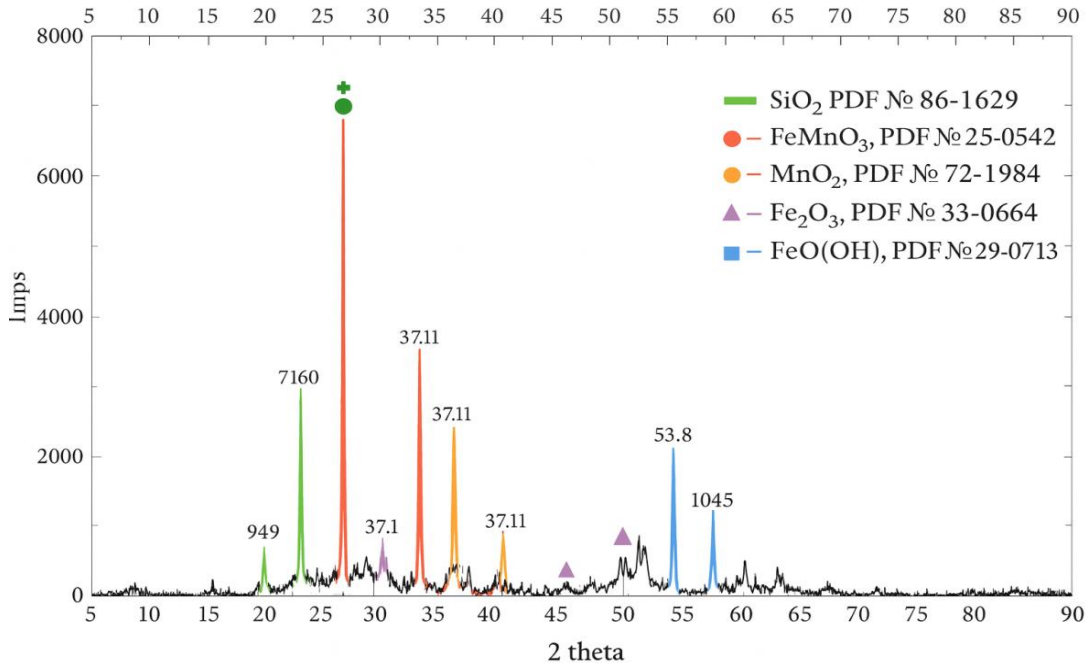

Figure 2. X-ray diffraction pattern of the initial iron–manganese ore
Note – prepared by the authors

To investigate the changes occurring in iron–manganese ores during heating in an air atmosphere, homogeneous lump samples from the "Keregetas" deposit were placed in a corundum crucible and heated in a Nabertherm muffle furnace. The heating rate was 200 °C/h, the target temperature was 1000 °C, and the holding time at this temperature was 2 hours.

RESULTS AND DISCUSSION

According to the X-ray diffraction data (Figure 3), the following phases were identified in the samples after calcination in an air atmosphere: Fe_2O_3, Mn_2O_3, Mn_3O_4, $FeMnO_3$, and Mn_7SiO_{12}.

During oxidative heating, oxygen is released from the crystal lattice of manganese dioxide (MnO_2), resulting in its partial reduction to lower oxides (Mn_3O_4 and Mn_2O_3). In addition, goethite FeO(OH) loses structural water and transforms into hematite (Fe_2O_3).

As a result of calcination in an air atmosphere, the total mass loss amounted to 13.24%, which is associated with dehydration and partial reduction of manganese oxides.

X-ray diffraction analysis, elemental distribution maps, and microstructural studies of the initial iron–manganese ore from the "Keregetas" deposit (Figures 1, 2, and 3) confirm its complex mineralogical composition and the predominance of iron and manganese in oxide forms. Such an ore structure can create certain technological difficulties in the production of manganese alloys from this raw material.

Therefore, experiments on the selective reduction of iron using hydrogen as a reducing agent were carried out. Reductive roasting was performed at temperatures of 700, 800, 900, 1000, and 1100 °C with a holding time of 60 minutes.

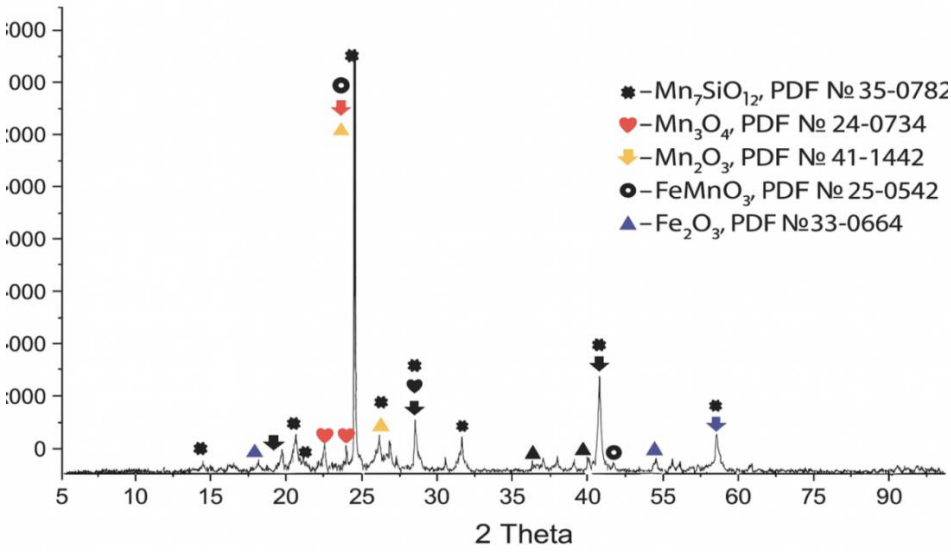

Figure 3. X-ray diffraction pattern of iron–manganese ore after oxidative calcination
Note – prepared by the authors

Figure 4 shows the dependence of sample mass loss on reduction temperature. At 700 °C, the mass loss was 18.41%, while increasing the temperature to 1000 °C led to a mass loss of 22.1%, which is associated with active reduction of iron and release of oxygen from oxides. However, when the temperature was further increased to 1100 °C, sintering of ore particles was observed, which reduced the interaction between hydrogen and the particle surfaces and hindered metal reduction, resulting in a decrease in mass loss to 19.8%.

Figure 4 presents the results of reductive roasting of iron–manganese ore samples from the "Keregetas" deposit in a hydrogen atmosphere at 700–1000 °C for 60 minutes at a hydrogen flow rate of 0.5 L/min.

Thermodynamic background (Fe–O–H and Mn–O–H systems)

The direction of metal reduction processes in a hydrogen atmosphere primarily depends on the equilibrium in metal–oxygen systems and the H_2/H_2O ratio in the gas phase. In general, the reduction of iron oxides by hydrogen proceeds through the following stages:

$$Fe_2O_3 \rightarrow Fe_3O_4 \rightarrow FeO \rightarrow Fe,$$

with the formation of water vapor (H_2O) as a reaction product. In the temperature range of 700–1000 °C, hydrogen effectively binds oxygen from iron oxides, enabling deep and intensive reduction to metallic iron. This is consistent with the increase in mass loss shown in Figure 4 and the formation of metallic Fe phase confirmed by XRD analysis (Figure 6).

For manganese oxides, reduction is thermodynamically more complex. Although MnO_2 and Mn_2O_3 can be relatively easily reduced to lower oxides (Mn_3O_4 and MnO), further reduction of MnO to metallic manganese requires a higher reducing potential in the gas phase (higher H_2/H_2O ratio) and higher temperatures. Therefore, at 700–800 °C, manganese remains

predominantly in oxide phases, whereas at temperatures above 900 °C, metallic manganese begins to appear (Table 2). This confirms the mechanism of selective reduction: iron is reduced first, followed by partial reduction of manganese at higher temperatures.

At 1100 °C, sintering of ore particles reduces gas–solid contact and increases diffusion resistance, which can slow down the reduction rate. In addition, at high temperatures, the formation of difficult-to-reduce complex silicate phases in the Fe–Mn–Si–O system (such as $FeMnSiO_4$ and Mn_2SiO_4) becomes more likely, which limits further metal reduction and may explain the observed decrease in mass loss at 1100 °C.

The general trend is consistent for all temperature regimes: as temperature increases, reduction processes in the ore become more intensive and deeper. After reduction, the formation of a metallic phase is observed both on the surface and inside the samples, with iron and arsenic being the main metallic components.

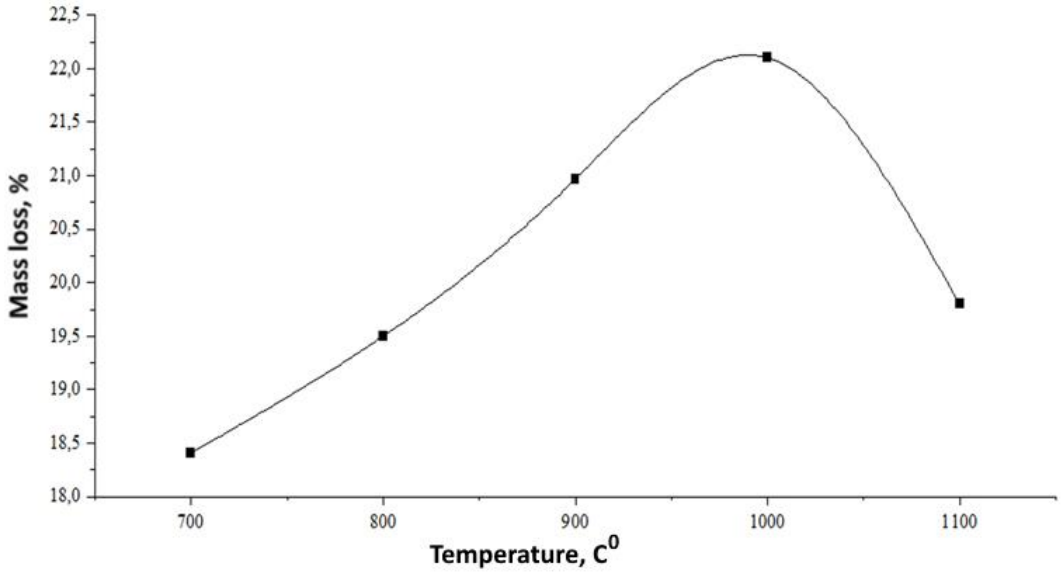

Figure 4. Mass loss of samples after reductive roasting in a hydrogen atmosphere (hydrogen flow rate 0.5 L/min)

Note – prepared by the authors

As the reduction temperature increases, a small amount of manganese appears in the metallic phase, indicating that its reduction begins at temperatures above 900 °C (Figure 5, Table 2).

In the micrographs shown in Figure 5, two main structural regions are observed: (i) light-colored metallic inclusions and (ii) a dark-colored oxide–silicate matrix. According to the micro-X-ray spectral analysis results presented in Table 2, at temperatures of 700–800 °C the metallic inclusions consist mainly of Fe (98.7–99.5 at.%) and As (0.5–1.3 at.%), indicating that hydrogen selectively reduces iron to the metallic state in this temperature range and promotes the accumulation of arsenic in the metallic phase.

In contrast, the dark matrix region exhibits high contents of O and Mn (approximately O ≈ 38–42 at.% and Mn ≈ 52–58 at.%), while the Fe content remains low. This suggests that the matrix is predominantly composed of manganese oxides and silicate phases, and that manganese largely remains in the oxide form at these temperatures.

At 900–1000 °C, the appearance of 2.8–4.4 at.% Mn in the metallic inclusions indicates the onset of partial reduction of manganese. Thus, the experimental results confirm that iron is predominantly reduced in the range of 700–900 °C, whereas manganese reduction becomes significant only at higher temperatures, demonstrating the selective nature of the process.

After roasting, the remaining oxide phase, regardless of temperature, mainly consists of manganese oxides and gangue silicate minerals, indicating that the ore material was partially, but not completely, reduced.

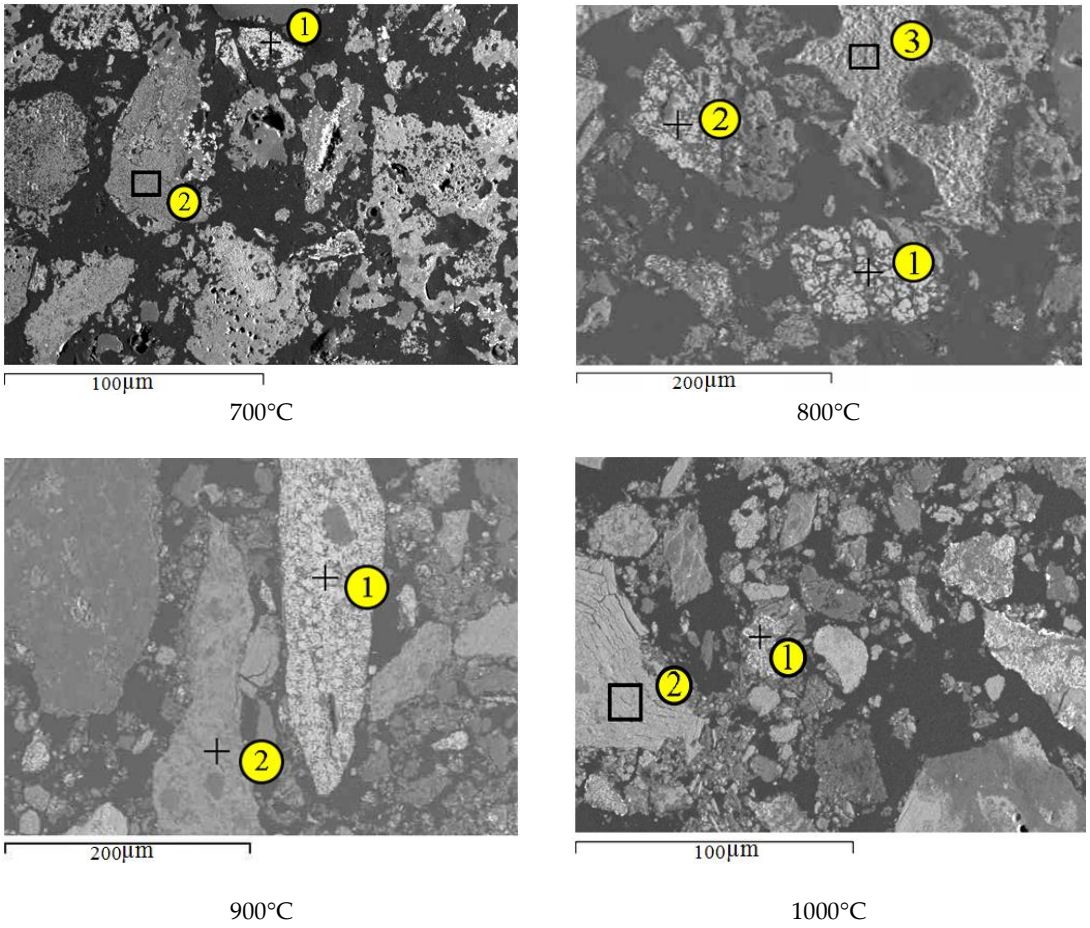

Figure 5. Microstructural appearance of phases in iron–manganese ore after reductive roasting

Note – prepared by the authors

Table 2. Results of micro-X-ray spectral analysis of the samples (Figure 5)

Sample	Element content, at.%						
	Analysis point	O	Al	Si	Mn	Fe	As
700°C	1	0,0	0,0	0,0	0,0	98,7	1,3
	2	39,5	0,0	2,4	52,1	6,1	0,0
800°C	1	0,0	0,0	0,0	0,0	99,5	0,5
	2	0,0	0,0	0,0	0,0	98,9	1,1
	3	42,0	2,0	0,7	53,0	2,2	0,0
900°C	1	0,0	0,0	0,0	2,8	95,3	1,9
	2	38,5	0,0	1,3	57,9	2,4	0,0
1000°C	1	0,0	0,0	0,0	4,4	93,6	2,0
	2	39,8	0,0	1,9	55,6	2,7	0,0
Note – prepared by the authors							

Figure 6 shows the diffractograms of iron–manganese ore samples after reductive roasting in a hydrogen atmosphere at temperatures of 700, 800, 900, 1000, and 1100 °C with a holding time of 60 minutes.

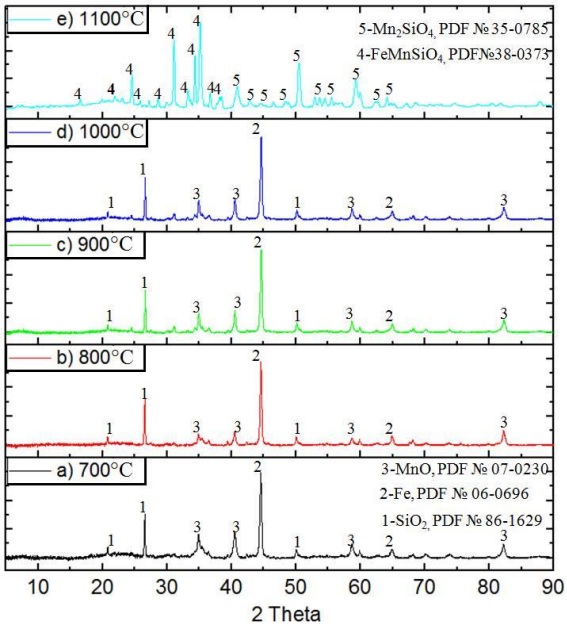

Figure 6. Diffractograms of samples after reductive roasting in a hydrogen atmosphere with a holding time of 60 minutes. Phases: 1 – SiO_2, 2 – Fe, 3 – MnO, 4 – $FeMnSiO_4$, 5 – Mn_2SiO_4.
Note – prepared by the authors

According to the X-ray diffraction data, reduction in a hydrogen atmosphere leads to the formation of metallic iron (Fe), manganese oxide (MnO), and quartz (SiO_2) phases in the samples. This indicates effective reduction of iron and partial reduction of manganese oxides at temperatures up to 1000 °C.

When the temperature is further increased to 1100 °C with the same holding time of 60 minutes, new complex phases such as $FeMnSiO_4$ and Mn_2SiO_4 appear in the ore.

Thus, it can be concluded that at 1100 °C the reduced components of iron, manganese, and silicon begin to interact, leading to the formation of difficult-to-reduce silicate compounds, which reduces the further efficiency of metal reduction.

CONCLUSIONS

Micro-X-ray spectral analysis of the iron–manganese ore from the “Keregetas” deposit revealed the presence of major elements such as Fe, Mn, Al, Si, Ba, and O. According to X-ray diffraction data, the initial ore contains the following phases: goethite (FeO(OH)), hematite (Fe_2O_3), manganese dioxide (MnO_2), a combined iron–manganese oxide phase ($FeMnO_3$), and silicon dioxide (SiO_2).

During oxidative calcination in an air atmosphere, dissociation of oxygen occurs from the crystal lattice of MnO_2, which reduces the oxidation state of manganese and leads to the formation of lower oxides such as Mn_3O_4 and Mn_2O_3. At the same time, goethite (FeO(OH)) undergoes dehydration and transforms into hematite (Fe_2O_3).

Reductive roasting of the ore in a hydrogen atmosphere at 700–900 °C with a holding time of 60 minutes makes it possible to obtain a soft oxide concentrate enriched in iron and manganese, which can subsequently be effectively separated by smelting or magnetic separation.

However, increasing the temperature to 1000 °C leads to partial reduction of manganese and its loss of up to 4.4 at.%, while further heating to 1100 °C causes sintering of ore particles, which worsens metal reduction and decreases overall mass loss.

Thus, the conducted experiments demonstrate that replacing carbon-containing reducing agents (C, CO) with hydrogen provides the following advantages:

- significant reduction of carbon dioxide emissions;
- improved environmental safety of metallurgical processes;
- selective reduction of iron without substantial loss of manganese;
- creation of prerequisites for developing low-carbon technologies for processing iron–manganese ores.

The development of hydrogen technologies and the decreasing cost of electricity from renewable sources open real opportunities for an economically viable transition to hydrogen use in Kazakhstan's metallurgy and for producing environmentally friendly ferroalloy concentrates.

CONFLICT OF INTEREST: The authors declare that they have no conflicts of interest.

FUNDING: This study was carried out within the framework of a grant-funded research project of the Ministry of Science and Higher Education entitled "Investigation of the possibility of obtaining high-manganese slags from non-conforming iron–manganese ores of Kazakhstan through selective reduction of iron using hydrogen gas" (project No. AR23490490).

ACKNOWLEDGMENTS: The authors sincerely thank Karaganda Industrial University, K. Zhubanov Aktobe Regional University, and South Ural State University (Laboratory of Hydrogen Technologies in Metallurgy) for their administrative and technical support, as well as for providing the necessary infrastructure and resources for this research.

DECLARATION ON THE USE OF ARTIFICIAL INTELLIGENCE TECHNOLOGIES: The authors did not use artificial intelligence (AI) tools at any stage of preparing this work.

REFERENCES

Baisanov, A., Maishina, Z., Isagulov, A., Smagulova, N., & Yudakova, V. (2021). Experimental melting of high-silicon ferromanganese with the use of ferromanganesian ore and manganese slag. Metalurgija, 60, 89–92.

Ernst, M.S., Tangstad, M., & Du Preez, S.P. (2024). Pre-reduction of Nchwaning manganese ore in CO/CO_2, H_2/H_2O, and H_2 atmospheres. Minerals Engineering, 216, 108854.

IRENA. (2023). World Energy Transitions Outlook 2023. International Renewable Energy Agency.

John, D. H. S., & Hayes, P.C. (1982). Microstructural features produced by the reduction of wustite in H_2/H_2O gas mixtures. Metallurgical Transactions B, 13, 117–124.

Kosdauletov, N. Y., & Roshchin, V. E. (2020). Estimation of selective reduction of iron and phosphorus from manganese ores of different genesis. IOP Conference Series: Materials Science and Engineering, 966(1), 012036.

Kosdauletov, N., Mukambetgaliyev, E.K., & Roshchin, V.E. (2021). Separation of ferromanganese ore components by non-contact and contact carbothermic reduction. Izvestiya. Ferrous Metallurgy, 64(10), 761–767.

Kosdauletov, N., Mukambetgaliyev, E.K., & Roshchin, V.E. (2022). Separation of ferromanganese ore components by reduction with carbon and carbon monoxide. Steel in Translation, 52(4), 416–421.

Matthew, S.P., Cho, T.R., & Hayes, P.C. (1990). Mechanisms of porous iron growth on wustite and magnetite during gaseous reduction. Metallurgical Transactions B, 21, 733–741.

Matthew, S.P., & Hayes, P.C. (1990). Microstructural changes occurring during the gaseous reduction of magnetite. Metallurgical Transactions B, 21, 153–172.

Naseri Seftejani, M., & Schenk, J. (2018). Thermodynamic of liquid iron ore reduction by hydrogen thermal plasma. Metals, 8(12), 1051.

Ngoy, D., Sukhomlinov, D., & Tangstad, M. (2020). Pre-reduction behaviour of manganese ores in H_2 and CO containing gases. ISIJ International, 60(11), 2325–2331. https://doi.org/10.2355/isijinternational.ISIJINT-2020-120

Sarkar, A., Schanche, T. L., & Safarian, J. (2023). Isothermal pre-reduction behavior of Nchwaning manganese ore in H_2 atmosphere. Materials Proceedings, 15, 58. https://doi.org/10.3390/materproc2023015058

Schanche, T. L., & Tangstad, M. (2021). Prereduction of Nchwaning ore in $CO/CO_2/H_2$ gas mixtures. Minerals, 11, 1097. https://doi.org/10.3390/min11101097

Suleimen, B., & Salikhov, S. P. (2022). Behavior of extrusion briquettes (Brex) and pellets from oolite iron ore in solid-phase metallization. AIP Conference Proceedings, 2456(1).

Yerbolat, M., Yesmurat, M., & Asyylbek, A. (2024). Modeling the ferrosilicomanganese smelting process using manganese-rich slag. Acta Metallurgica Slovaca, 30(1), 29–33.

Павлов, М. В., Шабанов, В. Ф., & Павлов, В. Ф. (2012). Комплексная переработка высокофосфористых марганцевых руд Новониколаевского месторождения. Химия в интересах устойчивого развития, 20(4), 443–448. // Pavlov, M. V., Shabanov, V. F., & Pavlov, V. F. (2012). Kompleksnaya pererabotka vysokofosforistykh margantsevykh rud Novonikolaevskogo mestorozhdeniya [Comprehensive processing of high-phosphorus manganese ores of the Novonikolaevsk deposit]. Khimiya v interesakh ustoychivogo razvitiya, 20(4), 443–448. (In Russ.)

Рощин, В. Е., Гамов, П. А., Рощин, А. В., & Салихов, С. П. (2023). Перспективы освоения водородных технологий в отечественной металлургии. Черная металлургия. Бюллетень НТЭИ, 79(2), 144–153. https://doi.org/10.32339/0135-5910-2023-2-144-153 // Roshchin, V. E., Gamov, P. A., Roshchin, A. V., & Salikhov, S. P. (2023). Perspektivy osvoeniya vodorodnykh tekhnologiy v otechestvennoy metallurgii [Prospects for the development of hydrogen technologies in national metallurgy]. Chernaya metallurgiya. Byulleten' NTEI, 79(2), 144–153. (In Russ.)

Tastanova, A. Y., Kuldeyev, Y. I., Temirova, S. S., Abdykirova, G. Z., & Biryukova, A. A. (2023). Processing of low-grade manganese-containing raw materials with pellet production for the manufacture of ferromanganese alloys. Engineering Journal of Satbayev University, 145, 10–18.

Government of the Republic of Kazakhstan. (2024). Concept for the development of hydrogen energy in Kazakhstan until 2030. Astana, Kazakhstan.

KazMunayGas Engineering. (2024). Assessment of underground water potential for hydrogen production needs. Atyrau, Kazakhstan.

Information about authors

Yerbol Kuatbay – Doctor of Philosophy (PhD), Karaganda Industrial University, Temirtau, Kazakhstan.
e-mail: ye.kuatbay@tttu.edu.kz
ORCID: https://orcid.org/0000-0002-8400-3537

Asylbek Nurumgaliev – Doctor of Technical Sciences, Professor, Abilkas Saginov Karaganda Technical University, Karaganda, Kazakhstan.
e-mail: anurumgaliyev@tttu.edu.kz ,
ORCID: https://orcid.org/0000-0002-8782-9975

Gulzat Bulekova – PhD doctoral student, Professor, Karaganda Industrial University, Temirtau, Kazakhstan.
e-mail: g.bulekova@tttu.edu.kz,
ORCID: https://orcid.org/0009-0008-0347-8532

Ainagul Otarbayeva – Master of Technical Sciences, K. Zhubanov Aktobe Regional University, Aktobe, Kazakhstan.
e-mail: aotarbayeva@zhubanov.edu.kz,
ORCID: https://orcid.org/0009-0005-3655-6662,

Salikhov Semyon Pavlovich – Candidate of Technical Sciences, South Ural State University (National Research University), Chelyabinsk, Russian Federation.
e-mail: salikhovsp@susu.ru ,
ORCID: https://orcid.org/0000-0002-8818-0450

https://doi.org/10.51885/3134-7983_CATMSP_2026_1_7
SRSTI 67.11.33

STRENGTHENING MASONRY WITH CARBON FIBER REINFORCED POLYMER

Aida Sharapiden [1], **Kuanysh Makashev** [1]*, **Kuandyk Sakanov** [1], **Amangeldy Zhumabaev** [1], **Sultan Makhanov** [1]
[1]Toraighyrov University, Pavlodar, Kazakhstan
*Corresponding author: Makashev Kuanysh Toktarbekovich, e-mail: m.kuanysh87@mail.ru

Keywords:
masonry, carbon, textile-reinforced masonry, epoxy resin, reinforcement, composite material.

ABSTRACT
This study examines the effectiveness of carbon fiber reinforced polymer (CFRP) in enhancing the strength properties of masonry structures. The study focuses on applying epoxy-coated carbon fiber textiles to masonry specimens and analyzing their effects on load-bearing capacity and deformation resistance. The experimental methodology involved testing masonry walls comprising three bricks stacked together. For comparative testing, part of the prepared specimens was reinforced with CFRP, while the other half was left unreinforced. The strengthening specimens' failure mode was the detachment at the junctions of the bricks, which showed joined mortar weakens. Compared, to that the strengthening specimens represent increased ductility, indicating improved structural stability. The study confirms that CFRP is an effective method for strengthening masonry structures. The results indicate that CFRP reinforcement can significantly enhance the durability and service life of masonry buildings. Future research should focus on the long-term performance of CFRP under various environmental conditions and its application in large-scale construction projects.

INTRODUCTION

Prolonging life cycle of unreinforced masonry (UM) structures is an active and innovative field of engineering research. The need for such strengthening is an indisputable fact that a significant part of the buildings currently in operation have long exceeded their originally calculated service life (Askouni & Papanicolaou, 2017). Moreover, the reinforcement of building structures is related to the fact that their technical condition does not meet the requirements of modern building regulations (Babatunde, 2017).

Stone structures are the earliest building systems in the world. Today, it is estimated that stone structures contain more than 70% of the world's housing stock. Moreover, a significant part of these structures includes historical buildings which need to be preserved for the next generation. It is often necessary to strengthen such expensive and historically significant structures since their dismantling and replacement can be more expensive or impossible to repair

(Erdogmus, 2015). Aging structures need to withstand increased loads due to increasing operational requirements, but also withstand the adverse effects of an ever-changing and dynamic environment, such as earthquakes, floods etc.

Reinforcement of masonry structures with composite materials is an effective method that significantly improves the operational characteristics and extends the service life of masonry structures (Can, 2018). Recently developed fibre-reinforced composite material (FRP), comprised of high strength, lightness, corrosion resistance, and flexibility, emergent a promising solution for strengthening existing UM buildings and structures (Tan & Patoary, 2004). The FRP comprise the textile fibre materials embedded in a polymer solution such as epoxy resin. The primary material used in composite structures is a textile which comprises a variety of solutions namely: glass, basalt, and carbon.

Despite numerous experimental and numerical studies conducted in this field, the use of FRP solutions remains largely unexplored in the Kazakhstan region. However, the extreme weather conditions highlight the need for modern composite materials to strengthen ageing buildings against natural hazards or manmade hazards. Enhancing material properties is a fundamental objective in modern engineering practice. Various techniques are employed to improve the key characteristics of materials, one of which involves the application of epoxy resin to textile materials. This coating process has the potential to enhance the mechanical performance of the base material by reinforcing and protecting textile fibers, thereby increasing durability and resistance to external factors. By ACI 549.4 R-13, fabric coating is defined as the application of a polymer intended either for coating or for glueing filaments without completely penetrating and impregnating the fibers, as is observed in fibre-reinforced polymer (FRP) materials. A number of previous studies have shown that impregnation of fabric with epoxy resin increases the mechanical strength of the joint, and the strength of adhesion under friction and stiffness. After impregnation with epoxy resin, textiles take on the appearance of a stiff, thin fabric, effectively reducing slippage between the threads. In cases where a coating is applied, the filaments experience a more uniform stress distribution, which leads to an increase in the participation of filaments in load-bearing functions (Vega & Torres, 2018). This observation provides valuable information about the structural improvements achieved through epoxy impregnation and coating of fabric mater

The basic concept of external reinforcement is following carbon fiber reinforced polymer with high tensile strength prevent transverse deformation of the masonry during axial compression. This makes it possible to restrain the formation of force cracks and limit their width, which in turn increases the load-bearing capacity of the masonry

MATERIALS AND METHODS OF RESEARCH

1 Sample preparation and deposition process

1.1 Tensile test

The reason for the tensile test is to compare the effect of epoxy resin application on the textile. In this project, commercially available textile-fibre materials, i.e., carbon, were used. The textile was strengthened with epoxy resin, and the material characteristics are shown in Table 1. The adhesive comprised of two components, was used as a binder for the production of samples: A – modified epoxy resin, B – plasticizer-hardener. The properties of the textile material, as provided in the manufacturer datasheets, are presented in Table 2. The epoxy-resin is prepared by thoroughly mixing 10 parts of the modified epoxy resin with 1 part of the hardener. The property of epoxy resin are given in Table 1.

Table 1. Property epoxy-resin according to manufacturer data shed

Appearance	Transparent viscous mass without mechanical impurities
Full cure time	24 hours at room temperature from +20 to +25 ° C
Operating temperatures	+10...+35°C
Ultimate strength	at least 8.0 MPa
Note – compiled by the authors	

Table 2. Properties of textile material (manufacturer's data)

Material	W [g/m²]	t [mm]	f [MPa]	E [GPa]	K[N/mm²]
Carbon fiber	220	0.035	4800	225	13.95
Note – compiled by the authors					

The coating process can be described as follows:

– textiles were cut into strips with nominal dimensions: width -80 mm and length – 350 mm;

– the textile material was placed on a flat surface and secured with tape to prevent movement Figure 1a;

– the epoxy resin was applied with a brush Figure 1a;

– an 80x60 mm aluminum plate was attached to both sides of the samples to improve grip in the testing machine Figure 1b;

– the samples were left for two days before the tests Figure 1, c.

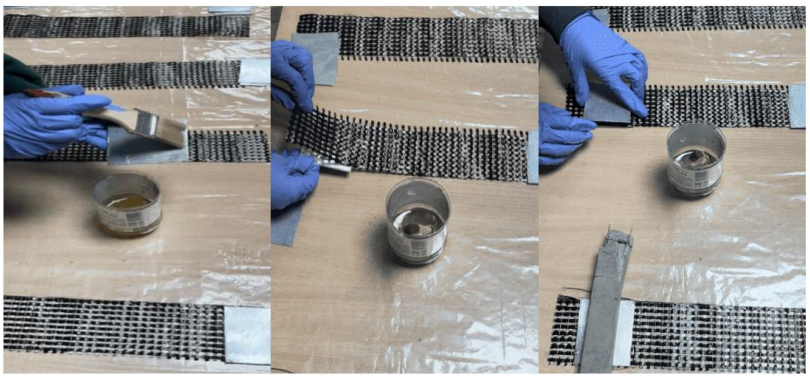

a b c

Figure 1. Sample preparation process: (a) – applying epoxy resin; (b, c) – attaching aluminum plates on both sides of the sample

Note – compiled by the authors

The tensile tests were carried out with motion control at a constant speed of 0.02 mm/sec on a universal testing machine WOW-200 equipped with a 200 kN load cell. It should be noted that the displacement was measured using measuring devices built into the testing machine, and no additional devices were used to measure elongation.

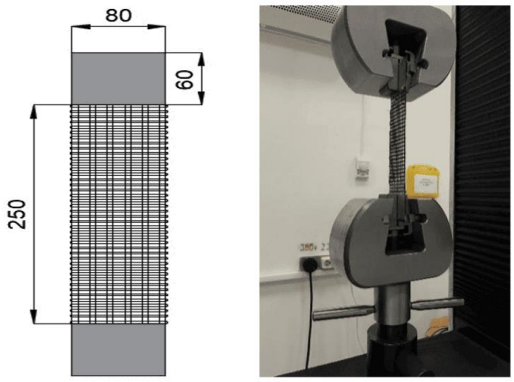

a) b)

Figure 2. STest scheme: (a) – geometry of the textile sample (all dimensions in mm); (b) – actual test scheme

Note – compiled by the authors

1.1 Tensile test

Compression testing of cement-sand mortar cubes is one of the main methods for determining the strength of a given building material.

In this study, a cement-sand mortar was used to connect the bricks to each other. The technical characteristics of the cement-sand mortar are presented in Table 2.

Table 2. Technical characteristics of cement-sand mortar

Brand of the solution	M150
Endurance	B12,5
Frost resistance	F50
Density	2000 kg/m^3
The ratio of cement and sand	1:4
Brand of cement	M400
Full cure time	28 days
Note – compiled by the authors	

The sample manufacturing process can be described as follows:

– a special prefabricated metal mold was used to make the sample cubes from cement-sand mortar. The size of 1 cube is 100x100 mm:

– the sample forms were lubricated with machine oil;

– each cell was filled with cement-sand mortar;

– then compacted the mixture inside the mold by bayoneting it with a rod to remove air bubbles and fill all the voids;

– a day later, the finished cubes were removed from the mold and left for 28 days to completely harden.

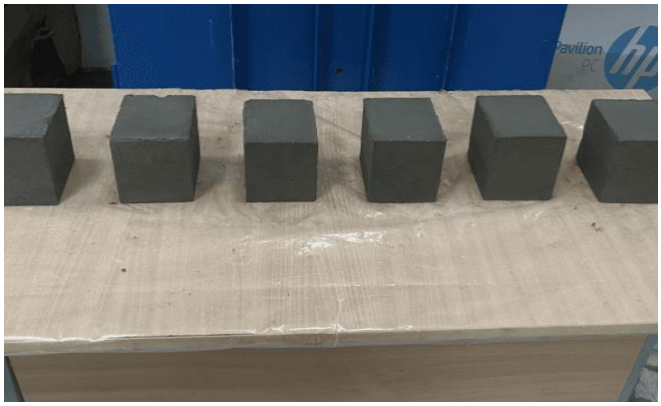

Figure 3. The process of making samples (cubes) from cement-sand mortar – finished samples every other day

Note – compiled by the authors

1.3 Brick triple test

In present experimental campaign, the masonry walls were reinforced with carbon fiber polymer. The samples were tested according to the European standard BS EN 1739:2007. In this method, special reinforced carbon fiber nets are glued to the outer surface of the masonry, which are then coated with epoxy resin. This creates an additional reinforcing structure that increases the strength and stability of the brickwork. The specimen reinforcement scheme is shown in Figure 4.

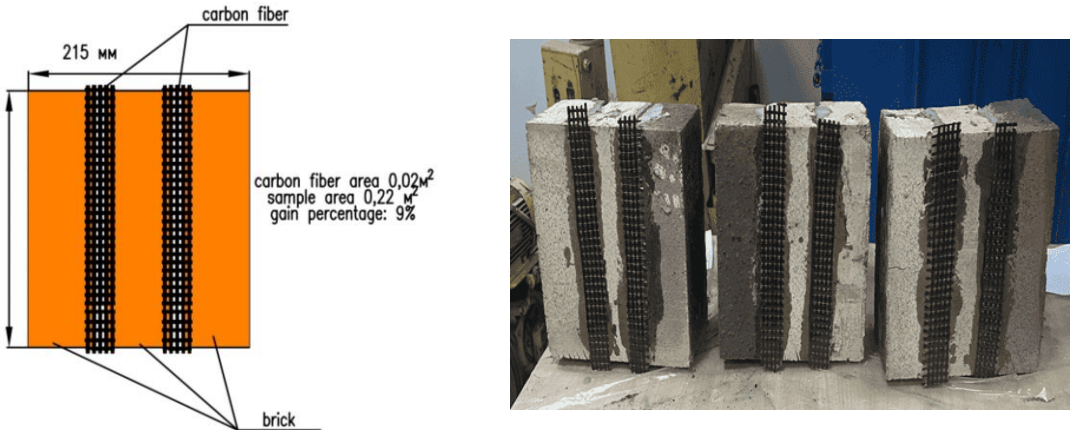

a) b)

Figure 4. Sample strengthening scheme (a) - schematic representation; (b) – real specimens
Note – compiled by the authors

Spacement was placed into the load cell, load was applied vertically from the top of the sample in the middle brick to determine the adhesive property between bricks. The load was applied with a load block using a hydraulics actuator the displacement and the load was recorded in each step. The reinforced part with FRP potentially can postpone the failure and increase the strength of the masonry wall.

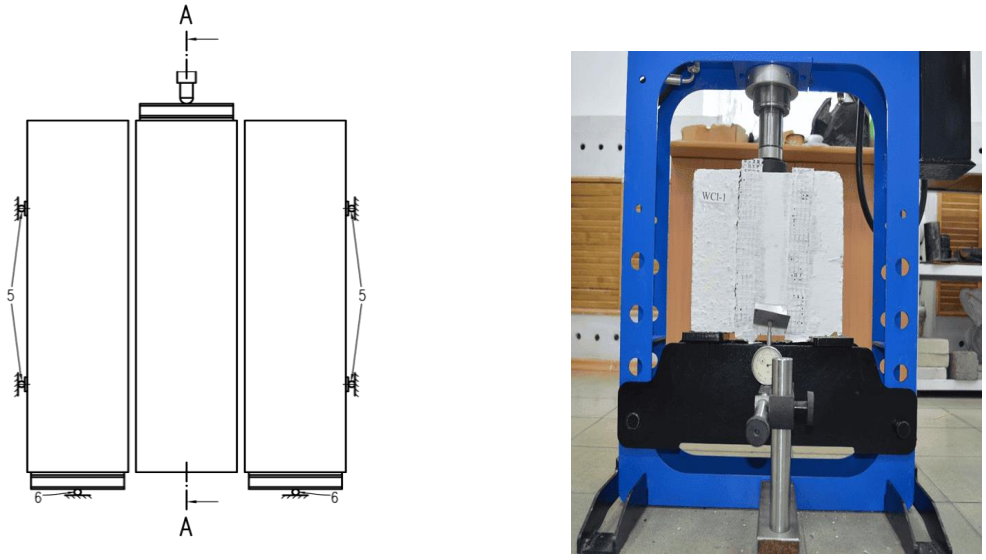

a) b)

Figure 5. Diagram of an alternative test facility: 1 – hydraulic jack; 2 – soft fiberboard; 3 – clock type indicator or motion sensor; 4 – mechanical or continuous connection; 5 – side supports with force sensor; 6 – steel roller; 7 – steel rollers with a diameter of 40 mm [53]
Note – compiled by the authors

The sample preparation process can be described as follows:

- commercially available ceramic hollow bricks with dimension of 250x120x65 mm were selected for testing;

- each sample consisted of 3 bricks, which were connected with a cement-sand mortar 10 mm thick, then the samples were left for 28 days to completely harden.;

- after 28 days, half of the samples were reinforced with carbon fiber. First, the first layer of epoxy resin was applied to the seams of the brick on one side using a brush. Then carbon fiber (260 mm long, 40 mm wide) was applied to this layer, smoothing it to ensure a tight fit. After that, a second layer of epoxy resin was applied over the carbon fiber, completely impregnating the fabric. The finished samples were left for two more days.

Compression tests were carried out at the hydraulic actuator with 200 kN load cell. The load cell is a consisting of racks, slats, upper and lower beams and a drive, the main working element of which is a bottle-type hydraulic jack. The movements were measured using a displacement sensor.

RESULTS AND DISCUSSION

Three trials were reviewed in this article.:

1) Carbon fiber tensile testing;

2) compression test of cement-sand mortar cubes;

3) compression testing of carbon fiber reinforced brick samples

The results of the tensile test shown in Figure 7a, b were textile rupture jccored in a centre part of the specimens. The graph of the stress-strain state is shown in Figure 7 c and Table 4 shows the maximum stress and modulus of elasticity. As expected, the trend was linear in all cases before the collapse.

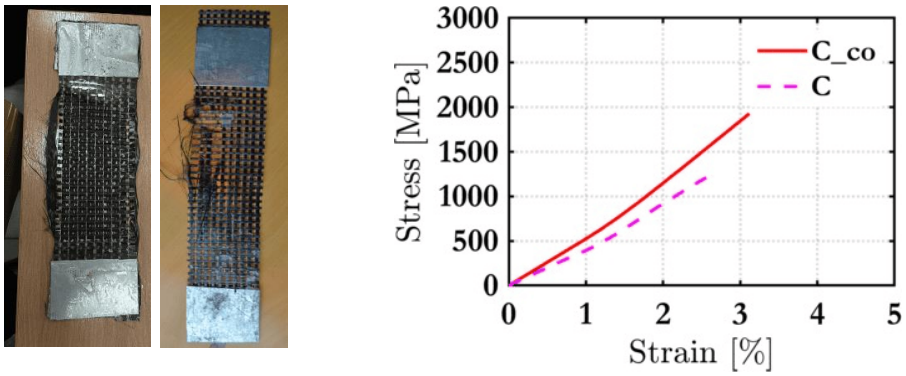

a) b) c)

Figure 7. Failure modes during tensile testing of textiles:
(a) – uncoated; (b) – coated; (c) – Stress strain plot

Note: compiled by the authors

Figure 7c shows a direct comparison of stress-strain graphs of coated (C_co) and uncoated (C) textile samples. The results show the positive effects of epoxy coating.

Table 4. Tensile test results

Textile	Tension [MPa]	Modulus of elasticity [GPa]
C	1207 (159) *(13) **	134 (6) * (4.4) **
C_co	1939 (52) *(2.71) **	165(3) *(1.8) **
Note – compiled by the authors		

*Standard deviation, **Coefficient of variation

Hardening textiles with epoxy resin increases load resistance by 60%, and the modulus of elasticity increases by 23%, which indicates a significant strengthening of the textile material, making it more durable.

However, the application of epoxy resin has a drawbacks. One of them is the reduced flexibility of textiles. Increased strength is achieved through flexibility, which limits the use of textiles on flat surfaces. This limitation may affect the versatility of the material, making it less suitable for use on curved or uneven surfaces.

The test results confirm the postponement of failure risks due to reinforcement with epoxy resin. These results highlight the potential benefits of epoxy coated textiles and the importance of considering specific application requirements in practical use.

From a practical point of view, the choice in favor of using textiles coated with epoxy resin should be based on the specific requirements of the intended application, such as the shape of the applied surface.

Compression tests of cement-sand mortar cubes were carried out on a PGM-1500MG4 test hydraulic press for 1,500 kN. Structurally, the press is a machine consisting of a loading device and a force meter Figure 8.

Figure 8. Compression testing of samples (cubes)– samples after the test
Note – compiled by the authors

In general, the test showed that the cement-sand mortar in these samples has certain compressive strength limits, when exceeded, the material begins to break down. Cracks and splinters indicate points of maximum stress and structural failure. This behavior is typical for cement-based materials when they are subjected to high compressive loads.

Table 5 shows the test result of the samples.

Table 5. Compression test result (average value)

Sample	Load Pк [kN]	Load R [MPa]
Cube 100x100	23,75	2,256
Note – compiled by the authors		

Figure 9a shows the process of testing a sample on a hydraulic press. First, the samples were tested without reinforcement. They were tested without any additional enhancements, which allowed us to evaluate their natural properties and stability. Without reinforcement, the sample showed low strength, manifested in fracture and breaking apart. Based on this result, it can be concluded that without additional reinforcement, the material is not able to withstand high loads.

Figures 9b, show the process of testing a sample reinforced with FRP in a hydraulic press. It can be seen that the sample is under load, but the structure remains relatively intact, although there are noticeable cracks. Reinforcement with epoxy resin and carbon postponing failure, preventing its complete destruction and allowing it to withstand a higher load compared to a non-reinforced sample.

a) b)

Figure 9. The testing process:
(a) – a sample without reinforcement; (b) – a sample reinforced with FRP
Note – compiled by the authors

The graph of the load versus displacement (average value) for non-reinforced and reinforced samples is shown in Figure 10. For non-reinforced samples (W), the load increases rapidly, reaching a maximum load value of 21 kN with a displacement of 0.4 mm. After that, the load stabilizes and begins to decrease, which indicates the beginning of sample destruction. This shows that non-reinforced samples reach their ultimate strength with relatively little movement.

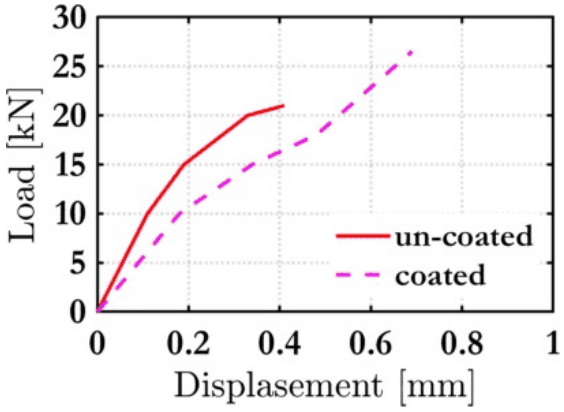

Figure 10. Comparison of reinforced and non-reinforced samples
Note – compiled by the authors

For reinforced samples (WC), the maximum applied load reached a maximum value of 27 kN with a displacement of 0.7 mm. Even though the reinforcement area was insignificant, carbon fiber-reinforced samples showed better load resistance compared to non-reinforced ones.

In general, the graph shows an improvement in the mechanical characteristics of reinforced samples compared to non-reinforced ones. Reinforced samples achieve higher strength, and withstand higher loads. The test results are shown in Table 6.

Table 6. Compression test results

Sample	Maximum load [kN]	Displacement [mm]
W	21	0,4
WC	27	0,7
Note – compiled by the authors		

CONCLUSION

According to the acquired results from the current experimental work, the following findings can be concluded:

– The reinforced samples showed a improvement in strength characteristics. The maximum load increased by 22 percent compared to unreinforced one.

– The reinforced samples showed more stable behavior under load: after reaching the peak, the load did not drop sharply, but showed a gradual decrease, which indicates better resistance to fracture.

– The increased strength and improved deformation characteristics can be explained by the use of carbon fiber and epoxy resin, which effectively distribute the load and prevent rapid destruction of the material.

– The results confirm the effectiveness of using carbon fiber and epoxy resin to improve the mechanical properties of materials. Future work should focus on the increasing percentage of the strengthening zone to develop an effective cover area.

CONFLICT OF INTEREST: The authors declare no conflict of interest.

FUNDING: This article was prepared without funding.

ACKNOWLEDGEMENTS: This section acknowledges individuals and organizations that contributed to the study. For example:

"The authors thank their colleagues for their methodological support and helpful discussions, as well as the anonymous reviewers for their valuable comments that helped improve the quality of the article.

STATEMENT ON THE USE OF ARTIFICIAL INTELLIGENCE TECHNOLOGIES: The authors declare that no artificial intelligence (AI) tools were used in the preparation on this article.

REFERENCES

Askouni, P. D., & Papanicolaou, C. G. (2017). Experimental investigation of bond between glass textile reinforced mortar overlays and masonry: The effect of bond length. Materials and Structures, 50(2), 164.

Babatunde, S. A. (2017). Review of strengthening techniques for masonry using fiber reinforced polymers. Composite Structures, 161, 246–255.

Белов, В. В., & Деркач, В. Н. (2010). Экспертиза и технология усиления каменных конструкций. Инженерно-строительный журнал, 17(7), 14–20. // Belov, V. V., & Derkach, V. N. (2010). Ekspertiza i tekhnologiya usileniya kamennykh konstruktsii [Expertise and technology of reinforcement of stone structures]. Inzhenerno-stroitel'nyi zhurnal – Magazine of Civil Engineering, 17(7), 14–20. (In Russ.)Can, Ö. (2018).

Investigation of seismic performance of in-plane aligned masonry panels strengthened with Carbon Fiber Reinforced Polymer. Construction and Building Materials, 186, 854–862.

de Andrade Silva, F., Butler, M., Hempel, S., Toledo Filho, R. D., & Mechtcherine, V. (2014). Effects of elevated temperatures on the interface properties of carbon textile-reinforced concrete. Cement and Concrete Composites, 48, 26–34.

Dushimimana, A., Ziada, M., & Tuhta, S. (2018). Effect of carbon fiber reinforced polymer (CFRP) composites applied to walls and slabs of masonry building. Development, 5(4), 2434–2442.

Erdogmus, E. (2015). Use of fiber-reinforced cements in masonry construction and structural rehabilitation. Fibers, 3(1), 41-63.

Hemeda, S. (2018, October). Carbon Fiber Reinforced Polymers (CFRP) for Strengthening and Seismic Retrofitting of Historic Circular Masonry Stone Columns. In International Congress and Exhibition "Sustainable Civil Infrastructures: Innovative Infrastructure Geotechnology" (pp. 114–137). Cham: Springer International Publishing.

Koeckritz, U., Cherif, C., Weiland, S., & Curbach, M. (2010). In-situ polymer coating of open grid warp knitted fabrics for textile reinforced concrete application. Journal of Industrial Textiles, 40(2), 157–169.

Makashev, K., Triantafyllou, S. P., Thermou, G. E., & Tizani, W. (2023). Bond behaviour of light and heavy carbon fibre TRM to masonry interfaces. Construction and Building Materials, 400, 132508.

Орлович, Р., Мантегатса, Д., Найчук, А., & Деркач, В. (2010). Современные способы ремонта и усиление каменных конструкций. Архитектура, дизайн и строительство, 1(44), 86–87. // Orlovich, R., Mantegatstsa, D., Naichuk, A., & Derkach, V. (2010). Sovremennye sposoby remonta i usilenie kamennykh konstruktsii [Modern methods of repair and reinforcement of stone structures]. Arkhitektura, dizain i stroitel'stvo – Architecture, Design and Construction, 1(44), 86–87. (In Russ.)

Tan, K. H., & Patoary, M. K. H. (2004). Strengthening of masonry walls against out-of-plane loads using fiber-reinforced polymer reinforcement. Journal of Composites for Construction, 8(1), 79–87.

Umair, S. M., Abbas, H., Ahmed, S., & Waheed, A. (2015). Fiber reinforced polymer and polypropylene composite retrofitting technique for masonry structures. Polymers, 7(5), 963–984.

Vega, C., & Torres, N. (2018). External strengthening of unreinforced masonry walls with polymers reinforced with carbon fiber. Ingeniería e Investigación, 38(3), 15–23.

Yin, S., Xu, S., & Li, H. (2013). Improved mechanical properties of textile reinforced concrete thin plate. Journal of Wuhan University of Technology – Mater. Sci. Ed., 28(1), 92-98.

Information about authors

Sharapiden Aida Zhumagalyevna – Master of Technical Sciences, Toraighyrov University, Pavlodar, Kazakhstan,
e-mail: aida.sharapyden@mail.ru,
ORCID: https://orcid.org/0000-0002-7179-9759,

Makashev Kuanysh Toktarbekovich – PhD, Toraighyrov University, Pavlodar, Kazakhstan,
e-mail: m.kuanysh87@mail.ru,
ORCID: https://orcid.org/0009-0005-2971-6322

Sakanov Kuandyk Timirovich – Candidate of Technical Sciences, Toraighyrov University, Pavlodar, Kazakhstan,
e-mail: kuan_altei@mail.ru,
ORCID: https://orcid.org/0000-0003-2897-2947

Zhumabaev Amangeldy Kayratovich – Master of Technical Sciences, Toraighyrov University, Pavlodar, Kazakhstan,
e-mail: aman_31_98@mail.ru,
ORCID: https://orcid.org/0009-0002-1203-1907

Makhanov Sultan Nurbolatovich – Master of Technical Sciences, Toraighyrov University, Pavlodar, Kazakhstan,
e-mail: mahanov-s@mail.ru,
ORCID: https://orcid.org/0000-0002-8758-3987

Vol. 1, Issue 1, March 2026.
CENTRAL ASIAN TRANSACTIONS ON MATERIALS STRUCTURE AND PROPERTIES

https://doi.org/10.51885/3134-7983_CATMSP_2026_1_8
SRSTI 55.22.23

COMPREHENSIVE EVALUATION OF THE CORROSION, EROSION, AND ABRASION RESISTANCE OF HVOF WC–CO–CR COATINGS ON 30KH13 STEEL

Nazerke Muktanova[1,2*], **Małgorzata Rutkowska-Gorczyca**[3], **Nurtoleu Magazov**[1], **Bauyrzhan Rakhadilov**[2]

[1]NJSC "D. Serikbayev EKTU", Ust-Kamenogorsk, Kazakhstan
[2]PlasmaScience LLP, Ust-Kamenogorsk, Kazakhstan
[3]Wrocław University of Science and Technology, Wrocław, Poland
*Corresponding author: Nazerke Muktanova, e-mail: muktanovan@gmail.com

Keywords:
metal-ceramic coating, HVOF method, erosion, corrosion, abrasion resistance, microstructure, wear resistance

ABSTRACT

This study presents a comprehensive experimental investigation of the corrosion, erosion, and abrasive wear resistance of WC–Co–Cr coatings deposited on 30Kh13 martensitic steel using the high-velocity oxygen-fuel (HVOF) spraying method. Corrosion tests were performed under cyclic salt fog conditions in a 5% NaCl solution, while erosion tests were carried out under the impact of an abrasive particle flow. Abrasive wear was evaluated using a standard method with the calculation of relative wear resistance. The results showed that the WC–Co–Cr coating significantly reduces mass loss and slows the development of corrosion and erosion damage compared with uncoated steel. Under abrasive wear conditions, the relative wear resistance of the coated samples is approximately nine times higher than that of 30Kh13 steel. Microstructural analysis revealed that coating degradation is localized and mainly associated with the destruction of the binder phase. The obtained results confirm the effectiveness of WC–Co–Cr HVOF coatings for protecting parts operating under combined corrosion-mechanical influences.

INTRODUCTION

Intensive wear and corrosion degradation of metallic materials remain one of the key problems in the operation of equipment in the oil and gas, energy, and pumping industries. Working elements such as valves, pump wheels, and gate valves are subjected to the combined effects of abrasive particles, erosive flows, and aggressive corrosive environments (Rao & Mulky, 2023; Gao et al., 2024; Xi et al., 2021; Wang et al., 2019).

Martensitic corrosion-resistant steel 30Kh13 is widely used due to its satisfactory mechanical properties and moderate corrosion resistance. However, under conditions of abrasive erosion and chloride exposure, its operational properties prove to be insufficient, leading to accelerated surface destruction and a reduction in product life (Sola et al., 2013; Scheuer et al., 2019; Xi et al., 2021).

One of the most effective ways to increase wear and corrosion resistance is to apply protective coatings using high-velocity oxygen fuel (HVOF) spraying. This method allows the formation of dense coatings with low porosity, high adhesion, and minimal decarburization of the carbide phase (Sidhu et al., 2005; Sahraoui et al., 2010; Kear et al., 2001; El Rayes et al., 2022).

Among carbide systems, WC–Co–Cr coatings are of particular interest, as the presence of chromium in the binder phase increases corrosion resistance compared to traditional WC–Co coatings, especially in chloride-containing environments (Picas et al., 2019; Magnani et al., 2007; Wang et al., 2019). It has been previously shown that such coatings effectively resist abrasive and erosive wear, but the nature of degradation significantly depends on the spraying parameters, coating thickness, and operating conditions (Sapate et al., 2021).

At the same time, there is insufficient systematic experimental data in the literature comparing the behavior of HVOF WC–Co–Cr coatings and martensitic steels under conditions of corrosion, erosion, and abrasive wear obtained in a single study.

The aim of this work is to conduct a comprehensive study of the corrosion, erosion, and abrasion resistance of WC–Co–Cr coatings applied by the HVOF method to 30Kh13 steel, with a quantitative comparison of their performance characteristics with untreated steel. Particular attention is paid to the kinetics of mass loss, surface morphology, and degradation mechanisms.

MATERIALS AND METHODS

Corrosion-resistant steel 30Kh13 and 86WC-10Co-4Cr coating (further WC-Co-Cr) applied to the surface of this steel were selected as the research materials. Before spraying, the samples were subjected to mechanical processing, degreasing, and abrasive jet cleaning to ensure the required surface roughness. The WC–Co–Cr coating was applied by high-velocity oxygen fuel (HVOF) spraying using commercial 86WC-10Co-4Cr powder with a fraction of 30-40 μm. The spraying distance was 300 mm. Propane was used as fuel, oxygen served as an oxidizer, and air was used to cool the nozzle. The main parameters of the spraying process are given in Table 1.

Table 1. HVOF spraying parameters

№	Propane pressure, bar	Oxygen pressure, bar	Air pressure, bar
HVOF method	2.9	5	3.2
Note – compiled by the authors			

The corrosion resistance of the samples was evaluated using a cyclic salt spray test in a 5% aqueous NaCl solution. One test cycle consisted of exposure to salt spray for 1 hour at a temperature of 25–35 °C, followed by drying of the samples at a temperature of 35 °C for 1 hour. After each cycle, the samples were rinsed with distilled water, dried, and weighed on analytical scales with an accuracy of 0.1 mg. The criteria for assessing corrosion resistance were the loss of sample mass and the appearance of visual signs of corrosion damage to the surface. Erosion resistance tests were conducted at room temperature in accordance with ASTM G76-04. During the experiment, a nozzle with an inner diameter of 5 mm was placed at a distance of 10 mm from the sample surface and oriented perpendicular (at an angle of 90°) to its surface. Quartz sand with a particle size of 50 μm was used as the erosion abrasive. The duration of one exposure cycle was 3 minutes. Before the start of the tests, the samples were weighed on electronic analytical scales with an accuracy of 0.01 mg, after which they were fixed in a holder and exposed to abrasive particles. At the end of the tests, the samples were removed, cleaned in acetone, and reweighed to determine the mass loss due to erosion wear. Samples made of 30Kh13 steel and samples coated with WC–Co–Cr were tested under identical conditions. Abrasive wear resistance was investigated in accordance with GOST 23.208–79. For 30Kh13 steel samples, the tests were carried out at a rotation speed of 600 rpm and a duration of 10 minutes, while for WC–Co–Cr coatings, the modes of 1800 rpm and 30 minutes at a load of 44 N were used. Steel 45 according to GOST 1050-88 in an annealed state with a hardness of 190–200 HV was used as a reference material. The wear resistance of the tested materials was evaluated by comparing their wear with that of the

reference sample. To determine mass loss, the samples were weighed on CRYSTAL 100 CALCE analytical scales with an accuracy of 0.1 mg before and after testing. Mass loss during wear was at least 5 mg. The relative wear resistance of the coatings was calculated based on the data obtained. The surface morphology and microstructure of the cross-sections of the coatings were studied using scanning electron microscopy (SEM) on a SEM3200 instrument equipped with an XFlash Detector 730M-300 (Bruker) energy-dispersive X-ray microanalysis (EDS) system.

All experiments were performed at least three times to ensure the reproducibility of the results.

RESULTS AND DISCUSSION

Figure 1 shows images of the surface of samples with WC–Co–Cr coating and samples of 30Kh13 steel without coating before and after exposure to cyclic salt spray.

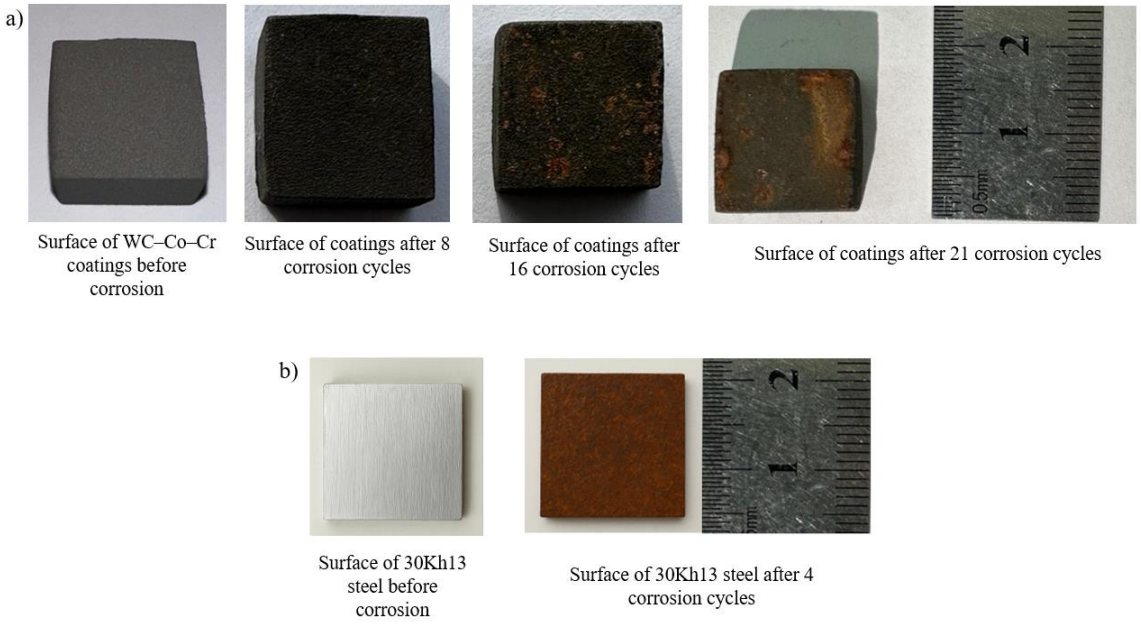

a) sample with 86WC-10Co-4Cr coating; b) sample made of 30Kh13 steel without coating

Figure 1. Surface of test samples before and after corrosion testing in a salt spray chamber

Note – compiled by the authors

The initial state of the WC–Co–Cr coating is characterized by a dense and uniform surface without visible defects. After 8 cycles of corrosion exposure, slight darkening of the surface is observed, with no signs of corrosion. After 16 cycles, local corrosion damage in the form of individual pitting is observed. Further exposure up to 21 cycles leads to more pronounced surface degradation and partial destruction of the coating in certain areas. In contrast to the coated sample, uncoated 30Kh13 steel exhibits low corrosion resistance. As shown in Figure 1b, after only 4 cycles of exposure, pronounced corrosion damage and the formation of rust products are observed, indicating intense degradation of the steel surface in a chloride-containing environment.

The quantitative assessment of corrosion resistance was carried out based on mass loss measurements (Figure 2).

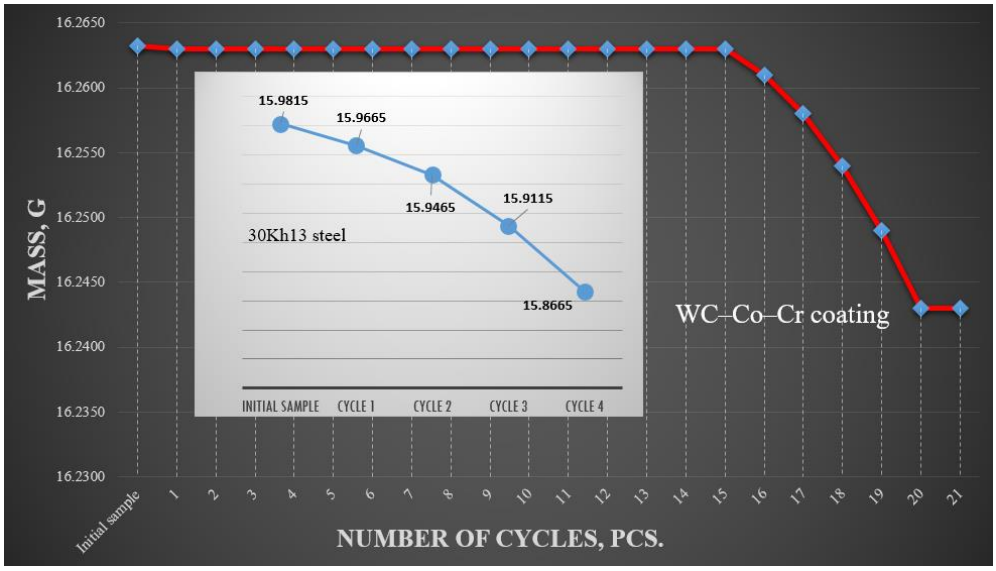

Figure 2. Graph showing the dependence of the mass loss of 30Kh13 steel and 86WC-10Co-4Cr coating on the number of cycles

Note – compiled by the authors

Uncoated 30Kh13 steel samples are characterized by a rapid decrease in mass starting from the first cycle of corrosion exposure. After four cycles, the total mass loss was 115 mg, which corresponds to intensive corrosion destruction of the surface. At the same time, samples with WC–Co–Cr coating retained virtually unchanged mass up to 15 cycles. A noticeable mass loss was recorded only after 16 cycles, and the total mass loss after 21 cycles was 20.2 mg, which is more than five times less than that of untreated steel.

Figure 3 shows a SEM image of the surface of 30Kh13 steel after 4 cycles of corrosion testing in cyclic salt spray conditions, as well as the results of energy-dispersive mapping of the distribution of chemical elements (Fe, Cr, O, Cl, C).

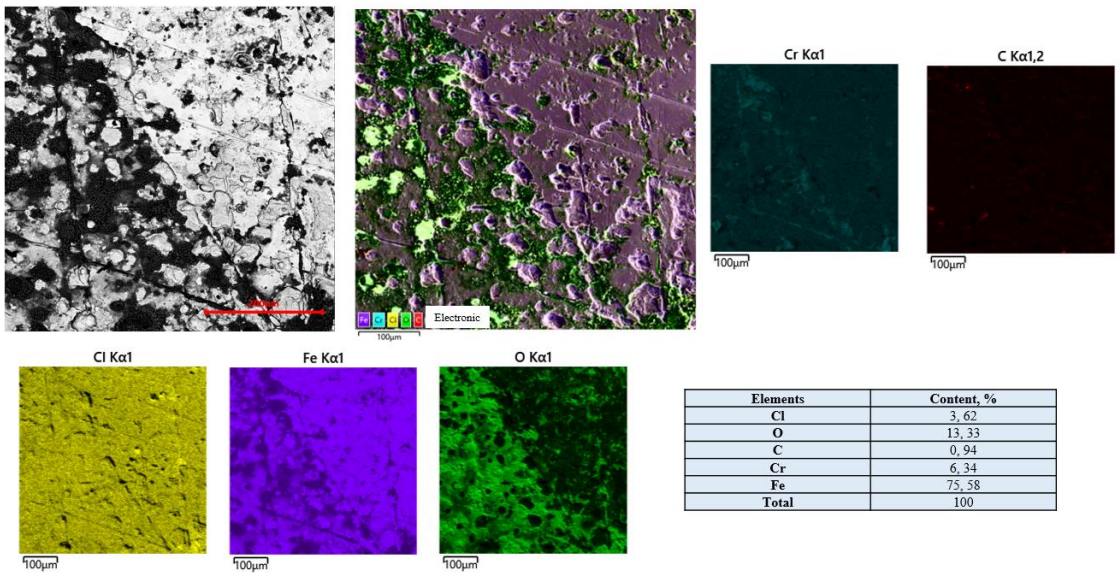

Elements	Content, %
Cl	3, 62
O	13, 33
C	0, 94
Cr	6, 34
Fe	75, 58
Total	100

Figure 3. SEM image of the surface of 30Kh13 steel and the results of elemental mapping after 4 cycles of cyclic salt spray exposure

Note – compiled by the authors

The SEM image shows pronounced localized corrosion damage to the surface, accompanied by the formation of pitting, pores, and areas with corrosion products. Element mapping reveals an increased concentration of oxygen and chlorine in the damaged areas, which indicates the formation of oxide and chloride-containing corrosion products and confirms the development of chloride-induced pitting corrosion. The distribution of iron remains relatively uniform and corresponds to the metal matrix of steel, while the chromium content is reduced, indicating a violation of the passive protective layer under the influence of an aggressive corrosive environment. Quantitative EDS analysis shows a predominance of iron (75.58 wt.%) and the presence of oxygen (13.33 wt.%) and chlorine (3.62 wt.%), confirming intense corrosion oxidation of the surface.

Figure 4 shows SEM images of the surface of the 86WC–10Co–4Cr coating after 21 cycles of corrosion testing in cyclic salt spray conditions: (a) general view of the coating surface, (b) surface areas with marked points for point energy dispersive (EDS) analysis (spectra 1–4).

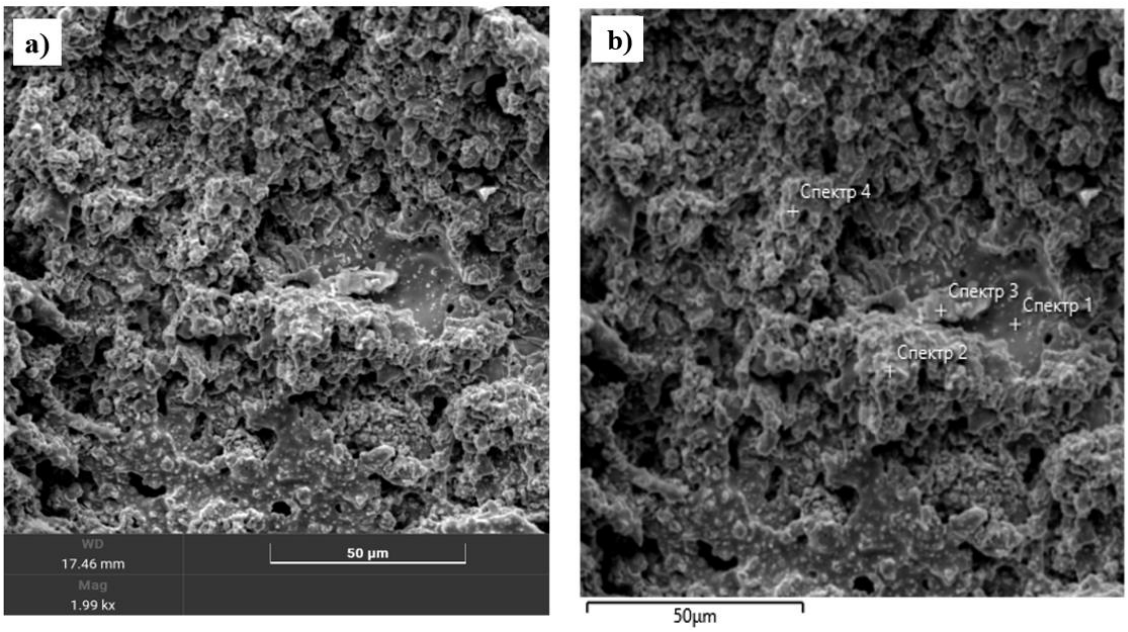

Figure 4. Surface morphology of the 86WC–10Co–4Cr coating (a) and results of point EDS analysis (b) after 21 cycles of cyclic salt spray exposure

Note – compiled by the authors

SEM images show a pronounced micro-relief and porous surface structure formed as a result of corrosion by a chloride-containing environment. Local areas of degradation of the binder phase, pores, and areas of loose corrosion products are observed, indicating the development of selective corrosion of the metal matrix of the coating. The results of point EDS analysis (Figure 4b, Table 2) show variations in elemental composition in different areas of the surface.

Table 2. Results of point EDS analysis of the 86WC-10Co-4Cr coating

Spectrum	O (mass %)	Cr (mass %)	Co (mass %)	W (mass %)
1	3.14	5.38	19.03	72.45
2	13.96	2.94	11.03	72.07
3	8.33	56.49	-	35.18
4	18.59	6.33	10.67	64.40

Note – compiled by the authors

The oxygen content varies in the range of 3.14–18.59 wt.%, reflecting different degrees of surface oxidation. The high mass fraction of tungsten (35.18–72.45 wt.%) confirms the preservation of the WC carbide phase, while fluctuations in the cobalt and chromium content indicate redistribution and partial leaching of the binder phase under the influence of the corrosive environment. The data obtained indicate the localized nature of the corrosion degradation of the coating without signs of its continuous destruction.

Analysis of the cross-section of the 86WC–10Co–4Cr coating using SEM (Figure 5) showed that the coating remains continuous after corrosion exposure, with an average thickness of about 59 μm. In the near-surface zone of the coating, porous areas, local defects, and cracks were observed, spreading mainly from the surface into the depth of the layer, which indicates the development of corrosion degradation under the action of a chloride-containing environment. No significant signs of through-corrosion or delamination of the coating from the substrate were observed.

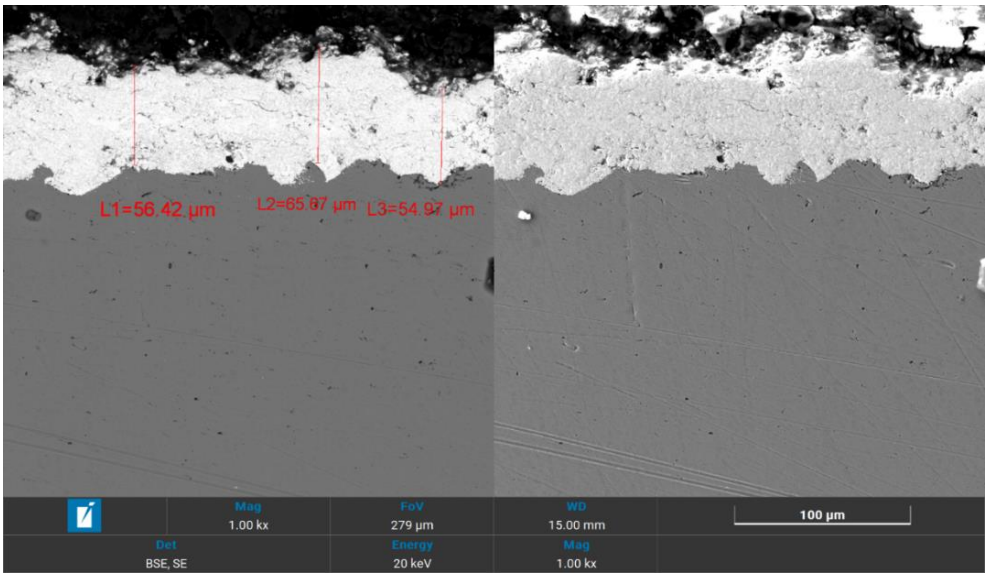

Figure 5. Microstructure of a cross-section of the WC-Co-Cr coating after exposure to a cyclic corrosion test in salt fog

Note – compiled by the authors

Figure 6 shows the results of elemental mapping and linear energy dispersive (EDS) analysis of the cross section of the WC–Co–Cr coating after corrosion testing in cyclic salt spray conditions: (a) distribution maps of the elements W, Co, Cr, Fe, O, and C; (b) profiles of EDS signal intensity changes along the line of analysis crossing the coating and substrate. Element mapping indicates that the compositional integrity of the coating is preserved throughout its thickness, with increased oxygen content localized mainly in the near-surface zone, indicating the development of oxidative processes. Cobalt and chromium signals correspond to the binder phase of the coating and are distributed uniformly throughout the thickness of the layer. Linear EDS analysis shows a sharp decrease in the intensity of the W signal and a simultaneous increase in the Fe signal at the coating-substrate interface, confirming a clear boundary between the layers.

Overall, the results obtained indicate that the application of a WC–Co–Cr coating significantly increases the corrosion resistance of 30Kh13 steel under cyclic salt spray conditions. The coating effectively delays the onset of corrosion damage and reduces the rate of mass loss, despite the development of local degradation of the binder phase during prolonged exposure to an aggressive environment.

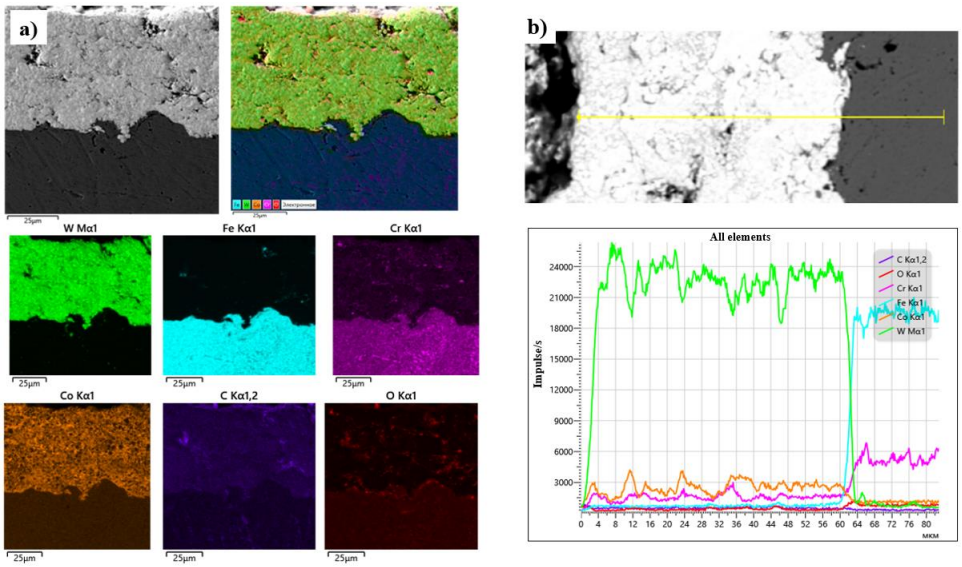

Figure 6. Elemental distribution (a) and linear EDS analysis of the cross-section of the WC–Co–Cr coating (b) after exposure to cyclic salt spray

Note – compiled by the authors

Under real operating conditions, materials and protective coatings are often exposed not only to corrosion but also to erosion caused by the action of solid particle flows. In this regard, for a comprehensive assessment of the operational reliability of 30Kh13 steel and WC-Co-Cr coatings, the next stage of work was to study their erosion resistance under identical test conditions.

Figure 7 shows the evolution of the surface of uncoated 30Kh13 steel during erosion testing. Already after the first cycle, the appearance of a matte zone in the center of the impact area is observed, which indicates the initial stage of abrasive wear. As the number of cycles increases, the eroded area expands and deepens. Starting from the third cycle, a pronounced crater-like depression forms, corresponding to the area of direct impact of abrasive particles. After the sixth cycle, the destruction becomes three-dimensional and is accompanied by significant thinning of the material, indicating high intensity of localized erosion wear.

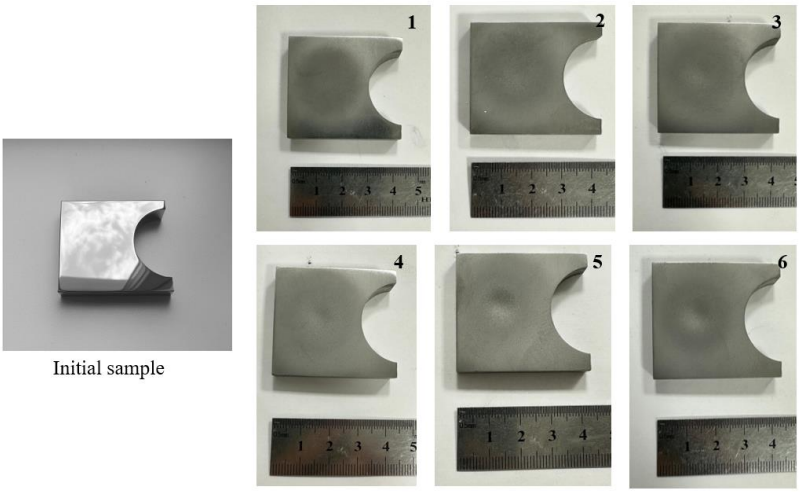

Figure 7. Change in the condition of the surface of uncoated 30Kh13 steel during erosion (cycles 1–6)

Note – compiled by the authors

A quantitative assessment of the erosion damage to 30Kh13 steel was carried out on the basis of cycle-by-cycle mass measurements (Table 3).

Table 3. Change in the mass of 30Kh13 steel during erosion tests

Cycle	Mass, g	Mass loss per cycle, g	Mass loss per cycle, mg
Initial	64, 2477	-	-
Cycle 1	64, 1560	0, 0917	91.7
Cycle 2	64.0512	0.1048	104.8
Cycle 3	63.9156	0.1356	135.6
Cycle 4	63.7109	0.2047	204.7
Cycle 5	63, 4013	0.3096	309.6
Cycle 6	63.0012	0.4001	400.1
Note – compiled by the authors			

The total mass loss after six cycles was 1.2465 g, which corresponds to approximately 1.94% of the initial mass of the sample. The nature of the mass change indicates progressive and accelerating wear, especially after the fourth cycle, when mass loss exceeds 200 mg per cycle. The data obtained indicate low erosion resistance of 30Kh13 steel under the specified test conditions.

To increase erosion resistance, a coating of 86WC–10Co–4Cr was applied to the surface of 30Kh13 steel using high-velocity oxygen fuel (HVOF) spraying. The average thickness of the formed coating was about 360 μm. The sequence of changes in the coating surface during erosion testing is shown in Figure 8.

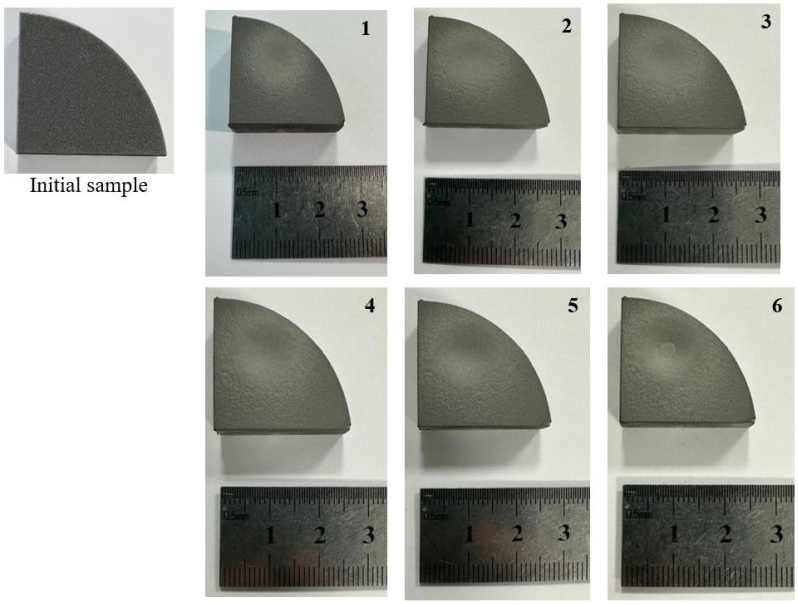

Figure 8. Changes in the surface of the 86WC-10Co-4Cr coating after each of the six cycles of erosion exposure

Note – compiled by the authors

At all stages of testing, three characteristic zones are clearly visible on the surface: a central zone of intense erosion, a zone of moderate wear, and a peripheral area with minimal damage.

Cycle-by-cycle weighing of coated samples (Table 4) showed that in the first four cycles, the mass loss increased relatively smoothly and did not exceed 121.6 mg per cycle.

Table 4. Change in mass of the WC-Co-Cr coated sample during erosion testing

Cycle	Mass, g	Mass loss per cycle, g	Mass loss per cycle, mg
Initial	31.4067	-	-
Cycle 1	31, 3412	0, 0655	65.5
Cycle 2	31, 2511	0.0901	90.1
Cycle 3	31, 1452	0.1059	105.9
Cycle 4	31, 0236	0.1216	121.6
Cycle 5	30.8213	0.2023	202.3
Cycle 6	30, 5200	0.3013	301.3
Note – compiled by the authors			

A significant increase in mass loss is observed after the fifth cycle, accompanied by a sharp deterioration in the surface condition, indicating the destruction of the binder phase and partial breakdown of the coating. In the sixth cycle, local exposure of the substrate is recorded, confirmed by an increase in mass loss to 301.3 mg. The total mass loss of the coated sample after six cycles was 0.8867 g (2.82% of the initial mass). Although the relative mass loss of the coating is comparable to that of steel, the nature of the wear is fundamentally different. The WC–Co–Cr coating effectively inhibits erosion damage in the initial and intermediate stages of exposure, while the sharp acceleration of wear is associated with the protective layer reaching a critical state and the abrasive reaching the substrate.

A comparative analysis of the mass loss curves (Figure 9) shows that uncoated samples are characterized by significantly more intense erosion wear, especially starting from the fourth cycle. At the same time, the WC–Co–Cr coating provides a smoother mass change and delays the development of intense erosion damage.

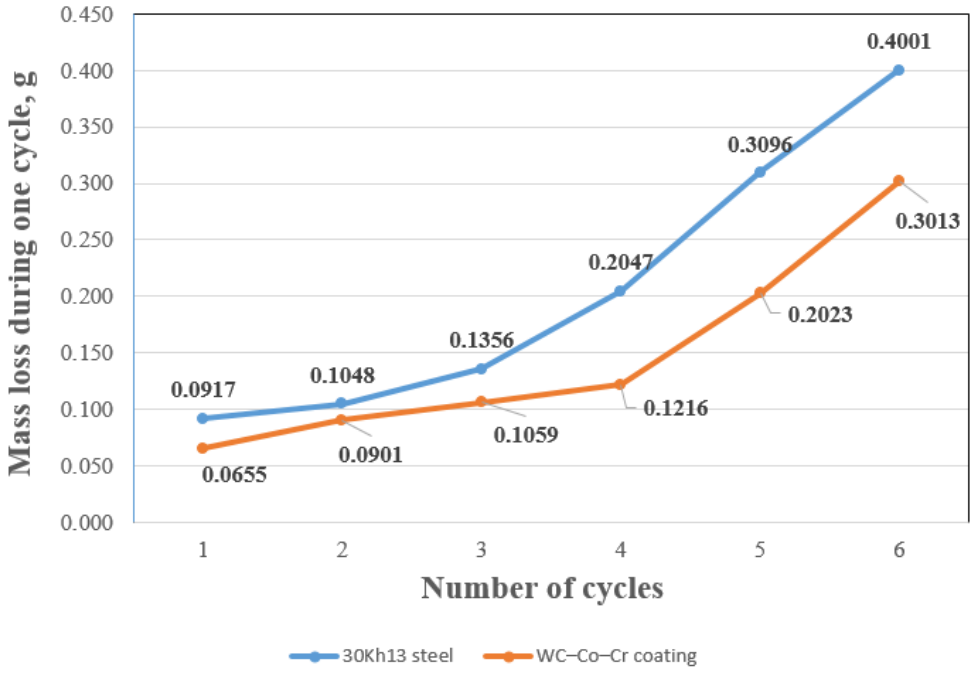

Figure 9. Graph of mass loss of samples with and without WC-Co-Cr coating depending on the number of erosion cycles

Note – compiled by the authors

Thus, the results of erosion tests confirm that the application of a WC–Co–Cr coating significantly increases the erosion resistance of 30Kh13 steel, especially in the early and intermediate stages of exposure to abrasive particles.

In addition to erosion wear, abrasive wear caused by prolonged contact of the surface with hard particles has a significant impact on the durability of parts. Figure 10 shows the results of weighing the samples before the abrasion tests, recording their initial mass.

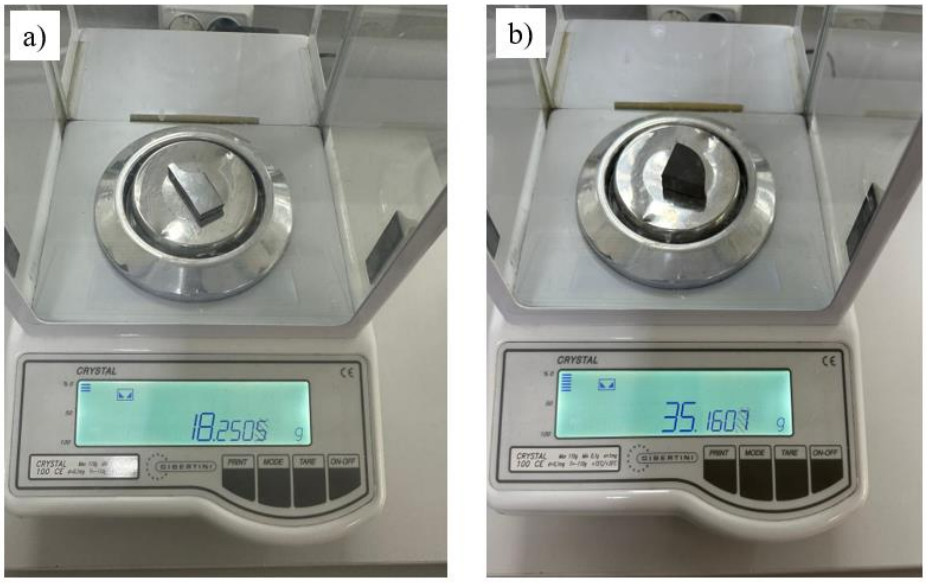

a) 30Kh13 steel; b) sample with 86WC-10Co-4Cr coating

Figure 10. Weighing of samples before testing

Note – compiled by the authors

The initial mass of the 30Kh13 steel sample was 18.2505 g, while the mass of the sample with WC–Co–Cr coating was 35.1607 g. These values were used as initial values in the subsequent determination of mass loss during wear. The appearance of the samples after abrasion testing is shown in Figure 11.

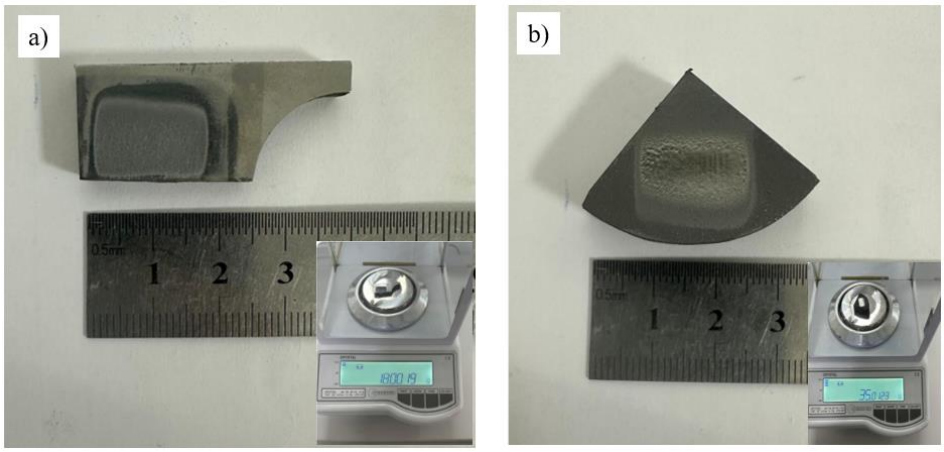

a) 30Kh13 steel; b) sample with 86WC-10Co-4Cr coating

Figure 11. Samples after abrasive wear testing

Note – compiled by the authors

Steel 30Kh13 is characterized by the formation of a more extensive and pronounced wear zone, while in the sample with a WC–Co–Cr coating, the wear zone is smaller and more localized. The quantitative results of the abrasion tests are given in Table 5.

Table 5. Results of abrasive wear tests on samples

No.	Sample	Test time, min	Mass before testing *m*, g	Mass after testing *m*, g	Mass loss, g
1	Steel 30Kh13	10	18.2505	18.0019	0.2486
2	WC-Co-Cr coating	30	35.1607	35.0123	0.1484
Note – compiled by the authors					

It was found that 30Kh13 steel is characterized by the greatest loss of mass, despite the shorter duration of exposure. At the same time, the sample with a WC–Co–Cr coating demonstrates a significantly lower loss of mass even with a longer test time, which indicates a higher resistance of the coating to abrasive wear. For a comparative assessment of wear resistance, the relative wear resistance K_i was calculated using formula (1), which takes into account mass loss, material density, and test conditions:

$$K_{\text{i}} = \frac{g_{\text{e}}\rho_{\text{i}}N_{\text{i}}}{g_{\text{i}}\rho_{\text{e}}N_{\text{e}}} \quad (1)$$

where g – is the mass loss, ρ – is the material density, N – is the number of revolutions, and the indices "e" and "i" correspond to the reference and test materials.

The results of the relative wear resistance calculation are presented in Table 6.

Table 6. Results of calculations of relative wear resistance (K_i) of the tested samples to abrasive wear

No.	Sample name	Mass loss g_i, g	Density ρ, g/cm^{3*}	Relative wear resistance K_i
1	Steel 30Kh13	0.2486	7.67	0.2
2	WC-Co-Cr coating	0.1484	14.5	1.8
3	Steel 45 (reference)	0.048	7.8	1
Note – compiled by the authors				

It has been established that for 30Kh13 steel, the value of K_i is 0.2, while for the WC–Co–Cr coating, this indicator reaches 1.8. The reference sample made of 45 steel is taken as a unit. Thus, the application of the WC–Co–Cr coating provides an increase in relative abrasive wear resistance by approximately 9 times compared to uncoated 30Kh13 steel.

Thus, the test results confirm that the WC–Co–Cr coating effectively increases the resistance of 30Kh13 steel to abrasive wear. Together with the data on corrosion and erosion resistance, this indicates the advisability of using these coatings to protect parts operating under combined corrosion, erosion, and abrasion conditions.

CONCLUSION

1. It has been shown that applying a WC–Co–Cr coating using the HVOF method significantly increases the corrosion resistance of 30Kh13 steel in cyclic salt spray conditions. The mass loss of coated samples is more than five times lower than that of uncoated steel, and the onset of intensive corrosion degradation is significantly delayed.

2. It has been established that during corrosion, the degradation of the coating is localized and is mainly associated with the oxidation and selective corrosion of the Co–Cr binder phase, while the WC carbide phase remains relatively stable.

3. The results of erosion tests showed that the WC–Co–Cr coating effectively reduces the intensity of erosion wear of 30Kh13 steel at the initial and intermediate stages of exposure to abrasive particles. Accelerated coating destruction is observed when the protective layer reaches a critical degree of thinning and the abrasive reaches the substrate.

4. Under conditions of abrasive wear, the WC–Co–Cr coating provides a significant increase in wear resistance: the relative wear resistance of coated samples exceeds that of 30Kh13 steel by approximately 9 times.

CONFLICT OF INTEREST: The authors declare no conflict of interest.

FUNDING: This study was funded by the Committee of Science of the Ministry of Science and Higher Education of the Republic of Kazakhstan (Grant number: BR24992854).

STATEMENT ON THE USE OF ARTIFICIAL INTELLIGENCE TECHNOLOGIES: Authors confirm that no artificial intelligence (AI) tools were used in the preparation of this scientific article. All stages of the work, including writing, editing, fact-checking, and data analysis, were carried out independently by the authors.

REFERENCES

Rao, P., & Mulky, L. (2023). Erosion-corrosion of materials in industrial equipment: a review. ChemElectroChem, 10(16), e202300152. https://doi.org/10.1002/celc.202300152

Lyphout, C., et al. (2013). Tungsten carbide deposition processes for hard chrome alternative: Preliminary study of HVAF vs. HVOF thermal spray processes. Proceedings of the International Thermal Spray Conference (ITSC 2013), 506–511. ASM International. https://doi.org/10.31399/asm.cp.itsc2013p0506

Sidhu, T. S. N., Prakash, S., & Agrawal, R. D. (2005). State of the art of HVOF coating investigations—A review. Marine Technology Society Journal, 39(2), 53–64. https://doi.org/10.4031/002533205787443908

Gao, G., Guo, S., & Li, D. (2024). A review of cavitation erosion on pumps and valves in nuclear power plants. Materials, 17(5), 1007. https://doi.org/10.3390/ma17051007

Xi, Y., et al. (2021). Improvement of erosion–corrosion behavior of AISI 420 stainless steel by ion-assisted deposition ZrN coatings. Metals, 11(11), 1811. https://doi.org/10.3390/met11111811

Sola, R., et al. (2013). Effect of quenching method on the wear and corrosion resistance of stainless steel AISI 420 (Type 30Kh13). Metal Science and Heat Treatment, 54(11–12), 644–647. https://doi.org/10.1007/s11041-013-9543-4

Scheuer, C. J., et al. (2019). AISI 420 martensitic stainless steel corrosion resistance enhancement by low-temperature plasma carburizing. Electrochimica Acta, 317, 70–82. https://doi.org/10.1016/j.electacta.2019.05.135

Sahraoui, T., et al. (2010). HVOF sprayed WC–Co coatings: Microstructure, mechanical properties and friction moment prediction. Materials & Design, 31(3), 1431–1437. https://doi.org/10.1016/j.matdes.2009.09.031

Kear, B. H., Skandan, G., & Sadangi, R. K. (2001). Factors controlling decarburization in HVOF sprayed nano-WC/Co hardcoatings. Scripta Materialia, 44(8–9), 1703–1707. https://doi.org/10.1016/S1359-6462(01)00789-0

Seitov, B., et al. (2025). Review of physical and mechanical properties, morphology, and phase structure in Cr_3C_2–NiCr composite coatings sprayed by HVOF method. Coatings, 15(4), 479. https://doi.org/10.3390/coatings15040479

El Rayes, M. M., Sherif, E. S. M., & Abdo, H. S. (2022). Comparative study into microstructural and mechanical characterization of HVOF WC-based coatings. Crystals, 12(7), 969. https://doi.org/10.3390/cryst12070969

Picas, J. A., et al. (2019). Corrosion mechanism of HVOF thermal sprayed WC–CoCr coatings in acidic chloride media. Surface and Coatings Technology, 371, 378–388. https://doi.org/10.1016/j.surfcoat.2018.11.090

Wang, H., et al. (2019). Corrosion resistance enhancement of WC cermet coating by carbides alloying. Corrosion Science, 147, 372–383. https://doi.org/10.1016/j.corsci.2018.11.021

Magnani, M., et al. (2007). WC–CoCr coatings sprayed by high velocity oxygen-fuel (HVOF) flame on AA7050 aluminum alloy: Electrochemical behavior in 3.5% NaCl solution. Materials Research, 10, 377–385. https://doi.org/10.1590/S1516-14392007000400008

Sapate, S. G., et al. (2021). Effect of coating thickness on the slurry erosion resistance of HVOF-sprayed WC-10Co-4Cr coatings. Journal of Thermal Spray Technology, 30(5), 1365–1379. https://doi.org/10.1007/s11666-021-01206-6

Information about authors

Nazerke Muktanova– doctoral student of the specialty "Technical Physics", East Kazakhstan Technical University named after D. Serikbaev, Ust-Kamenogorsk, Kazakhstan,
e-mail: muktanovan@gmail.com,
ORCID: https://orcid.org/0000-0002-4823-6640,

Małgorzata Rutkowska-Gorczyca – Doctor of Technical Sciences, Department of Automotive Engineering, Wrocław University of Science and Technology, Wrocław, Poland,
e-mail: malgorzata.rutkowska-gorczyca@pwr.edu.pl,
ORCID: https://orcid.org/0000-0003-2712-5914,

Nurtoleu Magazov – doctoral student of the specialty "Technical Physics", East Kazakhstan Technical University named after D. Serikbaev, Ust-Kamenogorsk, Kazakhstan,
e-mail: magazovn@gmail.com,
ORCID: https://orcid.org/0000-0002-9941-9199,

Bauyrzhan Rakhadilov – Doctor of Technical Sciences, Professor, General Director of PlasmaScience LLP, Ust-Kamenogorsk, Republic of Kazakhstan,
e-mail: rakhadilovb@mail.ru,
ORCID: https://orcid.org/0000-0001-5990-7123

CONTENT

CENTRAL ASIAN TRANSACTIONS
ON MATERIALS STRUCTURE AND PROPERTIES

Scientific journal
Published since 2026
Registered with the Ministry of Culture and Information
of the Republic of Kazakhstan.
Certificate No. KZ93VPY00129402 dated September 16, 2025.

Editors O. Nikolaenko, S. Mamyrazdykova
Copy editors O. Nikolaenko, S. Mamyrazdykova
Head of the editorial and publishing center O. Nikolaenko

Text Layout, lead out production of the original layout S. Mamyrazdykova

Signed to print on March 31, 2026.
Format 84´108/16. Offset paper.
Volume: conventional printing plate 9.45, estimated printing plate 9,49.
Printed version. Circulation 30 copies. Order No. 52-2026.
The price is negotiable.

D. Serikbayev East Kazakhstan Technical University.
070004, Ust-Kamenogorsk, 69 Protozanov Street.